Prepared by:

Guidance and Control Group
The Bendix Corporation

Approved by:

S. Calvin Rybak
Program Manager

O. Taylor
Technical Manager

M. Brown
Manager,
Denver Operations

THE BENDIX
CORPORATION

GUIDANCE SYSTEMS
DIVISION
DENVER OPERATIONS

FLOATED PALLET DEFINITION STUDY

FINAL REPORT

JULY 1975

VOLUME IV
SUMMARY VOLUME

PREPARED FOR:

GEORGE C. MARSHALL
SPACE FLIGHT CENTER
HUNTSVILLE, ALABAMA

NASA CONTRACT NO.
NAS8-30889

FOREWORD

This final report is submitted in accordance with the requirements of NASA-GSFC, Contract No. NAS8-30889. The report includes:

Volume I - Evaluation of Alternate Telescope Pointing Schemes

Volume II - Suspended Pallet Pointing Performance Study

Volume III - Retention/Suspension Systems, Pallet Common Module Configuration Study

Volume IV - Summary Volume

CONTENTS

CONTENTS (Continued)

Figure

CONTENTS (Continued)

CONTENTS (Continued)

CONTENTS (Concluded)

1. INTRODUCTION

With the maturation of the space shuttle concept of a reusable launch vehicle for earth orbital missions, two divergent modes of operation have been defined. One mode involves the use of the shuttle as a logistics vehicle placing free flying experiment packages in orbit and replacing, repairing or servicing existing packages. In addition it will perform a crucial role as a manned experiment base, remaining in earth orbit from 7 to 30 days performing various experiments with equipment mounted in the payload bay. The shuttle flight system is shown in figure 1-1.

Current assessments of the experiments proposed for operation in low earth orbit in conjunction with a manned vehicle indicate that nearly 45 percent of the payloads require pointing accuracy greater than that afforded by the orbiter capability using the Reaction Control System (RCS). It is therefore apparent that a second level of control or alternately, an Instrument Pointing System (IPS), is required to meet the precise pointing accuracies required by a substantial percentage of experiments that can fly on the orbiter. In general, the experimental payloads will be mounted on a pallet structure carried in the orbiter payload bay as shown conceptually in figure 1-2. Figure 1-3 shows a typical pallet segment and a conceptual drawing of a three bay pallet.

There are presently three concepts that have been proposed for the Instrument Pointing System. They are the Inside-Out Gimbal (IOG) system proposed by the European Spacelab project, the Standard Experiment Pointing Base (SEPB), and the Floated Pallet. The latter two concepts were developed by Marshall Space Flight Center (MSFC) personnel.

The material presented in this final report is the result of three interrelated studies. The first consisted of an evaluation of the three Instrument Pointing System concepts, the results of which are presented in volume I of this final report. The second was a Floated Pallet pointing performance study treated in volume II. The third was a pallet hardware conceptual design study including suspension and retention systems, experiment erection, CMG mounting, etc., with results presented in volume III.

The IPS evaluation study was performed not only to evaluate the operation of the three concepts mentioned previously, but also to determine the relative advantages and disadvantages of each of the systems. Of particular interest was the effect of structural flexibility on the performance of each of the proposed concepts. The approach taken in evaluating these effects was to

assume a rigid structure for determining the control loop bandwidths and other system parameters (i.e., suspension characteristics, sensor characteristics, etc.) required to meet a pointing stability limit of ± 1 sec for each of the proposed systems in the presence of crew motion disturbances. Crew motion disturbances are projected to be the most severe disturbance presented to the IPS. Once these parameters were identified, structural flexibility was inserted and its effect on overall system stability and performance was determined for each of the proposed concepts.

The Floated Pallet pointing performance study involved sizing and selection of a Control Moment Gyroscope (CMG) system for pallet pointing control. A complex nonlinear CMG actuator model including internal compliances, frictional characteristics, deadbands, and shockmount characteristics was derived and programmed for analog simulation in order to evaluate the actuator characteristics, in particular the frequency response. At the same time the model was simplified as far as possible while retaining all significant nonlinearities. Control loop studies were performed and included analytic studies to determine single axis loop stability, provisional gain selections, compensation analysis and determination, and linear error analysis. The actual pointing performance study was initiated with the definition of a three axis hybrid simulation model assuming rigid body dynamics for the orbiter and pallet, the pallet suspension characteristics, the nonlinear shockmounted CMG models derived earlier and the various control laws and compensations. Using this model, the pointing performance that could be achieved with the selected CMG actuators was studied, including response to short period (man-motion) disturbance profiles with emphasis on the amplitude of limit cycles incurred, the conditions of their occurrence and their variations as a function of CMG parameter variation.

The final study involved the conceptual design of a suspension system for the Floated Pallet and a retention system to support the pallet during launch, maneuvering and descent. In addition a CMG support equipment configuration study including installation and an experiment mount and erection study were performed. The impact of these separate hardware studies on the existing pallet configuration was assessed and a modified pallet common module defined.

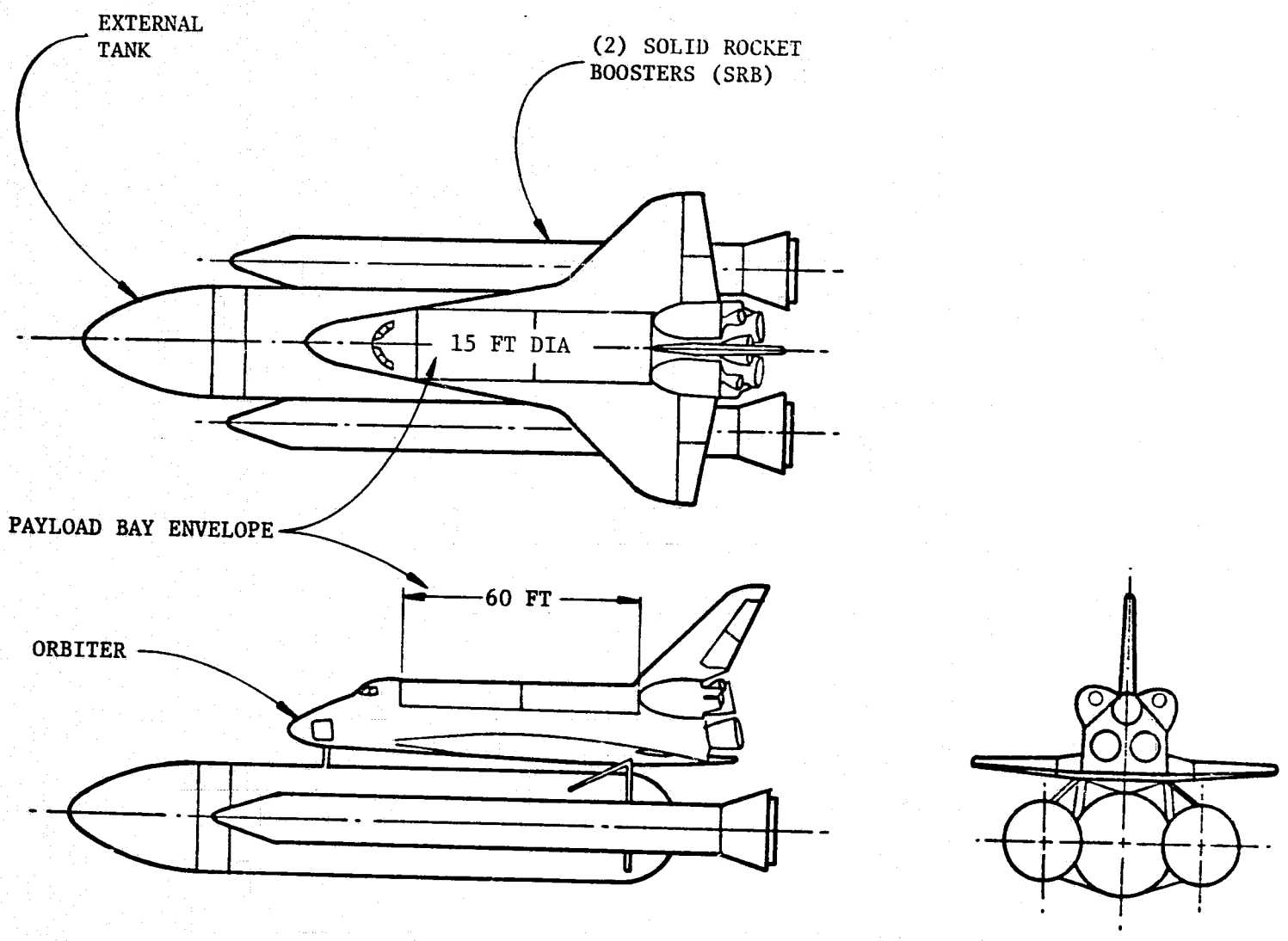

Figure 1-1. Space Shuttle Flight System

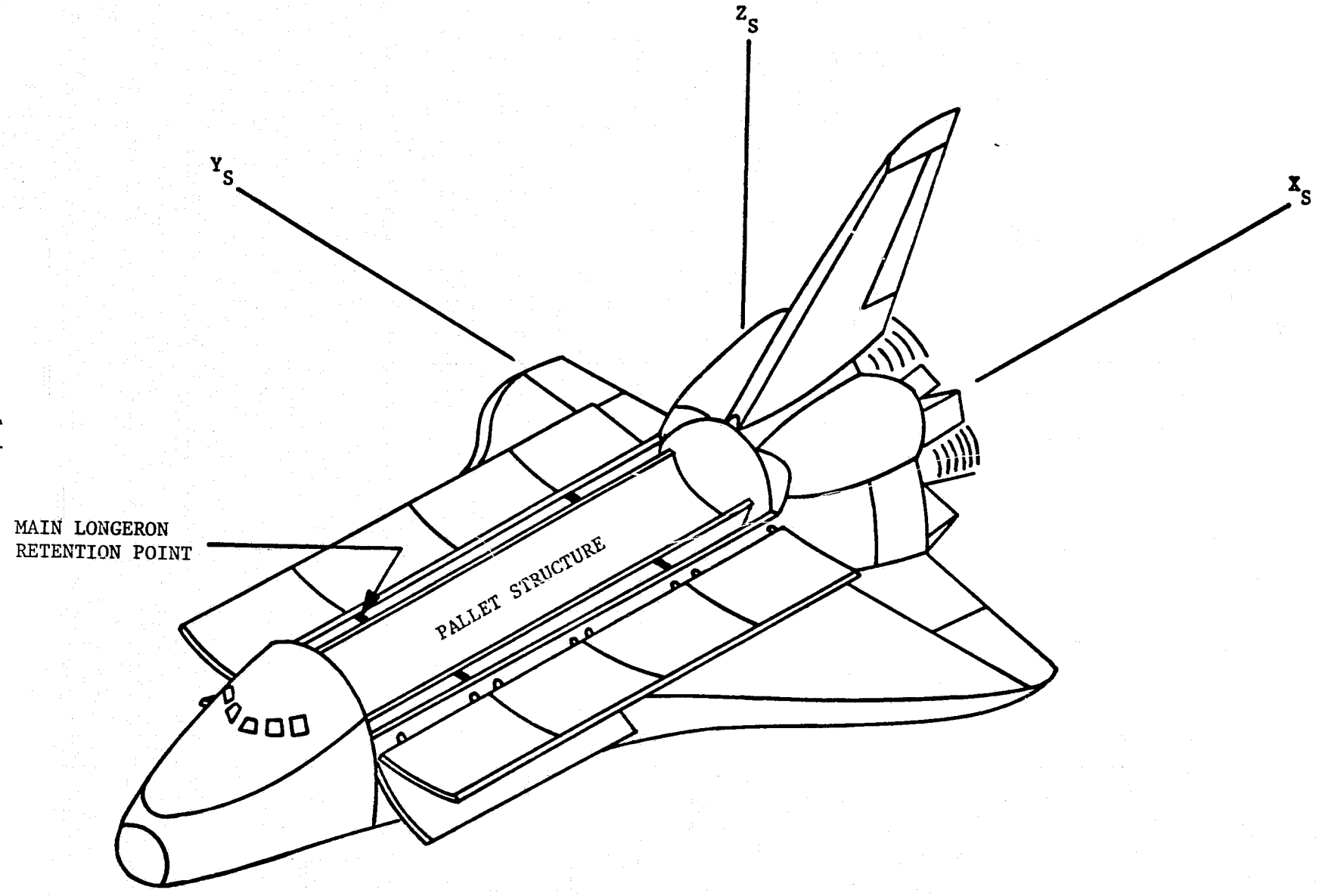

Figure 1-2. Orbiter/Pallet Configuration

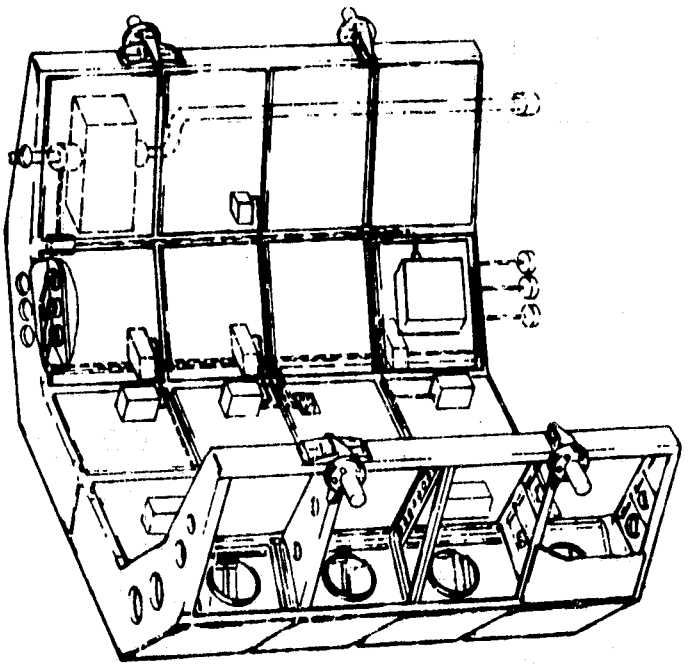

a) 3 METER PALLET SEGMENT

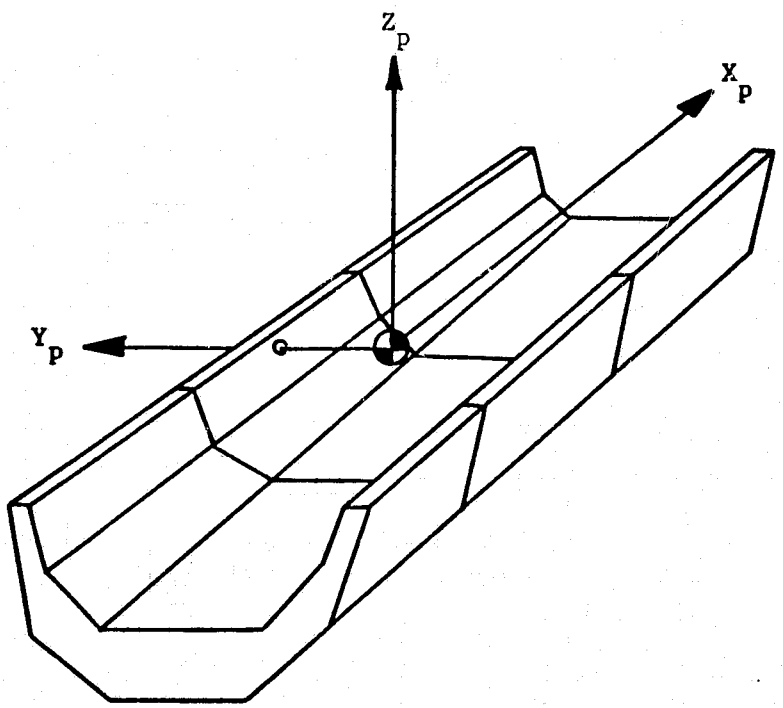

b) 3 SEGMENT PALLET

Figure 1-3. Pallet Configuration

2. CONTROL MOMENT GYROSCOPE (CMG) SYSTEM

2.1 CMG System Requirements - The torque and momentum storage requirements which determined the CMG actuator cluster capability for the Floated Pallet were calculated for an inertial attitude in which the orbiter/pallet composite vehicle X principal axis was constrained to lie in the orbital plane (XIOP). The XIOP attitude allows pointing of the pallet Z axis anywhere in the celestial sphere while minimizing the gravity gradient torques applied to the vehicle. The sizing was accomplished by considering the worst case XIOP gravity gradient environment which occurs when the vehicle Z axis is directed 45 degrees out of the orbital plane. In addition to the gravity gradient effects, aerodynamic effects and the impact of utilizing the CMG cluster for momentum desaturation maneuvering were considered in the basic sizing determination. A summary of the cluster requirements are given in table 2-1.

A CMG actuator cluster with a 12,200 n-m-sec momentum storage capability anywhere in the vehicle YZ plane and a 200 n-m torque output in any direction allows single orbit pointing capability for the XIOP attitude assuming cluster operation about a zero momentum state. Since the dominant gravity gradient momentum history is quite predictable, operation about a properly chosen nonzero momentum state would allow multiple orbit operation before desaturation maneuvering would be required or alternatively could allow relaxation of the momentum storage requirement.

With the specified cluster capability (based on the XIOP attitude), operation of the orbiter/pallet vehicle in any of the attitudes requiring local vertical pointing of the Z axis (ZLV) or X axis (XLV), or constraining the X axis perpendicular to the orbit plane (XPOP) can easily be accomplished due to the far less stringent momentum storage requirements.

2.2 CMG Actuator Selection - Based on the momentum storage and torque output requirements discussed in the previous section, a cluster of four modified Skylab ATM double gimbal CMGs was selected for this application. The modifications consist of redesign of the spin bearing lubrication system and changes in the internal power distribution allowing removal of the gimbal stops and thus unlimited gimbal freedom. The cluster of four actuators allows mission continuance with a single failure (fail operational).

Single gimbal CMGs were removed from consideration due to the limited momentum storage capabilities of any existing or planned actuator and due to the software problems associated with singularity avoidance and failure mode operation.

A survey of double gimbal CMGs revealed three actuators which could be clustered to meet the basic requirements with trade studies indicating the modified Skylab actuator was most effective for this application, particularly since it is the only launch and space qualified device and is available "off-the-shelf."

The basic envelope of the modified Skylab actuator (Bendix MA-2300 double gimbal CMG) is shown in figure 2-1, with pertinent physical data shown in tables 2-2 and 2-3. Dimensions are shown in inches since the actuator has been designed and built to American practice. It should be noted that the CMG Inverter Assembly (CMGIA) required for CMG spin motor power, gimbal resolver excitation and other CMG related functions has available regulated alternating current outputs which could be utilized by experimental or support hardware on the pallet or in the orbiter perhaps obviating the need of other inverter electronics packages.

2.3 CMG Installation - The primary design objectives for the installation of the CMG cluster on the suspended pallet included minimal structural modification to the pallet and to the CMG attachment fittings, while allowing adaptability to various payload configurations. In addition each actuator must be individually shock-mounted with a 20 Hz natural frequency in order to isolate high frequency vibrations arising within the CMG from the pallet.

The basic approach followed was the design of support frames made of welded aluminum tubing with machined aluminum fittings attaching directly to the existing pallet hard point spherical nuts. This approach requires no modification of the pallet structure. Frames were designed for two and four actuators as shown in figures 2-2 and 2-3, respectively. In both cases the CMGIAs are mounted on the support frame thus keeping all CMG hardware in one package.

The frames with two CMGs (of which two would be required) can be mounted at various locations on the three segment pallet and this arrangement is the more flexible in accommodating various payload configurations. The frame with four CMGs should be located on a single pallet and with such a mounting provides the stiffest structural interface between the actuators and pallet. Based on a conventional truss frame design, using 5 cm square aluminum tubing, the weight of the supporting structure in either case is approximately 90 kg (i.e., a four CMG frame weighing 90 kg or two frames for two CMGs at 45 kg each).

The 20 Hz isolation requirement indicates that military quality elastomer all-attitude mounts available off-the-shelf are likely candidates. Adaptation of such mounts to the CMGs require machined

adaptor fittings due to the isolator float requirements and the existing CMG mounting configuration. The adaptors can be bolted to the CMG so that no modification of the actuator is required. Detailed design of the fittings was not addressed in this study although the conceptual configuration is shown on the drawings.

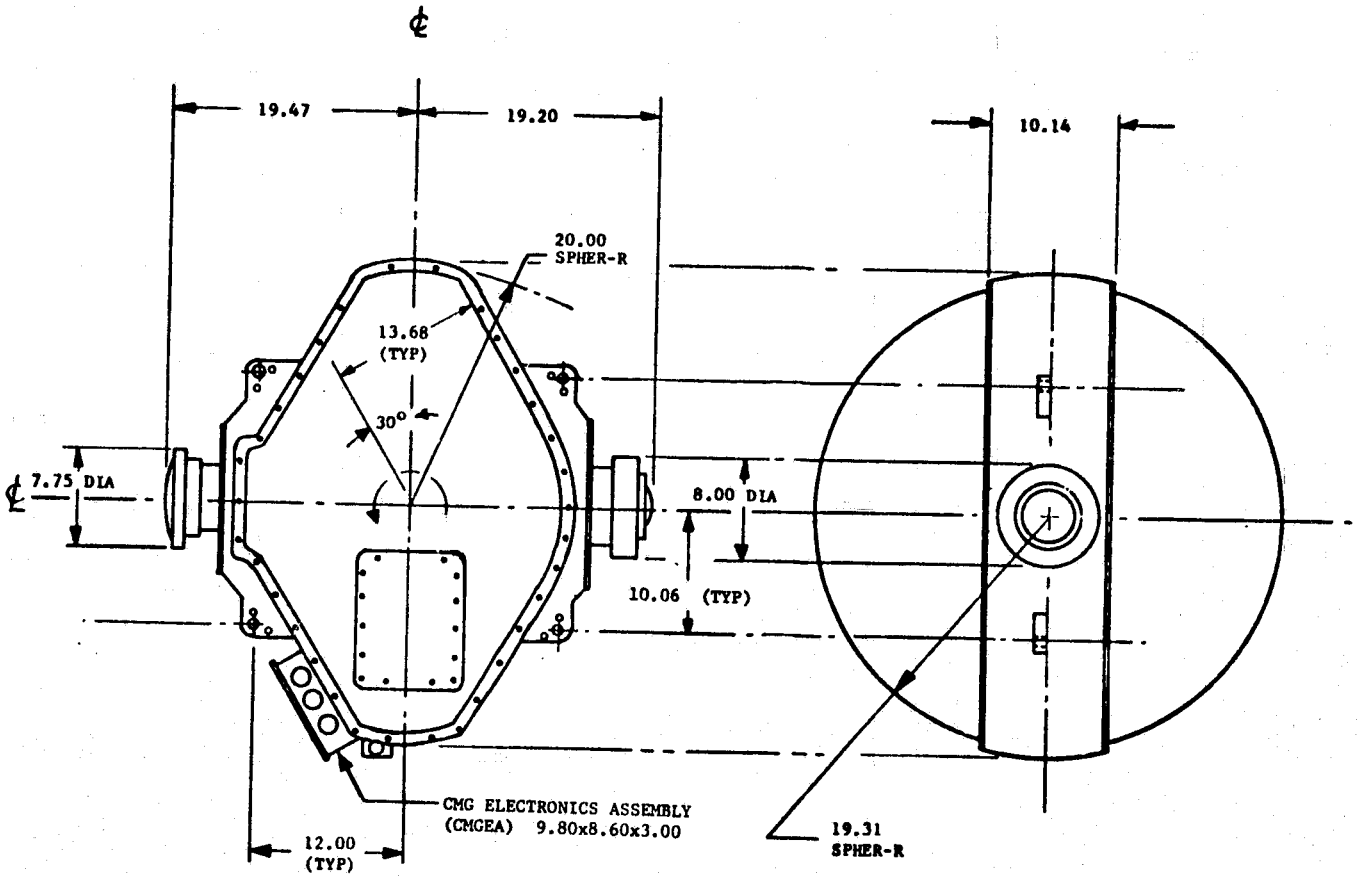

CONTROL MOMENT GYROSCOPE (CMG)

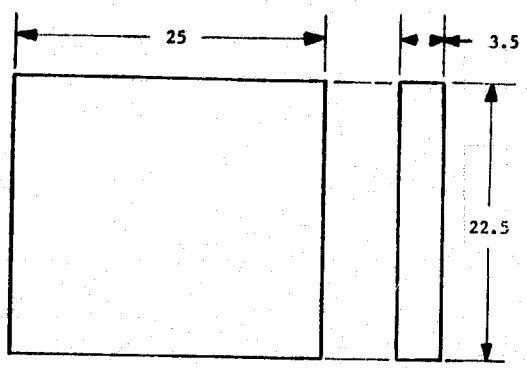

CMG INVERTER ASSEMBLY (CMGIA)

NOTE: ALL DIMENSIONS ARE GIVEN IN INCHES

Figure 2-1. Bendix MA-2300 Double Gimbal Control Moment Gyroscope

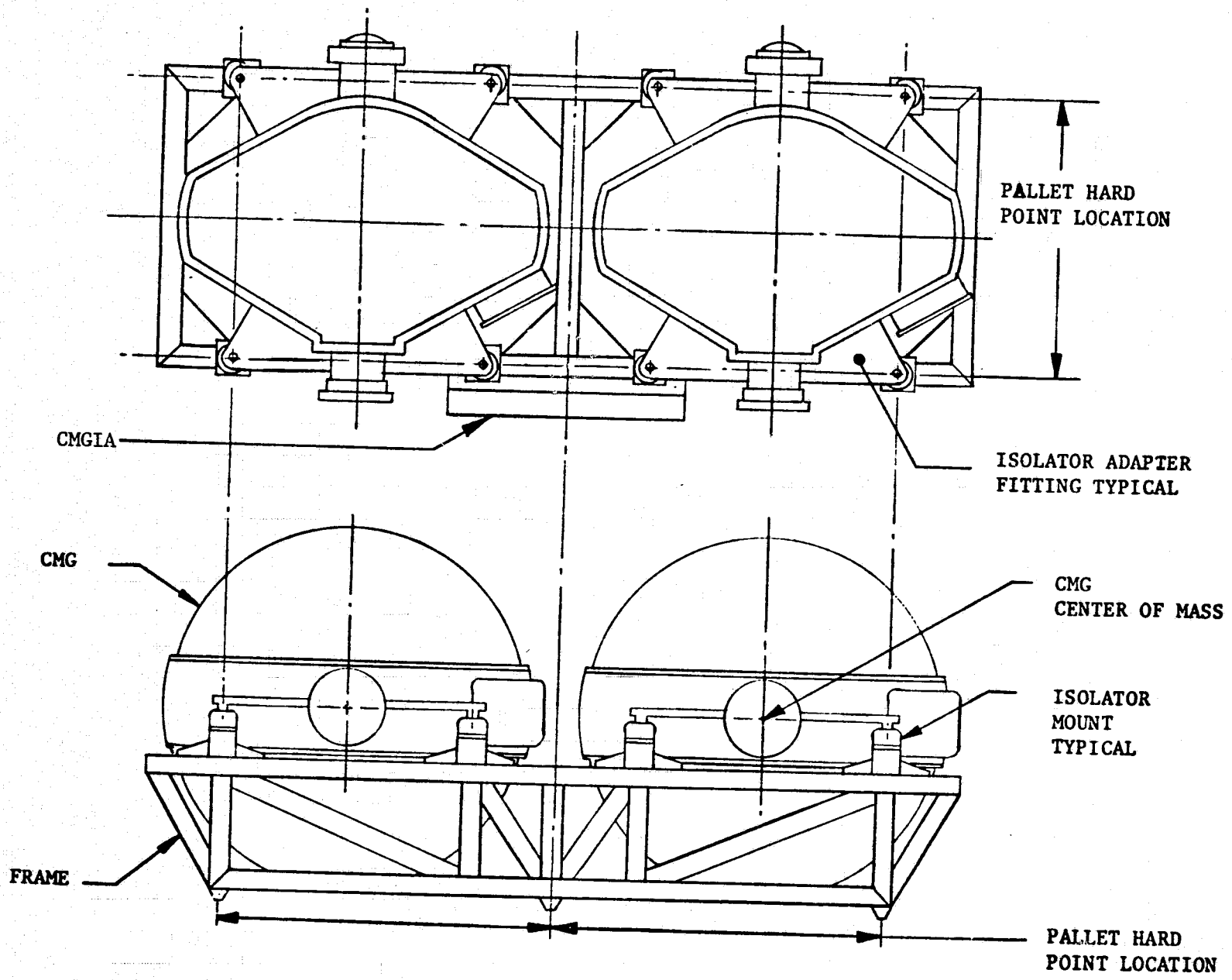

Figure 2-2. Support Frame With Two CMGs

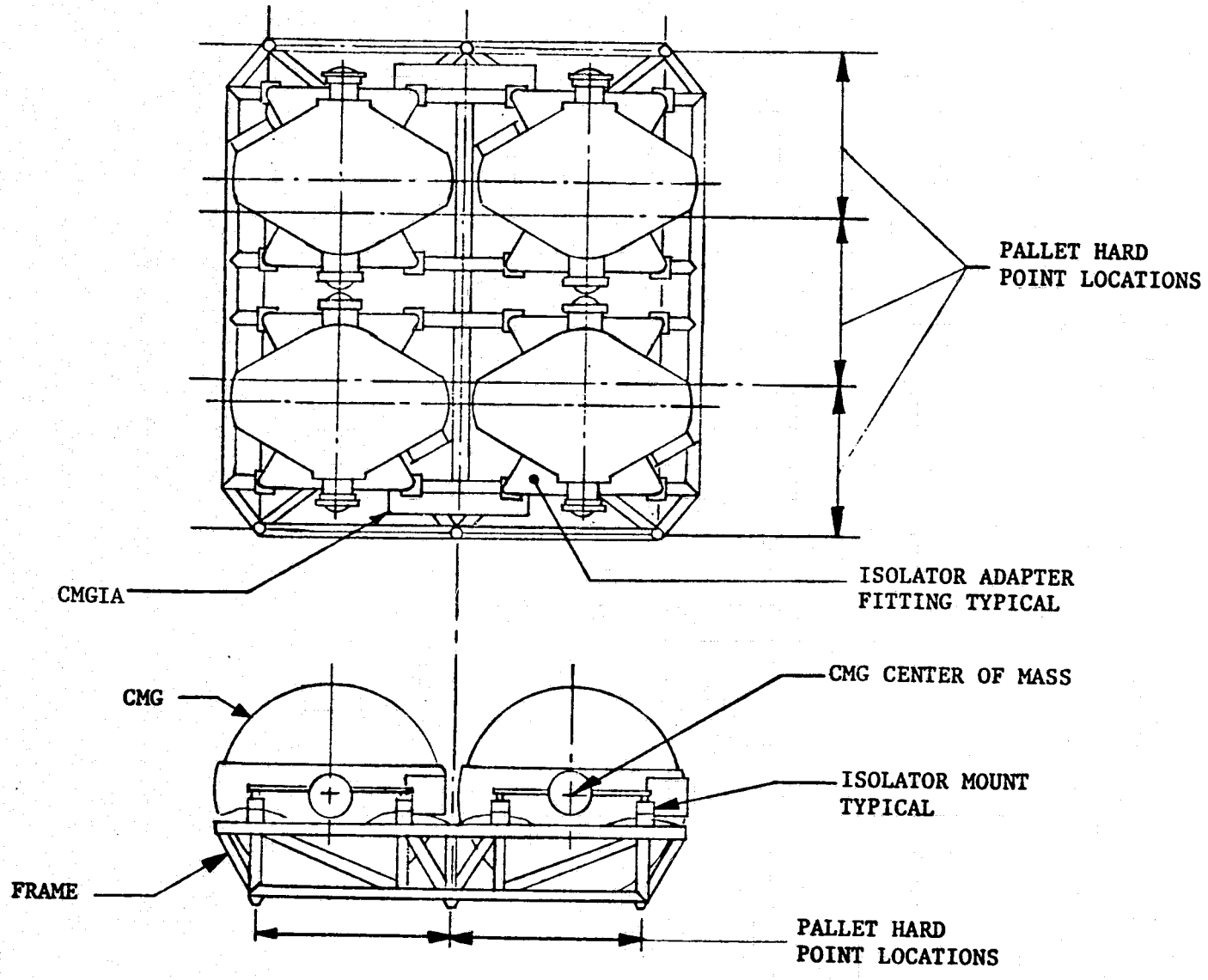

Figure 2-3. Support Frame With Four CMGs

Table 2-1. CMG Cluster Requirements

(XIOP, Z axis 45 degrees out of orbital plane)

Peak Gravity Gradient Torque (inertially held)	12.20 N-m
Peak Aerodynamic Torque (inertially held)	1.50 N-m
Maneuver Torque (momentum desaturation)	200.00 N-m
Peak Gravity Gradient Momentum (inertially held)	10,980 N-m-sec
Peak Aerodynamic Momentum (inertially held)	950 N-m-sec
Momentum Exchange (250 sec maneuver)	5,290 N-m-sec
Net Momentum Accumulation Per Orbit	1,125 N-m-sec
Root-Sum-Square Torque Requirements	200.43 N-m
Root-Sum-Square Momentum Requirements	12,239 N-m-sec

Table 2-2. Bendix MA-2300 Double Gimbal CMG

Actuator Characteristics:	
Stored Angular Momentum	3,120 N-m-sec
Peak Output Torque	165 N-m
Actuator Bandwidth	4-10 Hz
Wheel Rotation Rate	9,080 rpm
Wheel Spinup Time	14 hr
Physical Characteristics:	
Size	1 m sphere (a)
Weight	190 kg (b)
Power Requirements:	
Wheel Spin Control (steady)	80 watts
Spinup Peak	170 watts
Gimbal Torquers (peak)	170 watts
Spin Bearing Heaters (peak)	52 watts
Other	70 watts (c)
Miscellaneous:	
Spin Motor Type	AC (455 Hz, 3 phase)
Gimbal Torquer Type	Brush Type DC
Torquer Gimbal Drive	Geared (56.55:1)
Gimbal Freedom	Unlimited

Notes:

a) Includes CMG Electronics Assembly (CMGEA), 25x22x7.5 cm.
b) Includes CMG Electronics Assembly (CMGEA), 4 kg.
c) Allocated to CMG Inverter Assembly (CMGIA) functions.

Table 2-3. Bendix MA-2300 CMG Inverter Assembly (CMGIA)

Physical Characteristics:	
Size	64x57x9 cm
Weight	23 kg
Electrical Input:	
Voltage	28 vdc + 4 vdc
Current	10 amps (peak)
Performance Characteristics:	
Voltage Regulation	±5%
Frequency Regulation	±0.002% (primary)
Voltage Distortion	5%
Power Output	
455 Hz, 130 v, 3 phase	600 VA
800 Hz, 28 v, 1 phase	12.5 watts
4.8 kHz, 10 v, 1 phase	6.0 watts
Distributor Bus	
455 Hz	100 VA
800 Hz	12.5 watts
4.8 kHz	6.0 watts

3. PALLET SUSPENSION AND RETENTION SYSTEMS

The primary considerations in the conceptual design of hardware as it affected the Floated Pallet involved the selection of a suspension system configuration including isolator characteristics and definition of a retention system which met the basic study requirements. These requirements and the conceptual design results are outlined in the following paragraphs.

3.1 Pallet Suspension System - The suspension system is locked out during launch and descent of the orbiter with the retention system supporting the pallet during these periods. The design goal for the suspension was a natural frequency of 0.1 Hz in all axes both in rotation and translation with a damping ratio of 0.1. The configuration and location of the suspension cannot restrict experiment placement in the payload volume and in addition a system stable over a wide temperature range without thermal control is desirable.

Single point, two point, three point, and four point suspension systems were analyzed to determine if the systems could achieve the design goal of 0.1 Hz natural frequency in all axes for both rotation and translation. Wire rope helical springs, elastomeric isolators, solid wire helical or cantilever springs, and gas filled bellows were analyzed to determine if these configurations could achieve the design goal of the suspension system. The four point suspension system utilizing gas filled bellows was selected as the suspension system which most nearly meets the design objectives. The configuration of the decoupled four point suspension is shown in figure 3-1 with the frequency and damping characteristics given in table 3-1.

The required spring rates and damping constants are realized with a gas filled metal bellows design utilizing three of the bellows assemblies at each suspension point. For each assembly the spring constant is a function of both the metal bellows and the gas while the damping is a function of the gas flow through a circular orifice. The basic bellows design is shown in figure 3-2 with the physical characteristics given in table 3-2. A detailed layout of a typical suspension point is shown in figure 3-3 with estimated weight and volumes given in table 3-3. The bellows assemblies are installed between the pallet and orbiter with the installed length greater than the free length of the bellows resulting in a preloaded condition assuring linear response and allowing float of ± 1 inch along any pallet axis.

Performance of the suspension was evaluated for off nominal physical characteristics and failures in the isolators and for variation in the location of the pallet mass center with respect to the suspension points.

3.1.1 Spring Constant Sensitivity - Variation in spring constants can arise from manufacturing tolerances in fabricating the bellows and loss of gas from the bellows assembly. With the assumption of no center of mass offset, the following cases were considered:

a. Assembly spring constants varied ±10 percent.

b. Bellows spring constants varied ±10 percent.

c. Total loss of gas pressure leaving only the nominal bellows spring constants. (This is the worst case since no damping exists.)

d. Loss of gas pressure at one suspension point.

The changes in natural frequencies corresponding to the above variations are given in table 3-4 as cases 1 through 4, respectively. Case 2 (b above) represents reasonable manufacturing tolerances resulting in natural frequency variations of less than 5 percent. Case 4 (d above) represents a reasonable failure mode resulting in natural frequency variations of less than 10 percent.

3.1.2 Damping Sensitivity - Damping performance is a function of the damping constant and the gas pressure drop across the orifice. The damping constant is a function of the orifice length and hole diameter; the gas pressure drop is a function of the system disturbances. Therefore, if the initial gas pressure is greater than the required gas pressure drop, damping performance does not change. Reasonable orifice length and hole diameter tolerances are ±0.025 cm and -0.0015 cm, respectively. These tolerances are the basis of the numerical extremes shown in table 3-5.

3.1.3 Center of Mass Variation Sensitivity - If the pallet center of mass is not located at the elastic center of the suspension, coupling of rotational and translational motions occurs. Since center of mass offsets can occur as differing payload configurations are installed on the pallet, these coupling effects were investigated one axis at a time. For offsets along the X axis, Y and Z translations couple into Z and Y rotations, respectively, while for Y offsets X and Z translations couple into the Z and X rotations, respectively, and finally Z offsets result in

X and Y translations coupling into Y and X rotations. The natural frequencies as a function of offset along X, Y, and Z are shown in figures 3-4, 3-5, and 3-6, respectively, where in each case the frequencies along the axis of offset remain unchanged.

Center of mass offsets of ±0.5 m along any axis result in natural frequency variations of less than 10 percent for all axes. For combined axis offsets, the natural frequency variation should also be small, although translational to rotational coupling will exist for all axes. The suspension system can, however, accommodate reasonable center of mass offsets without modification.

3.2 Pallet Retention System - Because the orbiter structure warps under aerodynamic flight loads, launch accelerations, and thermal differences, the pallet must be isolated from the relative motions of the mounting points. The existing pallet retention system was designed to overcome the problem. Two retention points are located on the cargo bay main longerons near the aft end of the pallet to react forward and aft loads plus up and down loads. Two retention points are located on the cargo bay main longerons near the forward end of the pallet to react up and down pitching loads. A fifth retention point on the lower centerline of the cargo bay reacts side loads. This approach prevents any relative motion of the orbiter structure from inducing destructive loads into the pallet/payload. In order to allow the suspension system to be active during orbital operations, the existing retention system must be modified to provide a means of disengaging to allow the pallet to float on the suspension.

The recommended modification is based on moving the mounting shaft inside the pallet fitting. The cargo bay main longeron retention point with the mounting shaft in the extended position is shown in figure 3-7. The retracted position is shown in figure 3-8. Since the mounting shaft is sized for a free running fit to the orbiter trunnion, this feature is incorporated in the pallet fitting. The position of the mounting shaft is maintained through a positive friction device such as a set screw in the pallet fitting, plus the lead screw/nut combination.

Retraction of the mounting shaft is accomplished by turning the lead screw with an actuator. As shown in figure 3-8 the lead screw tip remains inside the orbiter trunnion thus providing a limit to the relative displacement between the pallet and orbiter.

Extension of the mounting shaft is dependent upon engagement to the orbiter trunnion. Since the engagement sequence occurs in orbit, resistance will be from radial misalignment and the tendancy

of the orbiter trunnion spherical bushing to rotate. Forces necessary to overcome radial misalignment can be expected to be small compared to launch loads. The rotational misalignment of the spherical bushing is overcome by the configuration of the mounting shaft tip. A typical engagement sequence is shown in figure 3-9. Maximum radial misalignment (caging) is controlled by the size of the lead screw tip and is not necessary for engagement. Maximum rotation of the spherical bushing is controlled by the outer race of the trunnion. Position I shows initial contact of the shaft to the bushing at A. Extension of the shaft into the bushing continues along A and contact B is made as shown in position II. Contact at B causes the bushing to rotate until contact at C is made as shown in position III. The shaft lead diameter and lead length is determined at this position to assure a gap D. The spherical bushing is now centered about the shaft allowing further shaft extension as shown in position IV. The engagement sequence is completed when the shaft actuates a limit switch to stop the lead screw drive motor.

This arrangement would necessitate a new pallet fitting to house the mounting shaft and drive mechanism. However, since this system can be used for captive pallet missions as well as the Floated Pallet missions, a natural conclusion would be to incorporate the system on all pallet common modules.

The weight increase of this system over the existing system is estimated at 20 kg, based on the drive mechanism at 1 kg and the movable mounting shaft at 3 kg per retention point. Detailed layouts of both a typical main longeron and the lower centerline retention points are shown in figure 3-10.

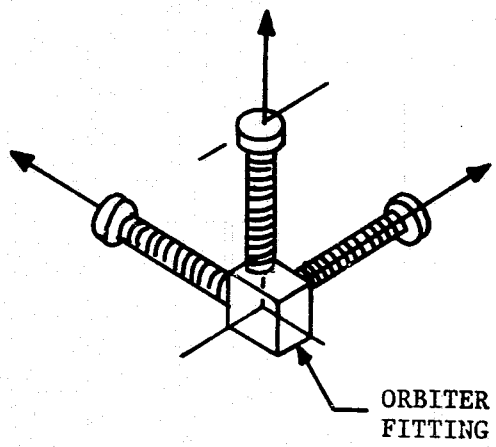

ISOLATOR - GAS BELLOWS
ARRANGEMENT

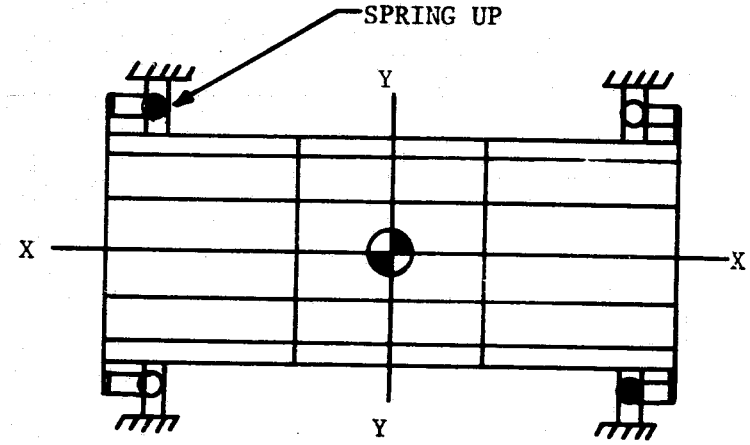

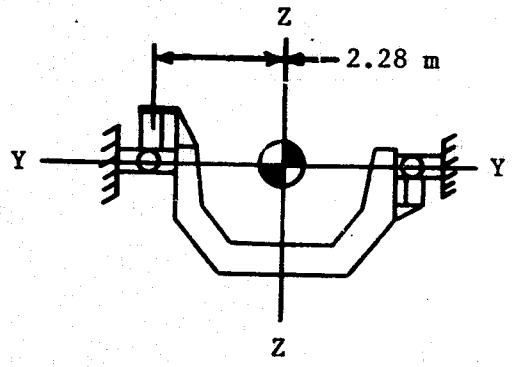

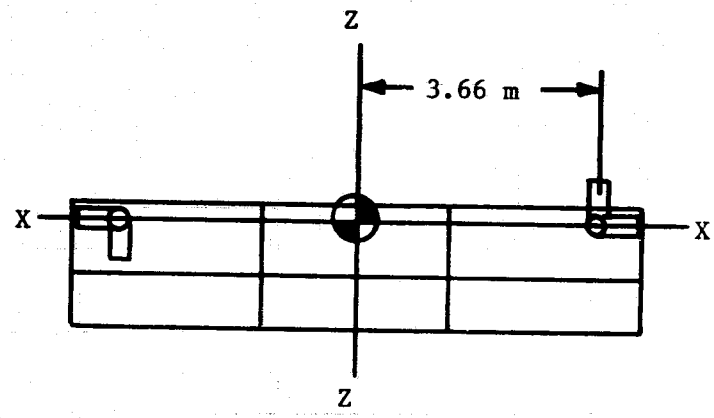

Figure 3-1. Four Point Suspension Containing the Center of Mass Gas Filled Bellows Isolaters

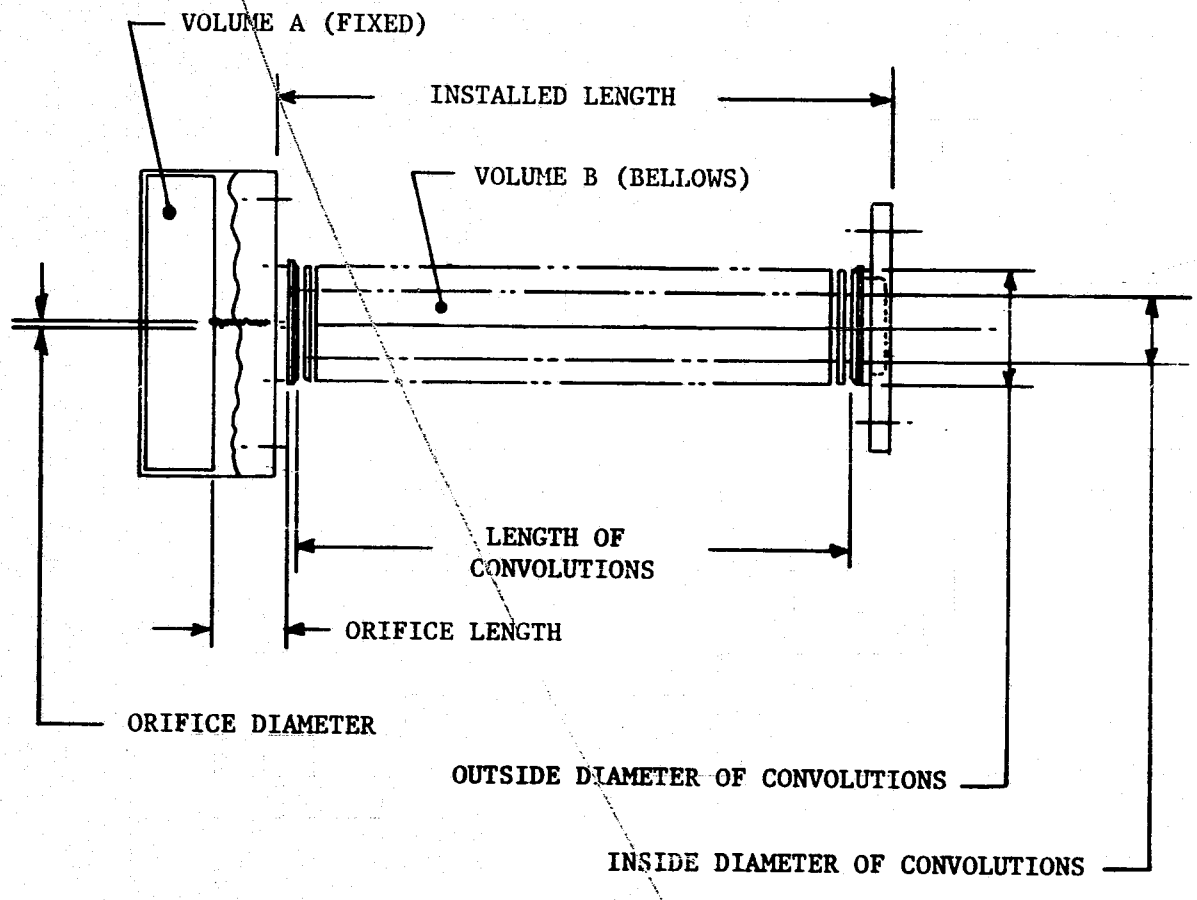

Figure 3-2. Gas Filled Bellows

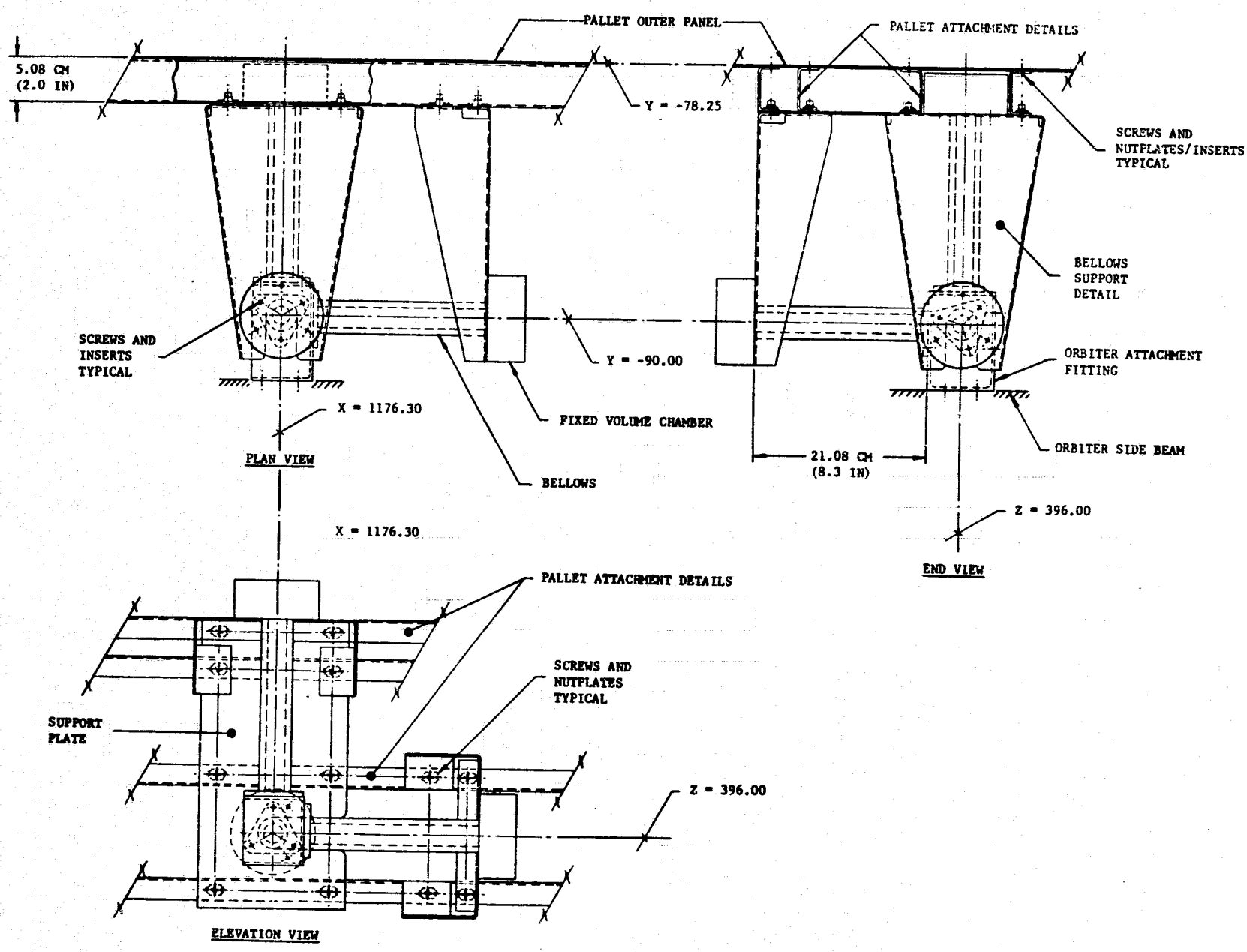

Figure 3-3. Suspension System - Gas Filled Bellows
Aft Left-Hand Location

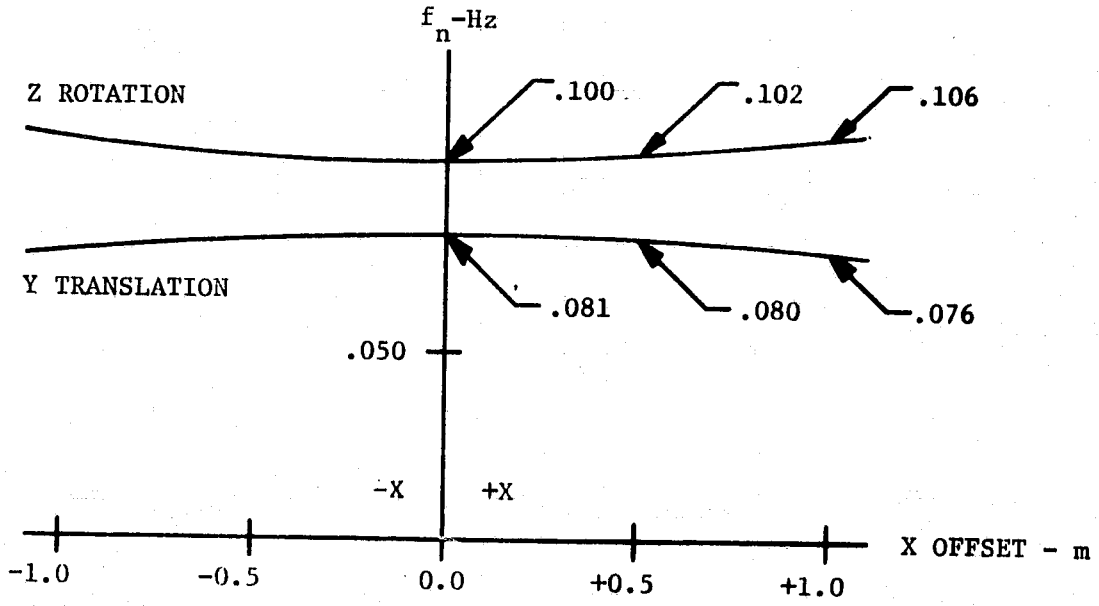

Y TRANSLATION - Z ROTATION COUPLING

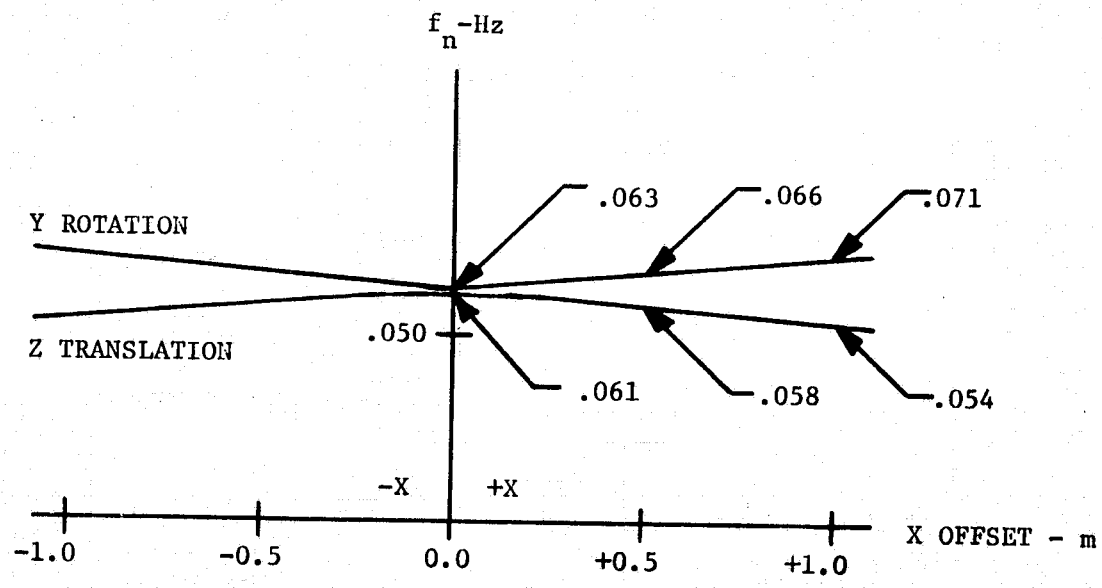

Z TRANSLATION - Y ROTATION COUPLING

Figure 3-4. Variation of Suspension Natural Frequencies With Longitudinal (X Axis) Center of Mass Offsets

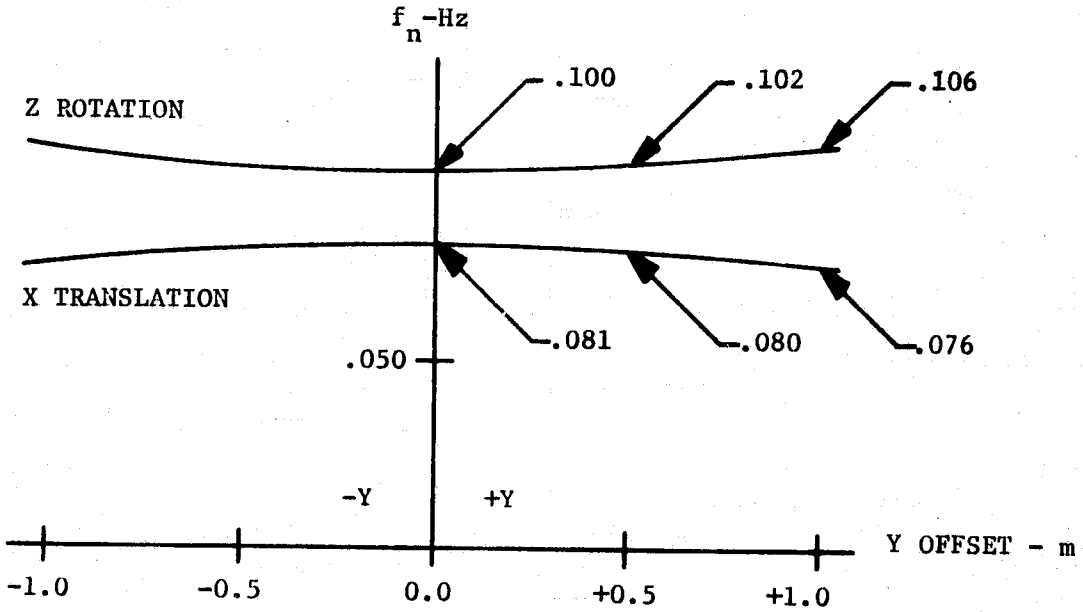

X TRANSLATION - Z ROTATION COUPLING

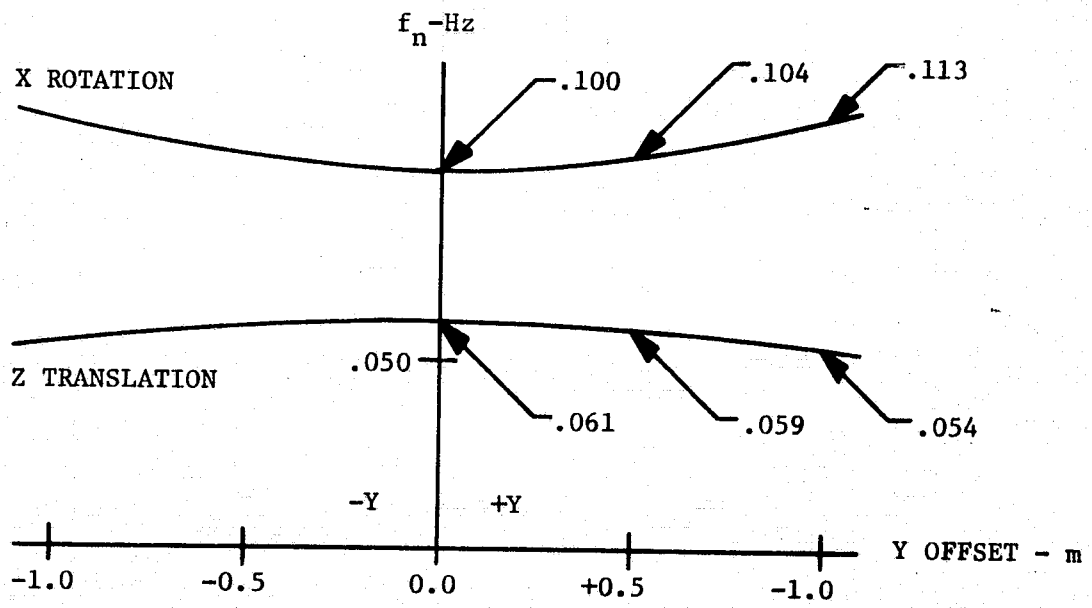

Z TRANSLATION - X ROTATION COUPLING

Figure 3-5. Variation of Suspension Natural Frequencies With Lateral (Y Axis) Center of Mass Offsets

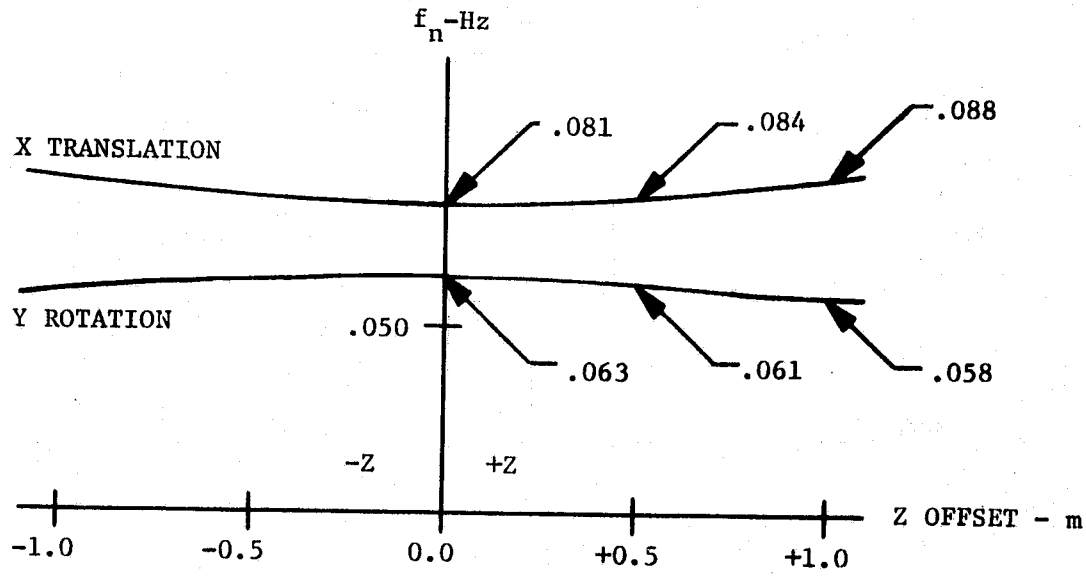

X TRANSLATION - Y ROTATION COUPLING

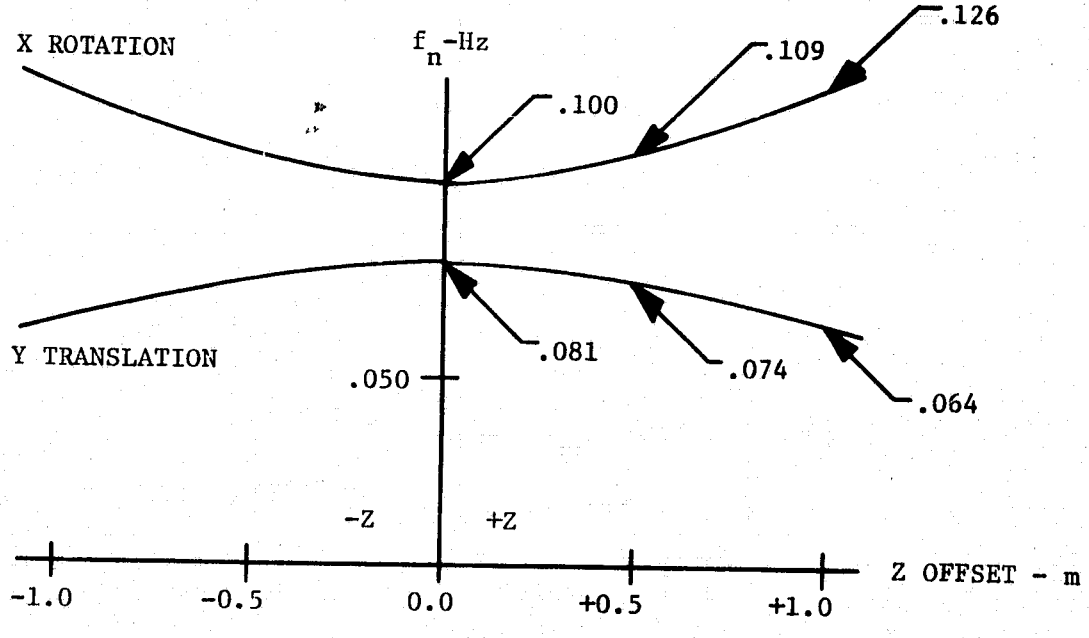

Y TRANSLATION - X ROTATION COUPLING

Figure 3-6. Variation of Suspension Natural Frequencies With Vertical (Z Axis) Center of Mass Offsets

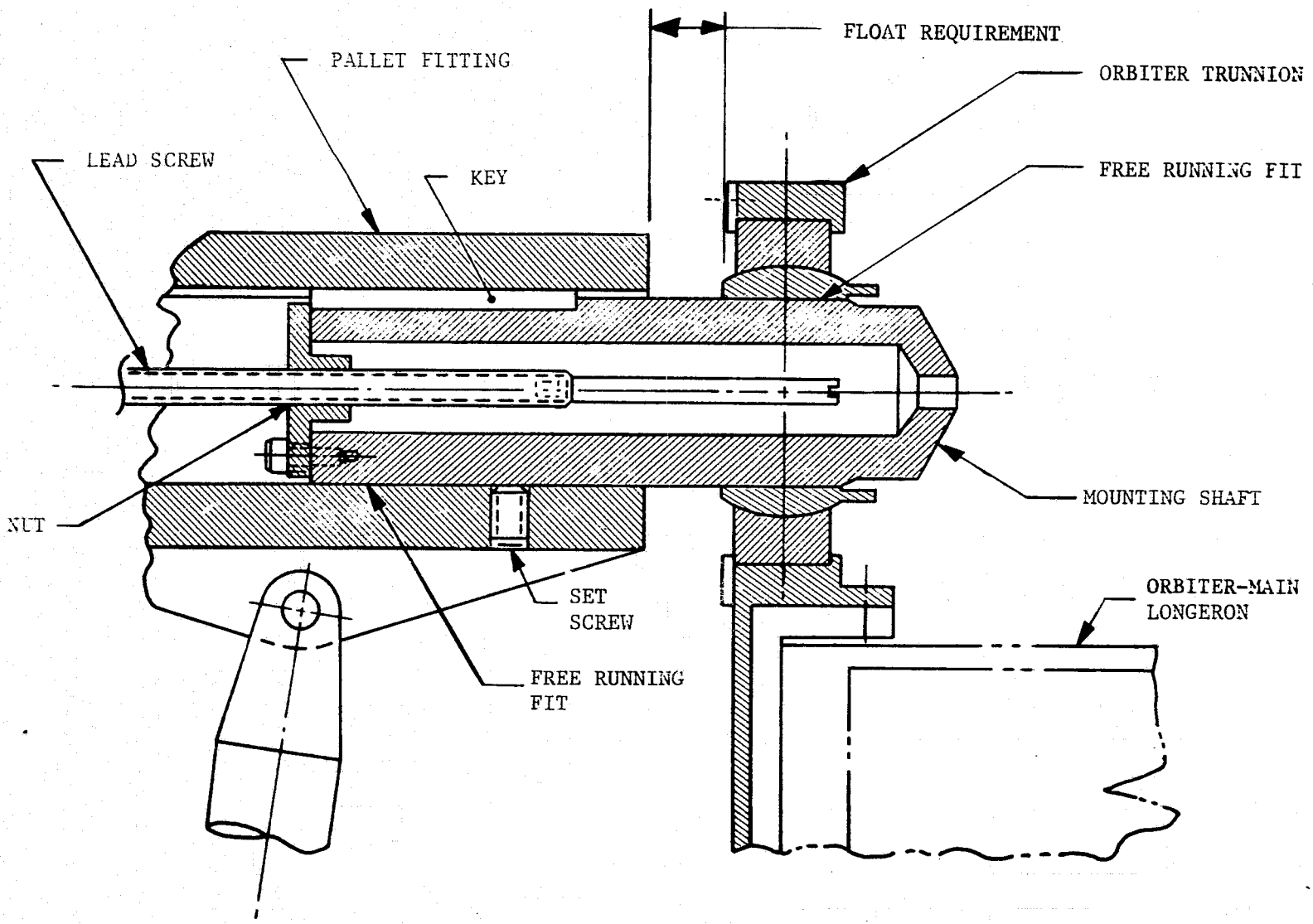

Figure 3-7. Cargo Bay Main Longeron Retention Point Mounting Shaft Extended Position

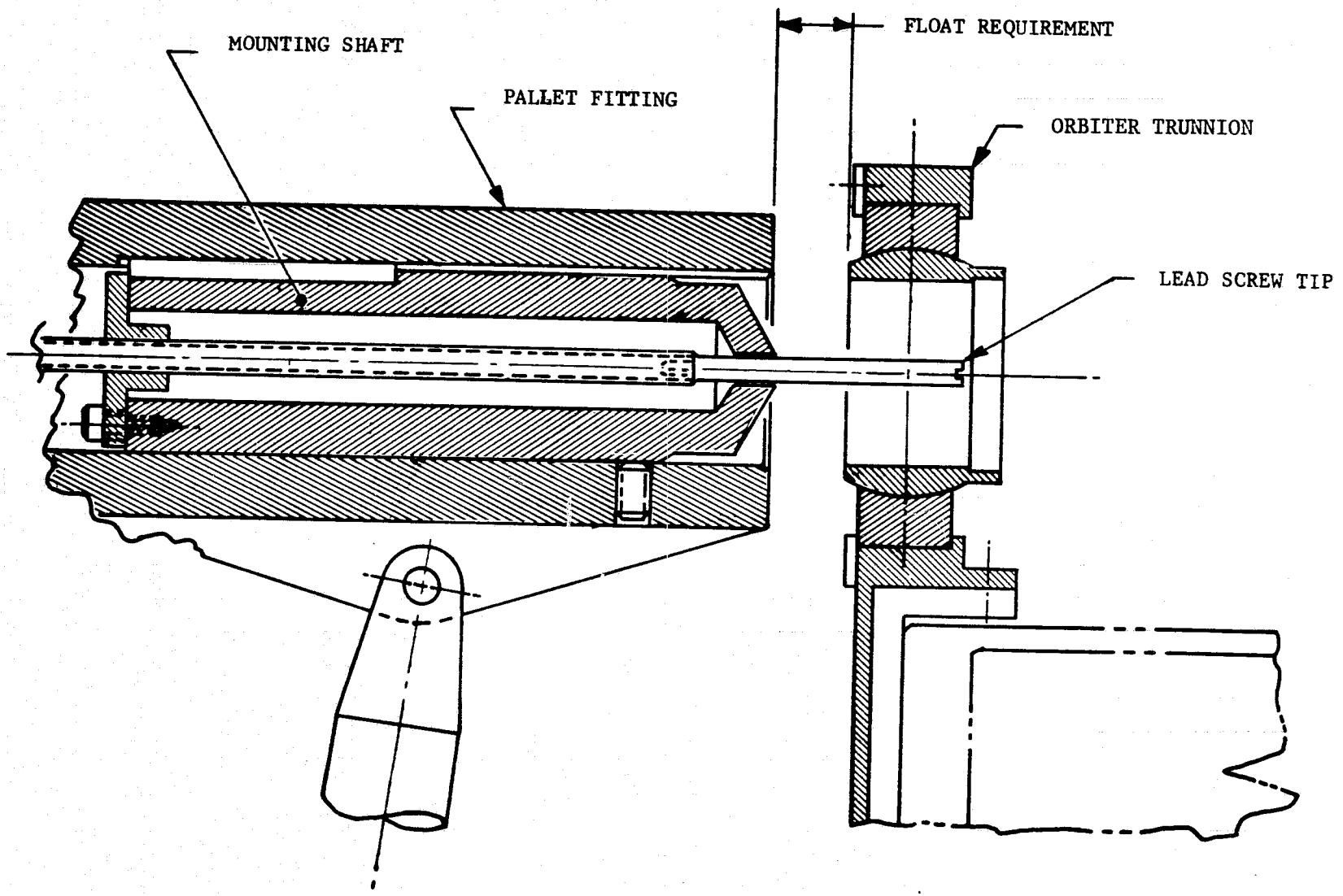

Figure 3-8. Cargo Bay Main Longeron Retention Point - Mounting Shaft Retracted Position

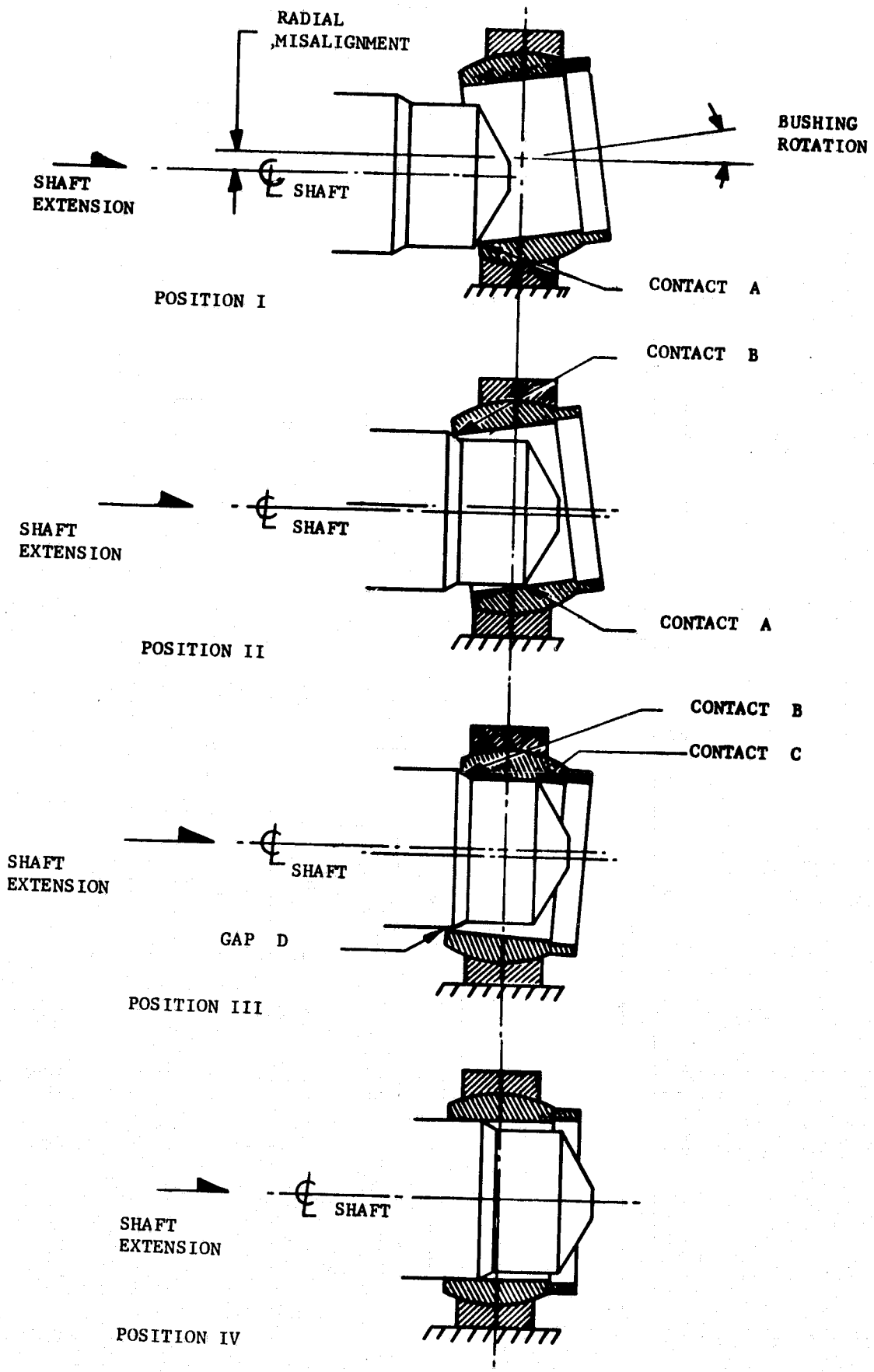

Figure 3-9. Engagement Sequence

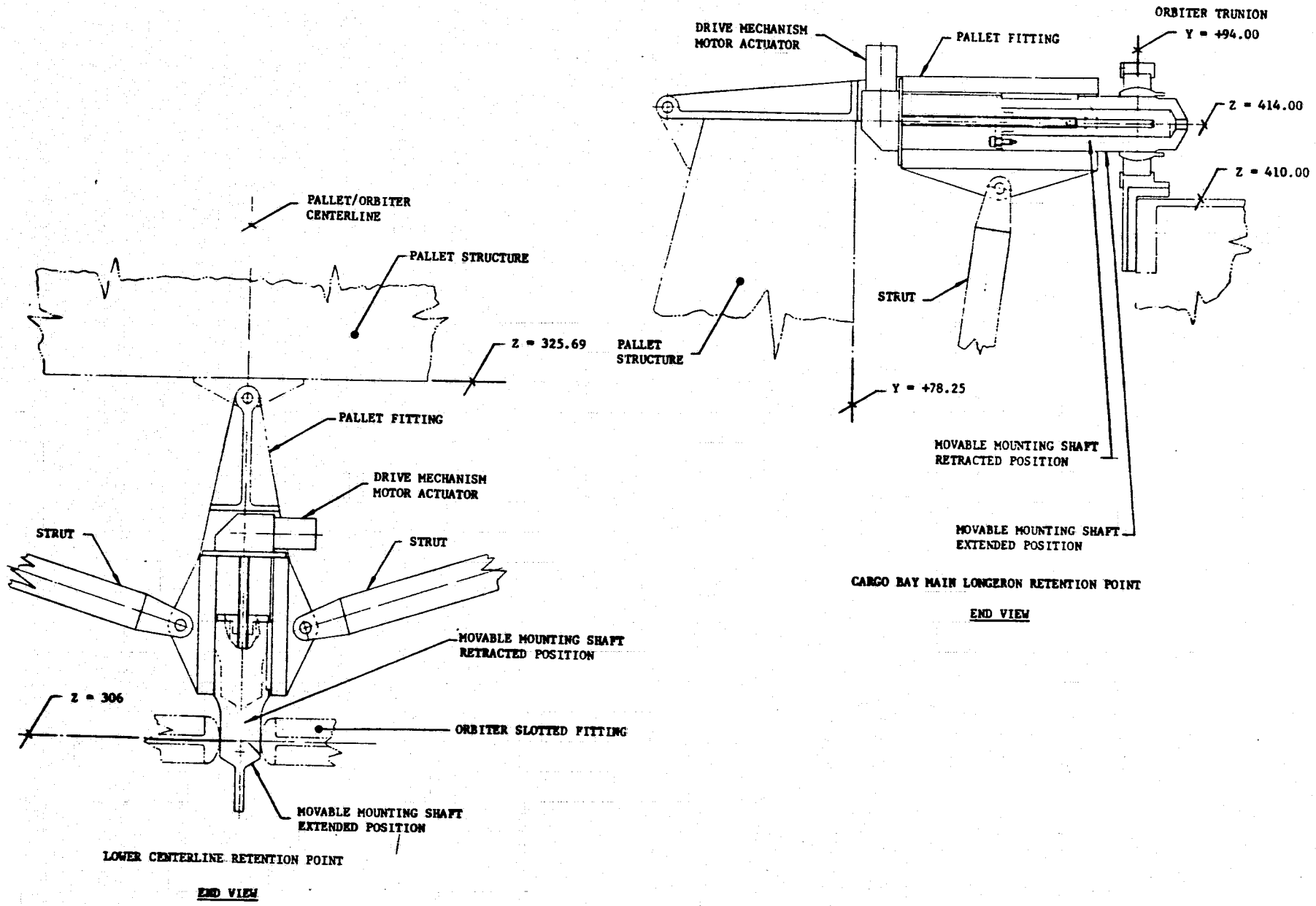

Figure 3-10. Retention System - Movable Mounting Shafts

Table 3-1. Four Point Suspension - Gas Filled Bellows Isolators Natural Frequencies and Damping Ratios

PALLET AXIS	X	Y	Z
Equivalent Linear Spring Constant, N/m	719	719	404
Equivalent Linear Damping Constant, N-sec/m	229	229	129
Translational Natural Frequency, Hz	0.081	0.081	0.061
Translational Damping Ratio	0.081	0.081	0.061
Rotational Natural Frequency, Hz	0.100	0.063	0.100
Rotational Damping Ratio	0.100	0.063	0.100

Table 3-2. Bellows Design Features

	X AND Y AXES	Z AXIS
Outside Diameter	3.81 cm	3.81 cm
Inside Diameter	2.29 cm	2.29 cm
Convolution Thickness	0.0112 cm	0.0094 cm
Convolution Pitch	0.38 cm	0.38 cm
Number of Convolutions	47	47
Effective Bellows Area	7.29 cm^2	7.29 cm^2
Bellows Volume	148 cm^3	148 cm^3
Fixed Volume	182 cm^3	182 cm^3
Orifice Diameter	0.030 cm	0.056 cm
Orifice Length	2.54 cm	2.54 cm
Bellows Pressure Rating	4,800 g/cm^2	3,380 g/cm^2
Initial (Fill) Pressure	1,510 g/cm^2	880 g/cm^2
Maximum Pressure	1,600 g/cm^2	940 g/cm^2
Bellows and Gas Weight	0.55 kg	0.55 kg
Free Length of Bellows	17.91 cm	17.91 cm
Maximum Stroke	7.21 cm	8.61 cm
Spring Constant	719 N/m	404 N/m
Damping Constant	229 N-sec/m	129 N-sec/m

Table 3-3. Suspension System Weight and Volume

	WEIGHT PER SUSPENSION POINT kg	TOTAL WEIGHT kg
Bellows	1.65	6.60
End Fittings	7.20	28.80
Structure	2.24	8.96
TOTAL	11.00	44.00

Volume Per Suspension Point

$V=(0.35\ m)^3=0.043\ m^3$

Table 3-4. Four Point Suspension - Gas Filled Bellows Isolators Spring Constant Sensitivity

	X	Y	Z
Nominal Natural Translational Frequency, Hz	.081	.081	.061
Nominal Natural Rotational Frequency, Hz	.100	.063	.100
Nominal Bellows Spring Constant, N/m	387	387	210
Nominal Gas Spring Constant, N/m	332	332	194
Nominal Assembly Spring Constant, N/m	719	719	404

Case 1 ±10% Variation in Assembly Spring Constant

	+10%			-10%		
	X	Y	Z	X	Y	Z
Spring Constant, N/m	791	791	444	647	647	364
Translational Frequency, Hz	.085	.085	.064	.077	.077	.058
Rotational Frequency, Hz	.105	.066	.105	.095	.060	.095

Case 2 ±10% Variation in Bellows Spring Constant

	+10%			-10%		
	X	Y	Z	X	Y	Z
Bellows Spring Constant, N/m	426	426	231	348	348	189
Assembly Spring Constant, N/m	758	758	425	680	680	383
Translational Frequency, Hz	.083	.083	.063	.079	.079	.059
Rotational Frequency, Hz	.103	.065	.103	.097	.061	.097

Case 3 Loss of Gas Pressure

	X	Y	Z
Spring Constant, N/m	387	387	210
Translational Frequency, Hz	.059	.059	.044
Rotational Frequency, Hz	.073	.046	.072

Case 4 Loss of Gas Pressure in One Corner

	X	Y	Z
System Spring Constant, N/m	2,544	2,544	1,422
Translational Frequency, Hz	.076	.076	.057
Rotational Frequency, Hz	.094	.059	.094

Table 3-5. Four Point Suspension - Gas Filled Bellows Isolators Damping Ratio Sensitivities

PALLET AXIS	X	Y	Z
Nominal Translational Damping Ratio	0.081	0.081	0.061
Maximum Translational Damping Ratio	0.092	0.092	0.069
Minimum Translational Damping Ratio	0.080	0.080	0.061
Nominal Rotational Damping Ratio	0.100	0.063	0.100
Maximum Rotational Damping Ratio	0.112	0.070	0.112
Minimum Rotational Damping Ratio	0.099	0.062	0.099

4. EXPERIMENT MOUNT AND ERECTION

The attachment of a specified Inside-Out Gimbal System and an alternative altazimuth type gimbal system to the pallet structure was defined conceptually. The approach selected was the design of a support frame, similar to that used in the CMG installation. The two configurations shown in figure 4-1 show the design parameters of pallet hard point locations, frame height and the mount/frame interface. Experiment constraints were not considered since the restraint system would tend to be dependent on the particular instrument configuration. The restraint system would consist of forward and aft supports. The aft support would interface with the experiment base plate and the frame. The forward support would interface with the experiment and the pallet hard points.

Frame attachment to the pallet is with threaded fasteners through the frame base fittings into the standard hard point spherical nuts. Alignment of the experiment/mount to the pallet reference system would require an adjustable interface between the mount and the frame; this can be achieved with the use of shims.

4.1 Line of Sight Errors Due to Mounting Misalignments - In general the ideal pointing of any instrument can only be approached due to various misalignments and inaccuracies in the mounting system. For an instrument with moderate power and resolution this would probably cause no difficulty, however, with an increase in magnification, the angular field of view decreases and it becomes important to examine the error in the line of sight due to physical inaccuracies. A limiting line of sight error can be loosely defined as no greater than the minimum instrument field of view to insure that after gimbal action is commanded, that the target object is in the viewing field and can be brought near the optical axis by fine adjustment as required.

The line of sight error can be bounded for both gimbal systems in terms of the physical inaccuracies by the following:

$$\varepsilon < m_o + \sqrt{z_o^2 + n_o^2} + z_i + n_i$$

where:

ε = the line of sight error

m_o = the angular misalignment of the gimbal base with respect to the pallet

Z_o = the total bias error of the outer gimbal zero point

n_o = the outer gimbal-inner gimbal nonorthogonality

Z_i = the total bias error of the inner gimbal zero point

n_i = the inner gimbal-optical axis nonorthogonality

4.2 Gimbal Motions Required for an Arbitrary Line of Sight Adjustment - Definition of the line of sight error caused by physical misalignments in the gimbal system immediately indicates that some fine pointing capability is required to bring the desired target point into alignment with the optical axis. Regardless of the implementation of the fine pointing control, the magnitude of gimbal motion required to move the optical axis by a small amount to center a target is an item of interest.

The gimbal motions required for an arbitrary change in the line of sight can be determined quite generally by considering the locus of all possible unit vectors $\hat{\rho}_o$ making an angle ε with an arbitrary line of sight vector ρ. This locus can be expressed in terms of a parameter γ which is merely the ccw rotation of the $\hat{\rho}_o$ vector away from the $X_p Z_p$ plane as shown in figure 4-2.

Differential gimbal motions required to move the optical axis through small angles δ_{xp} and δ_{yp} from an initial pointing direction were derived for both mounting arrangements. For the IOG the differential motions $\delta\theta$ (outer gimbal) and $\delta\phi$ (inner gimbal) are:

$$\delta\phi = -\delta_{yp}$$

$$\delta\theta = \frac{\delta_{xp}}{\cos\phi}$$

For the classical system the motions $\delta\alpha$ (outer gimbal) and $\delta\beta$ (inner gimbal) are:

$$\delta\beta = \delta_{xp}$$

$$\varepsilon = \sqrt{\delta_{xp}^2 + \delta_{yp}^2}$$

$$\left.\begin{aligned}\delta\alpha &= \tan^{-1}\frac{\delta_{yp}}{\beta+\delta_{xp}} && ,\ \beta+\delta_{xp}>0\\ &= \tan^{-1}\frac{\delta_{yp}}{\beta+\delta_{yp}}+\pi\,\mathrm{sgn}\{\delta_{yp}\},\ && \beta+\delta_{xp}<0\end{aligned}\right\}\ \beta<\epsilon$$

$$= \tan^{-1}\frac{\delta_{yp}}{\beta+\delta_{xp}} \qquad \epsilon\leq\beta<15\epsilon$$

$$= \frac{\delta_{yp}}{\beta+\delta_{xp}} \qquad 15\epsilon\leq\beta<60\epsilon$$

$$= \frac{\delta_{yp}}{\beta} \qquad 60\epsilon\leq\beta<4°$$

$$= \frac{\delta_{yp}}{\sin\beta} \qquad \beta>4°$$

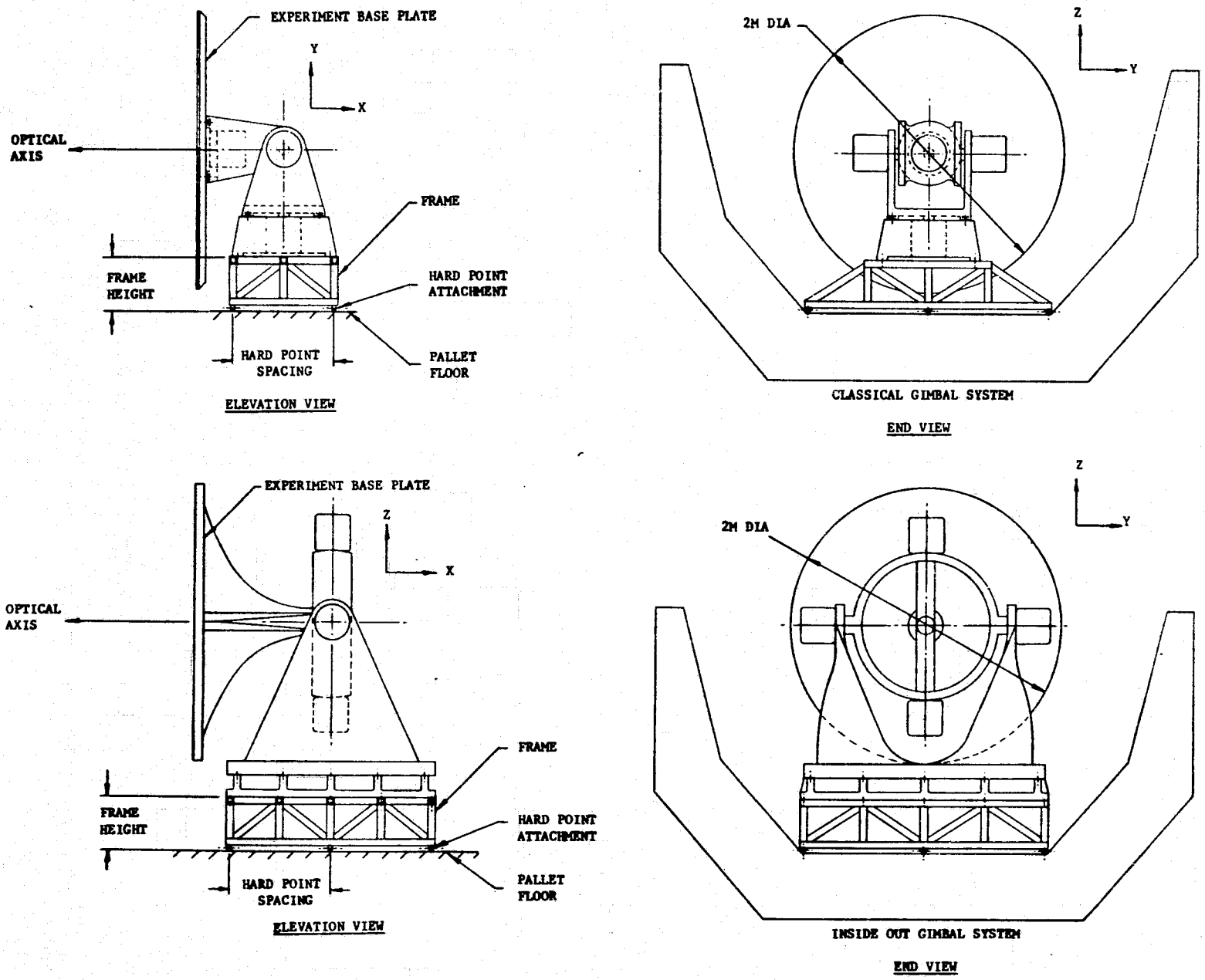

Figure 4-1. Experiment Base Mount Installation

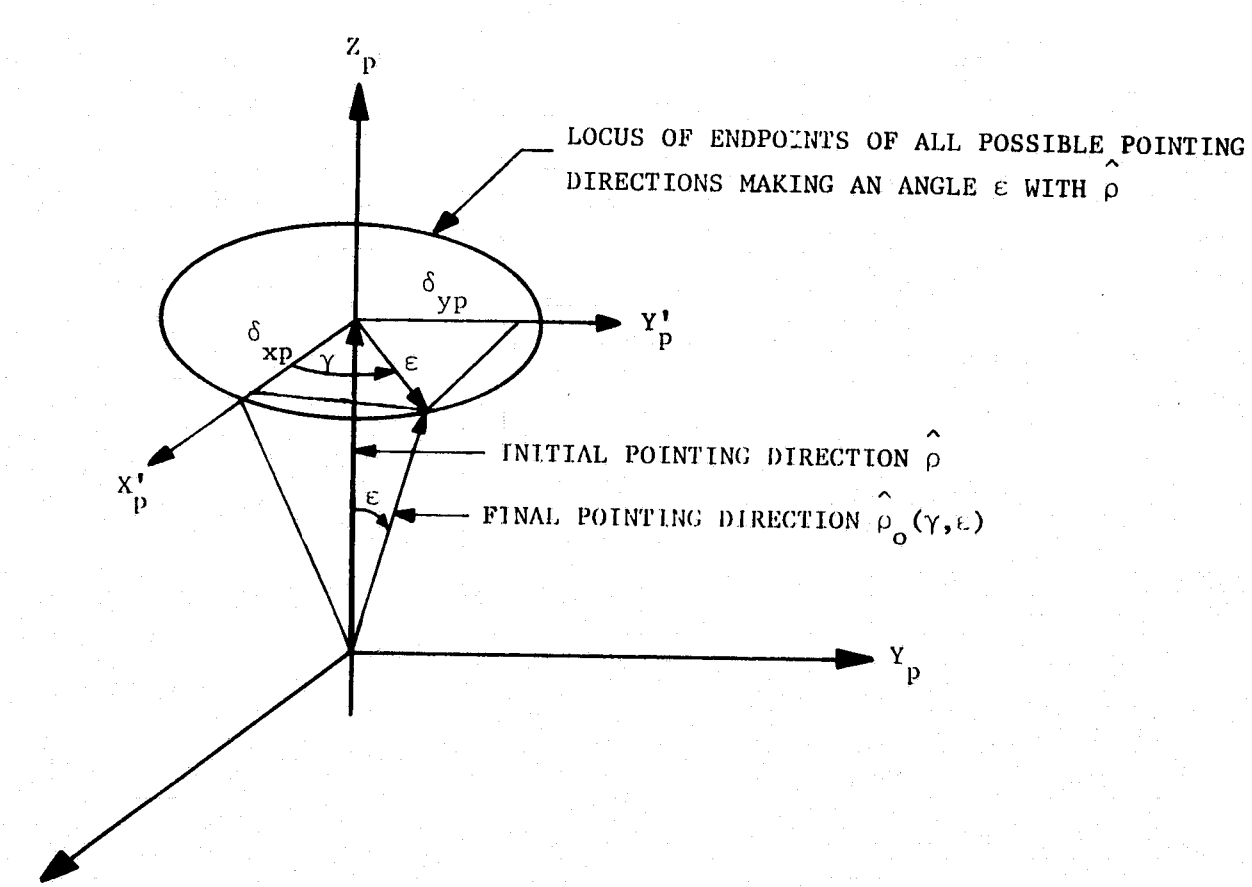

Figure 4-2. Relation of the Initial and Adjusted Lines of Sight

5. PALLET COMMON MODULE CONFIGURATION

The pallet common module was developed from existing pallet segments and modified to incorporate the features required for the Floated Pallet concept. Three of the 3 meter pallet segments were used as the basic pallet configuration. The common module includes:

a. A suspension system capable of supporting the pallet during orbital experimental operation while isolating the pallet from orbiter disturbances.

b. A retention system providing pallet support during launch and descent and also as required during orbital operations. When the retention system is disengaged the pallet is free to float on the suspension system.

c. The CMG actuator cluster providing pallet stabilization during experimental operations.

Figure 5-1 is a layout of the pallet common module showing the suspension and retention systems along with the CMGs mounted in pairs on the outer pallet segments. Figure 5-2 shows the installation of all four CMGs on a single frame mounted on one pallet segment, and in addition includes the payload bay inner profile showing the space available above the CMG cluster available for the installation of experiment hardware.

The suspension system installation is based on the gas filled bellows design discussed in section 3 with a typical suspension point shown in figure 3-3. The system is located in the space between the orbiter side beam and the pallet outer panel to minimize structural modification. The orbiter attachment fitting is machined from aluminum plate with the detailed design depending on the orbiter side beam configuration.

The retention system installation is based on the movable mounting shaft design of section 3 with typical retention points shown in figure 3-10. The orbiter retention fitting required is similar to some existing concepts and detailed design will depend on the orbiter trunnion arrangements.

5.1 Pallet Modifications - The pallet structure must be modified to accept the suspension system. Actual modification depends upon the stiffness of the pallet outer panels. If the pallet outer panels are of honeycomb construction with adequate attachments to the pallet framework, modification requirements are merely bonding

threaded inserts into the panels. If the pallet outer panels are aluminum sheet webs, modification requirements are based on stiffening the web with the attachment channels spanning the distance between pallet frames. As indicated, major modifications are not required and can be accomplished with simple tools at the time of installing the suspension system.

The existing pallet retention fittings can not be modified and must be replaced with new fittings. Since the existing fittings are probably forgings made from high strength materials replacement expense would involve forging tooling and procurement lead time. Therefore a reasonable improvement would be to incorporate the recommended retention system with movable mounting shafts on all pallets.

Since the installation of the CMGs utilizes existing pallet hard points, pallet modifications are not required for actuator mounting.

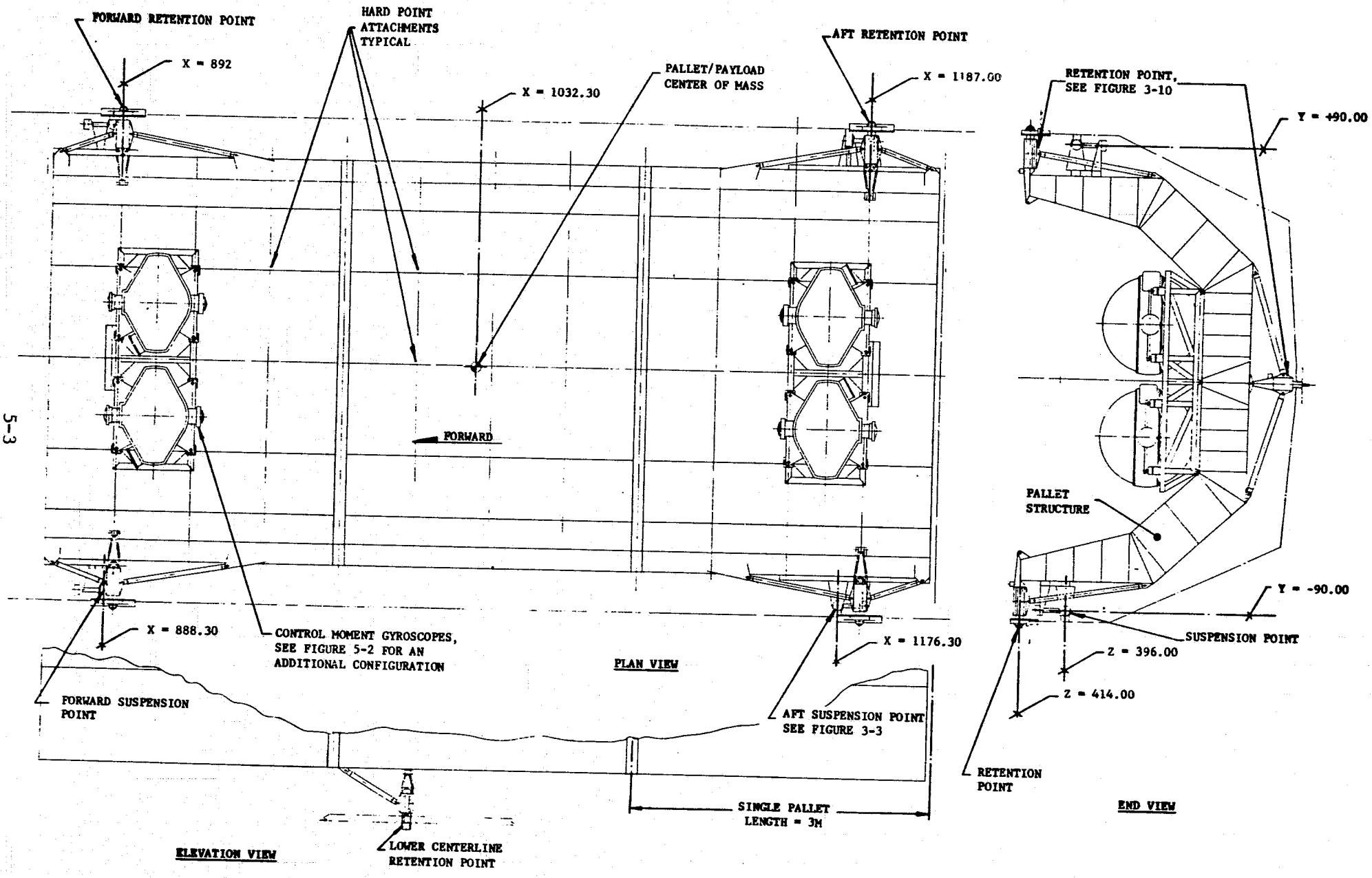

Figure 5-1. Pallet Common Module

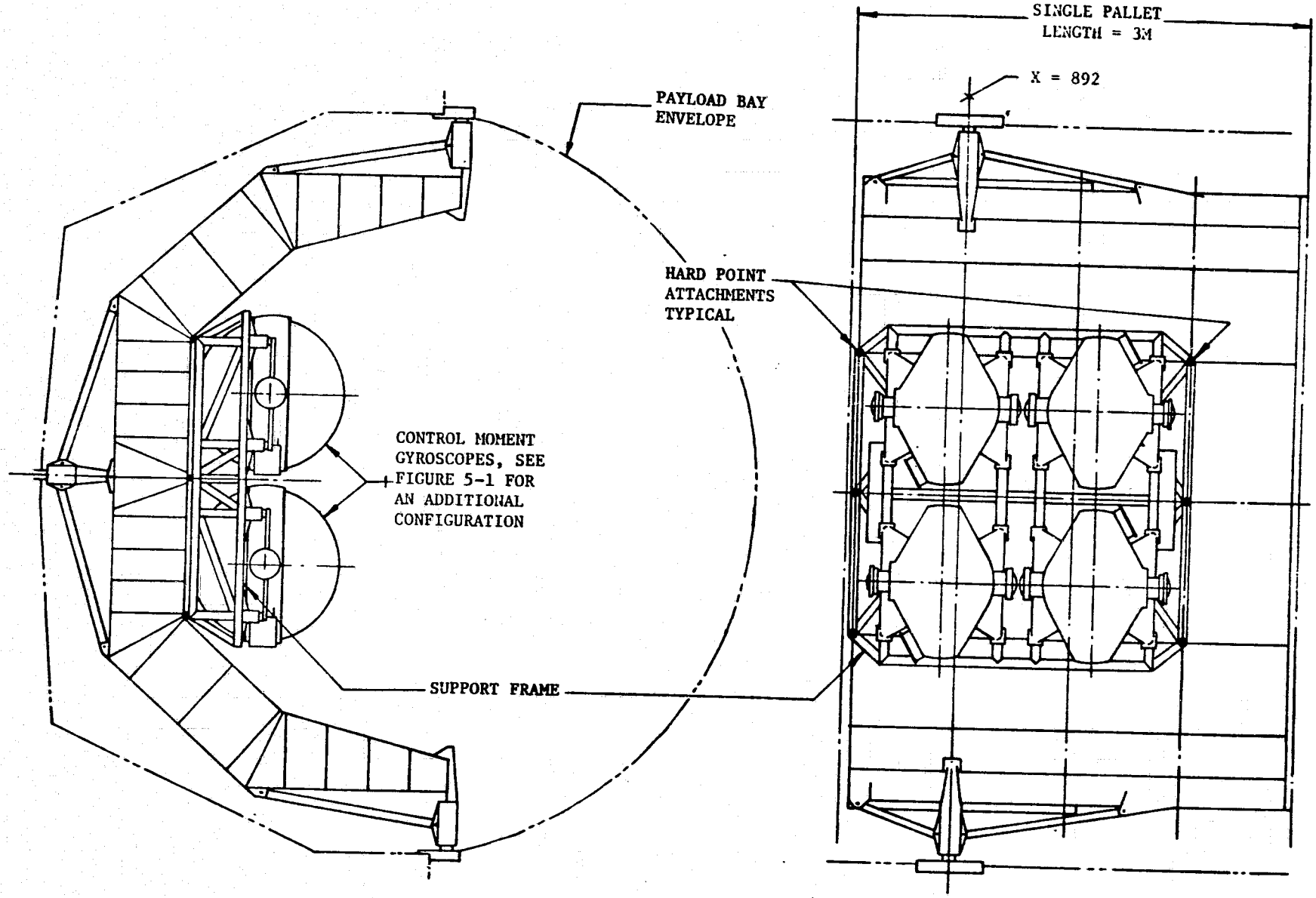

Figure 5-2. Four Control Moment Gyroscopes on a Single Pallet

6. FLOATED PALLET POINTING PERFORMANCE HYBRID SIMULATION MODEL

The simulation model used to evaluate the pointing performance of the Floated Pallet was implemented on a hybrid computer facility consisting of a Scientific Data Systems 86 digital computer interfaced to two Applied Dynamics AD-4 analog consoles and a Beckman EASE analog computer. The hybrid simulation model included the following:

a. Rigid body representation of the dynamics of both the orbiter and pallet, with the suspension system connecting the two rigid bodies. The suspension system was modeled assuming the pallet mass center coincided with the center of elasticity of the suspension system. In the original formulation three axis rotations of both orbiter and pallet along with relative translation of the two bodies were included. During the checkout of the model, it was determined that the translational dynamics and the suspension system torques acting on the orbiter could be neglected since they had negligible effect on the overall system response. The vehicle dynamics as implemented are shown in figure 6-1 with the parameters used shown in table 6-1.

b. Detailed actuator dynamics of the four shockmounted CMGs, initially including all pertinent limiters and dead zones, inner gimbal and gear train compliance dynamics, classical (stiction/running) friction on both motors and gimbals and a detailed representation of the shockmount dynamics of each actuator. The only simplifications made were removal of the various limiters contained in the rate loops. This was done since CMG operation involved low signal levels throughout, thus obviating the need for the limiters. The CMG model is shown in figure 6-2 with the parameters used shown in table 6-2. The frequency response of a single shockmounted actuator as determined from this model is shown in figure 6-3 for inner gimbal commands and figure 6-4 for outer gimbal commands.

c. A rate plus position plus position integral (i.e., rate, integral of rate, and second integral of rate) vehicle control law operating on the pallet rates about each of the three axes. Ideal sensors were assumed with the appropriate pallet rate feeding directly into the control law. The various gains for each axis and each loop bandwidth are shown in table 6-3.

d. A command torque compensator acting on the vehicle control law output composed of a second order over second order transfer function. The quadratic lead was placed at a natural frequency

of 12.5 rad/sec, 0.125 damped to minimize the shockmounted CMG poles occuring near those values. The quadratic log was placed at 70 rad/sec, .707 damped. These compensation values insured loop stability with adequate control loop phase and gain margins for each of the bandwidths considered.

e. An optimized digital CMG control law (pseudo-inverse for mutation) transforming compensated torque commands into gimbal rate commands derived such that the ideal control torque equaled the torque command while minimizing the CMG gimbal rates. The sample period was 7 milliseconds with A/D and D/A quantization approximately .006 percent of the maximum value.

A block diagram of the entire hybrid simulation model is shown in figure 6-5. In order to conserve computer hardware resources, the additional simplification of considering CMG gimbal angles as constant was implemented. This allowed all sine and cosine functions of gimbal angles in the CMG model and CMG control law to be replaced with numerical constants based on the initial gimbal angle state. This did not affect system response as only short time periods were considered during which the gimbal state does not change significantly.

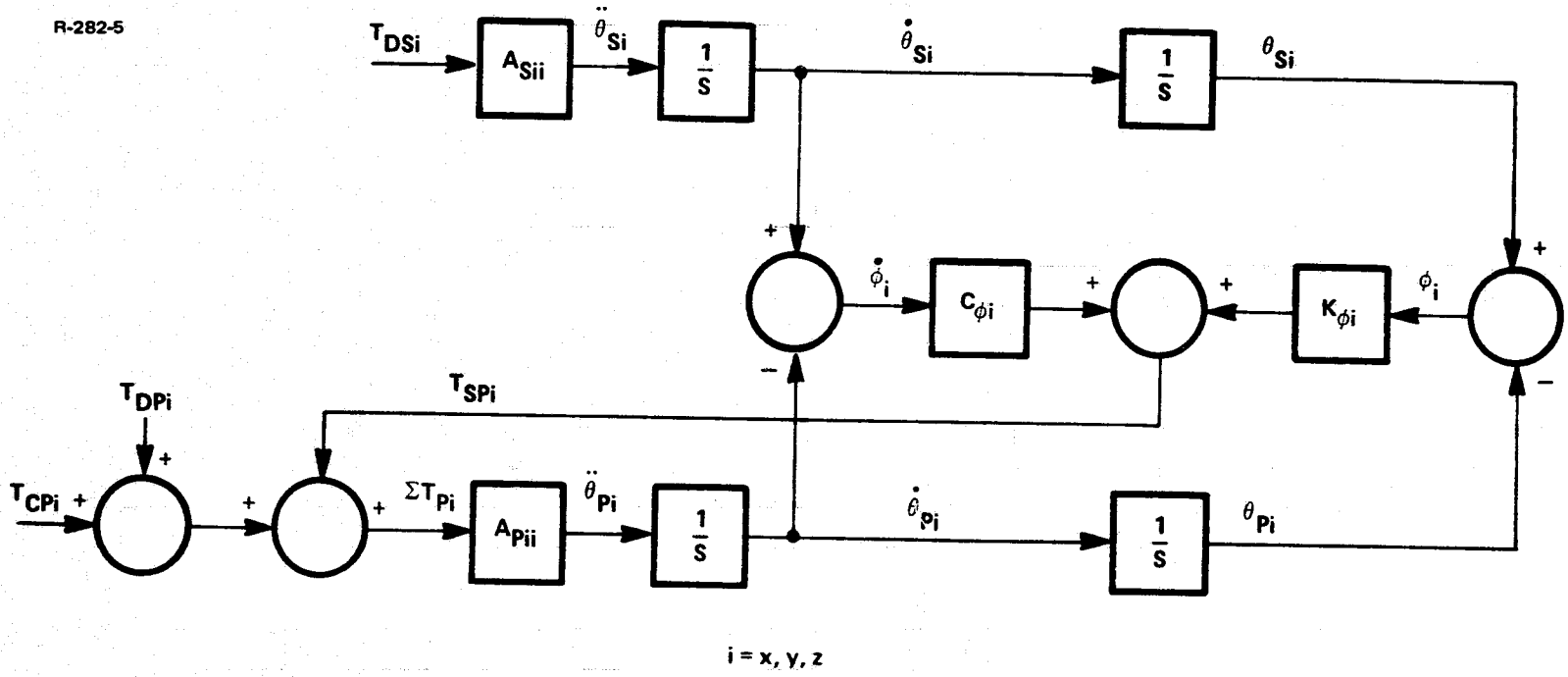

Figure 6-1. Floated Pallet Pointing Performance Study, Vehicle Dynamics

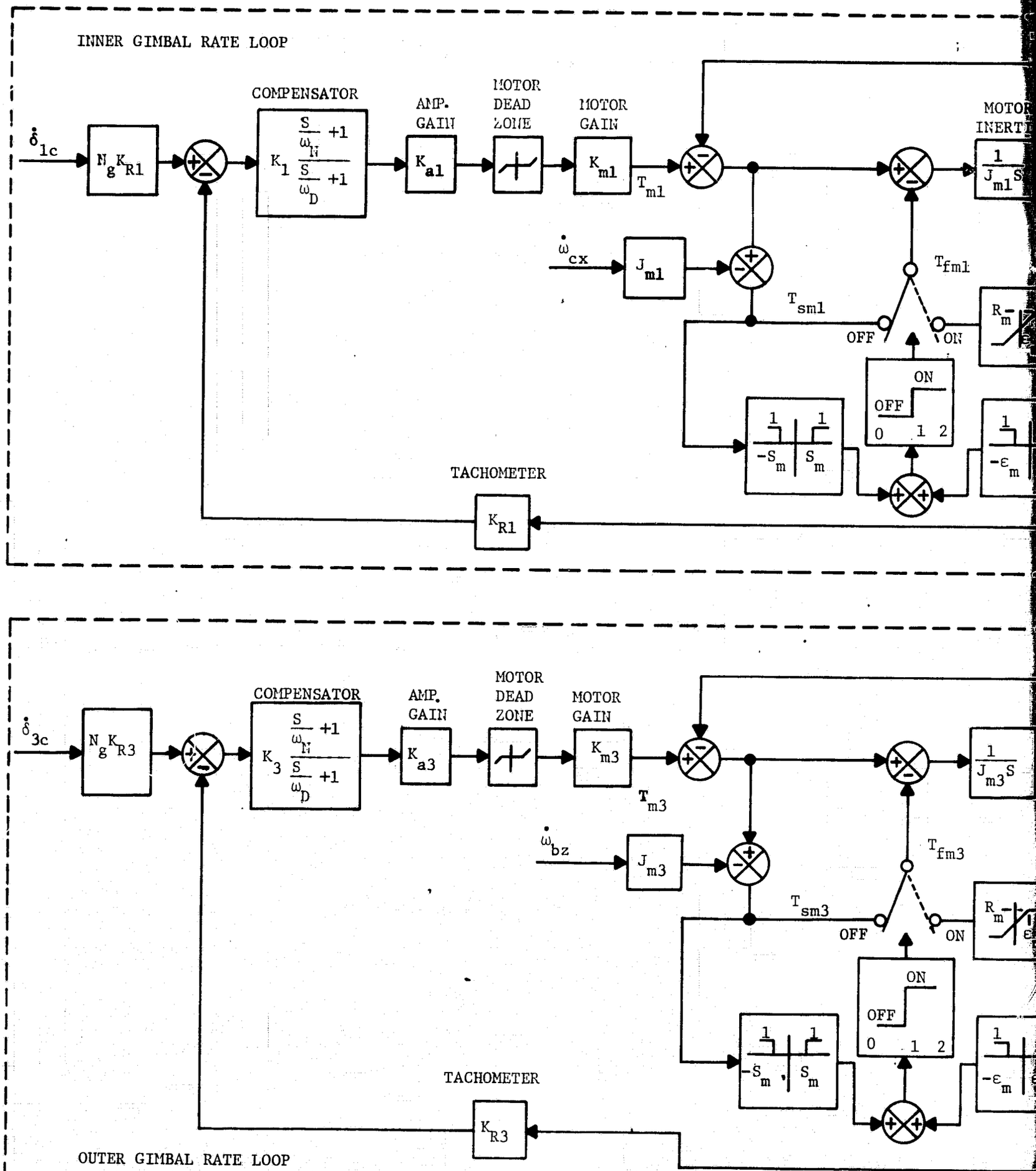
INNER GIMBAL RATE LOOP
COMPENSATOR
AMP. GAIN
MOTOR DEAD ZONE
MOTOR GAIN
MOTOR INERTI
$\dot{\delta}_{1c}$
$N_g K_{R1}$
$K_1 \frac{\frac{S}{\omega_N}+1}{\frac{S}{\omega_D}+1}$
K_{a1}
K_{m1}
T_{m1}
$\frac{1}{J_{m1}S}$
$\dot{\omega}_{cx}$
J_{m1}
T_{sm1}
T_{fm1}
OFF
ON
R_m
$-S_m$
S_m
$-\varepsilon_m$
TACHOMETER
K_{R1}
$\dot{\delta}_{3c}$
$N_g K_{R3}$
$K_3 \frac{\frac{S}{\omega_N}+1}{\frac{S}{\omega_D}+1}$
K_{a3}
K_{m3}
T_{m3}
$\frac{1}{J_{m3}S}$
$\dot{\omega}_{bz}$
J_{m3}
T_{sm3}
T_{fm3}
K_{R3}
OUTER GIMBAL RATE LOOP

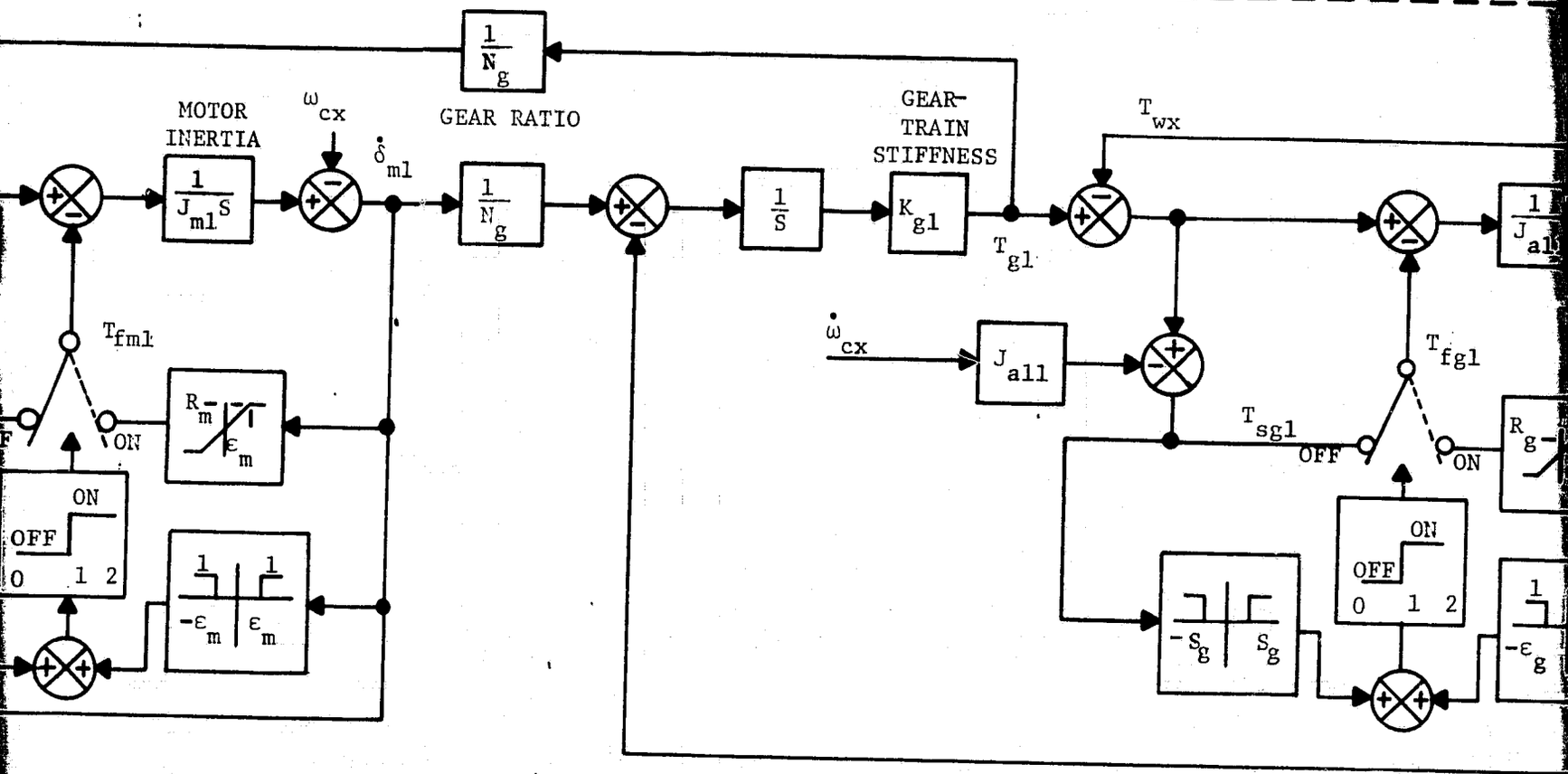

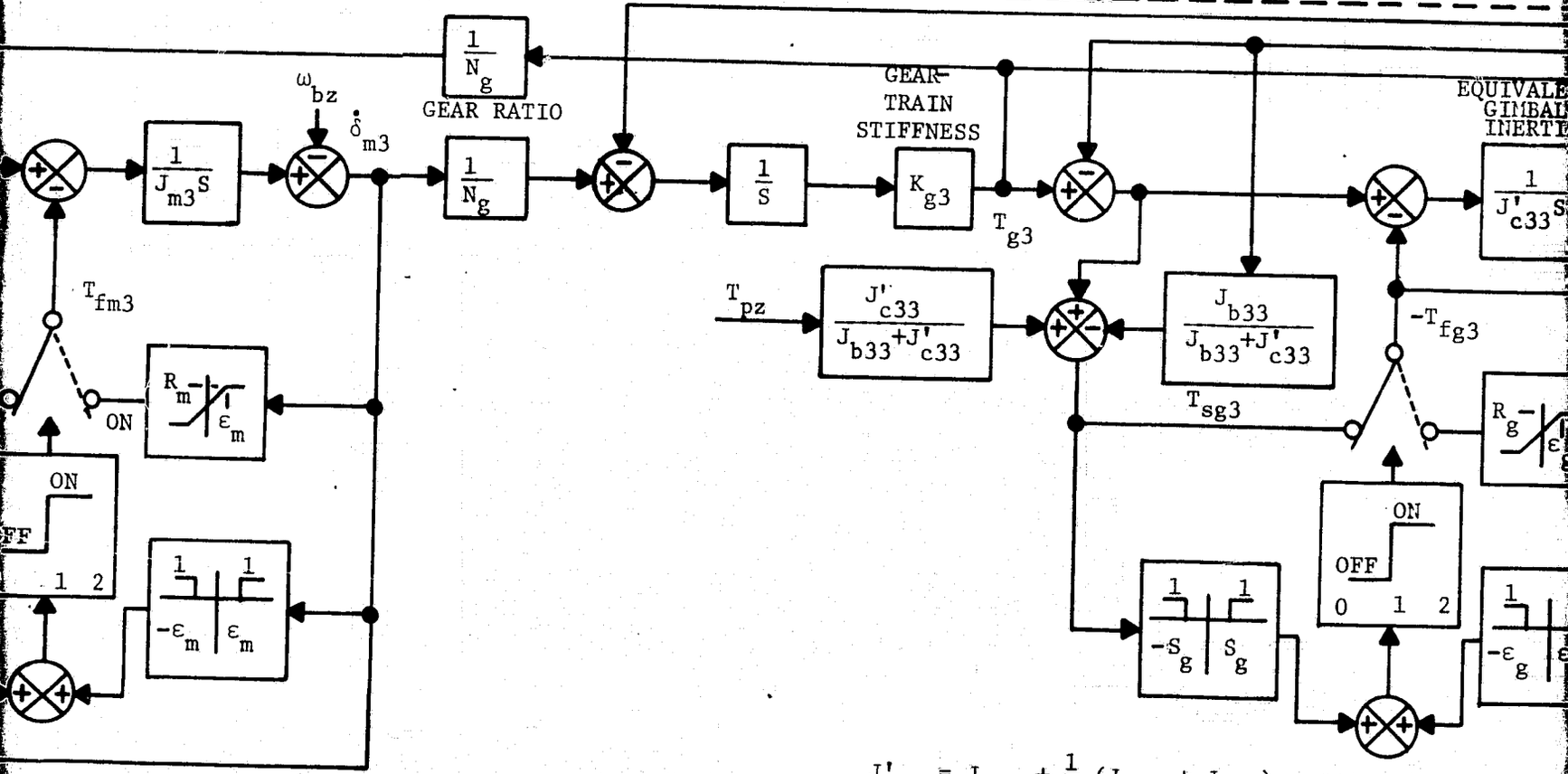

$$J'_{c33} = J_{c33} + \frac{1}{2}\left(J_{a22} + J_{a33}\right)$$

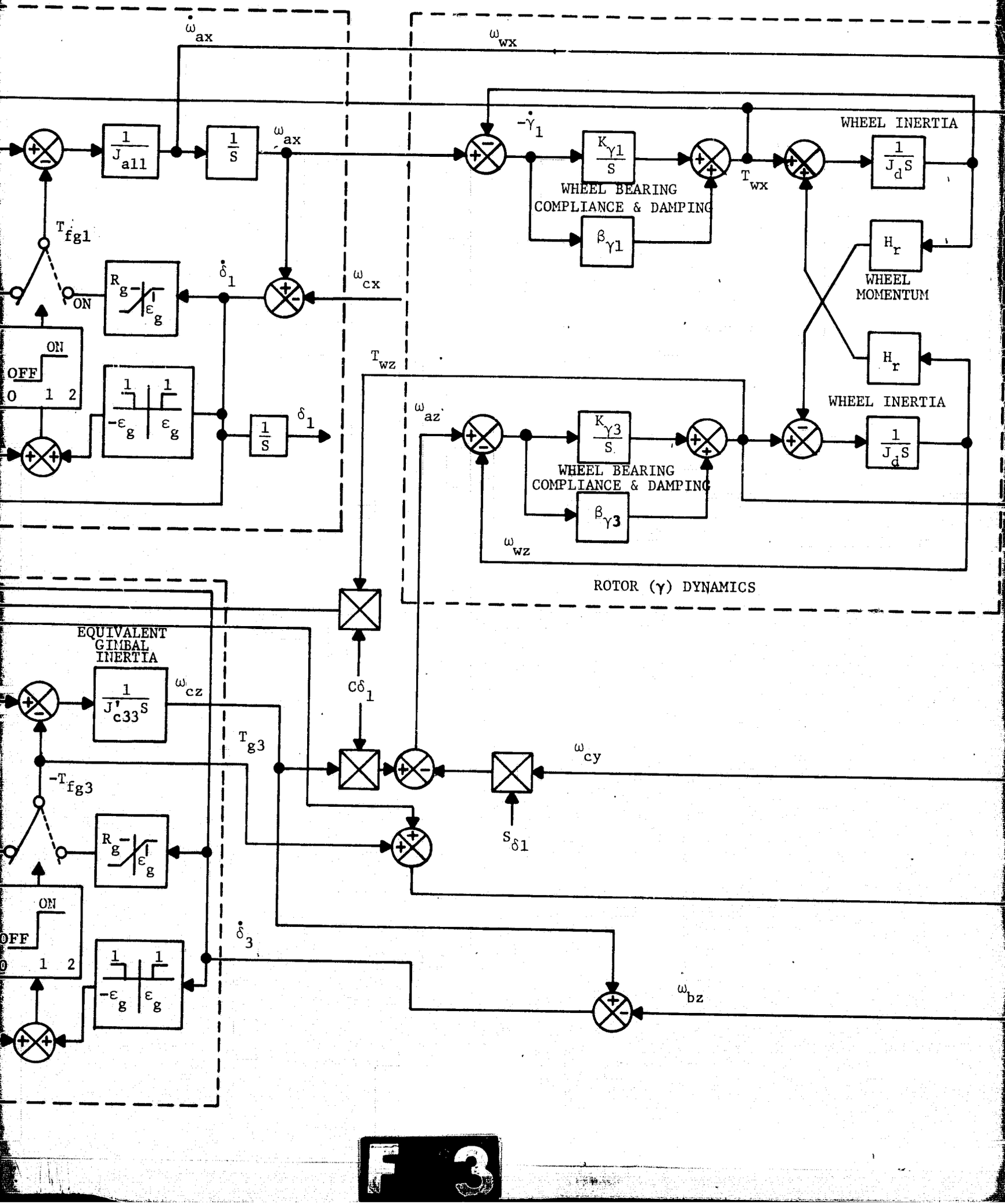
$\dot{\omega}_{ax}$
ω_{wx}
$\frac{1}{J_{all}}$
$\frac{1}{S}$
ω_{ax}
$-\dot{\gamma}_1$
$\frac{K_{\gamma 1}}{S}$
WHEEL INERTIA
$\frac{1}{J_d S}$
WHEEL BEARING
COMPLIANCE & DAMPING
T_{wx}
$\beta_{\gamma 1}$
T_{fg1}
H_r
WHEEL
MOMENTUM
R_g
ε_g
ON
$\dot{\delta}_1$
ω_{cx}
OFF
0 1 2
T_{wz}
ω_{az}
$\frac{K_{\gamma 3}}{S}$
WHEEL INERTIA
$\frac{1}{J_d S}$
WHEEL BEARING
COMPLIANCE & DAMPING
$\beta_{\gamma 3}$
ω_{wz}
ROTOR (γ) DYNAMICS
EQUIVALENT
GIMBAL
INERTIA
$\frac{1}{J'_{c33} S}$
ω_{cz}
$C\delta_1$
T_{g3}
$-T_{fg3}$
ω_{cy}
$S_{\delta 1}$
$\dot{\delta}_3$
ω_{bz}

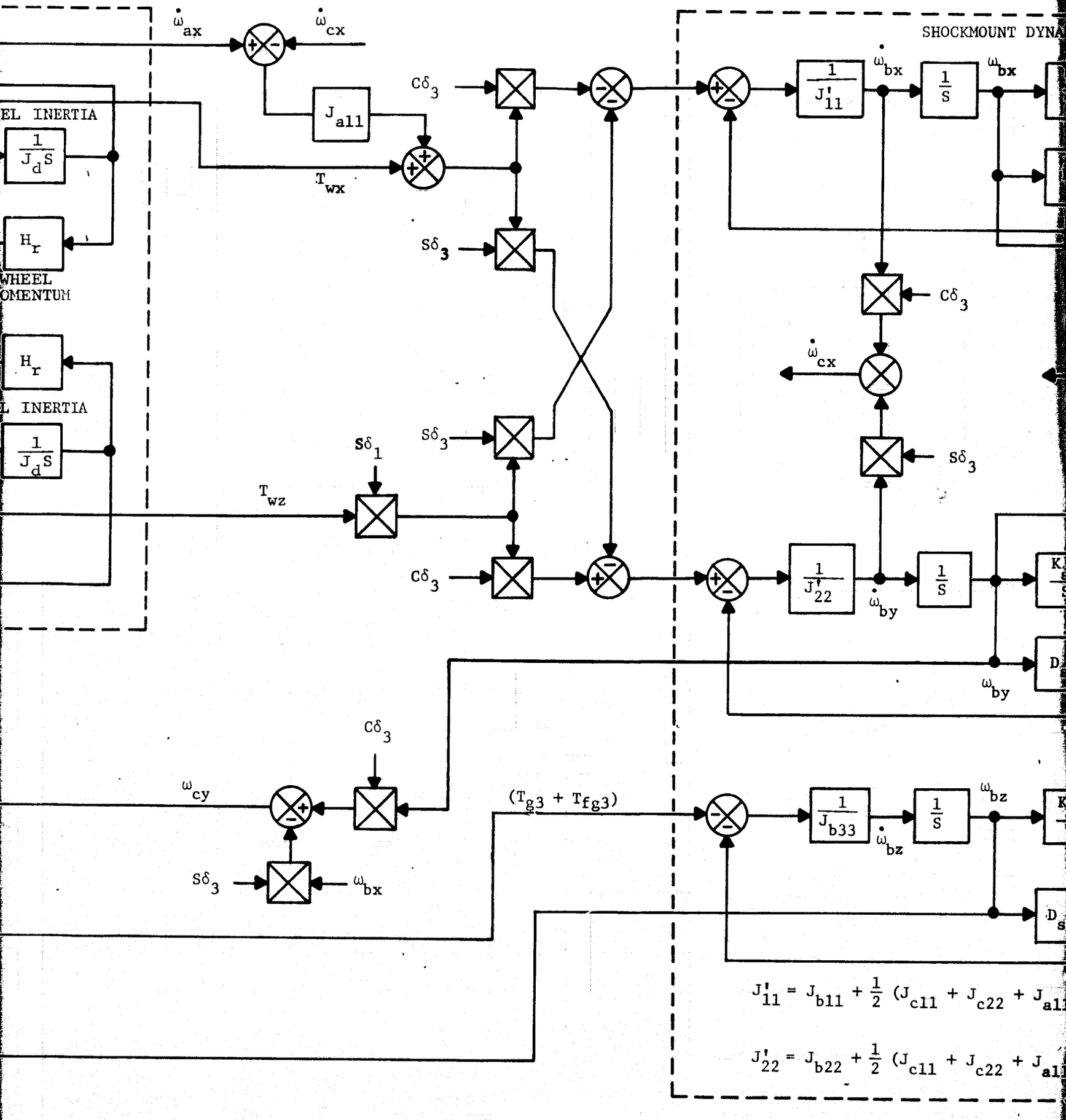

Figure 6-2. Shock Mounted Six Ma

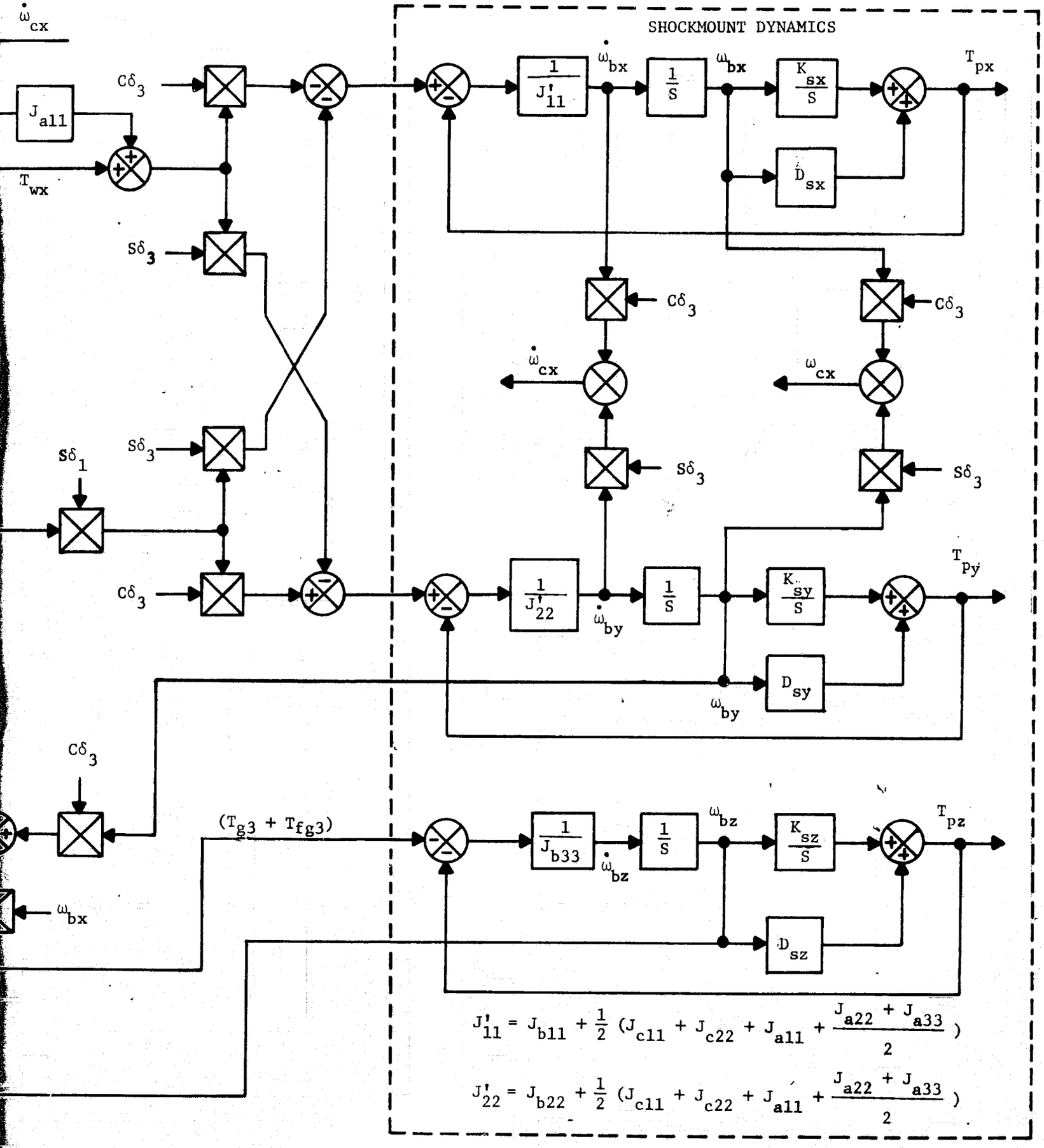

Figure 6-2. Shock Mounted Six Mass CMG Dynamic Model

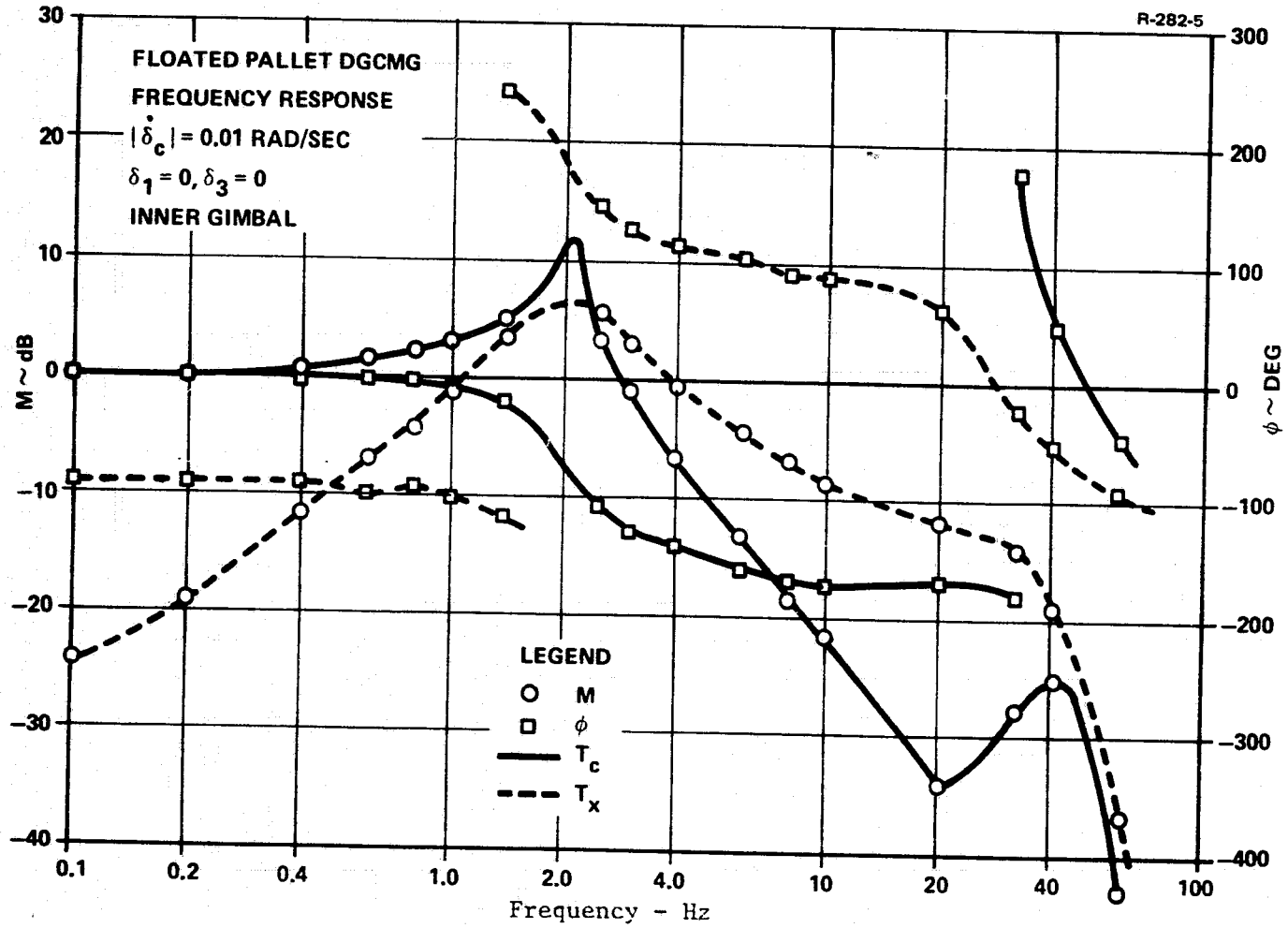

Figure 6-3. Floated Pallet CMG Frequency Response to Inner Gimbal Rate Command

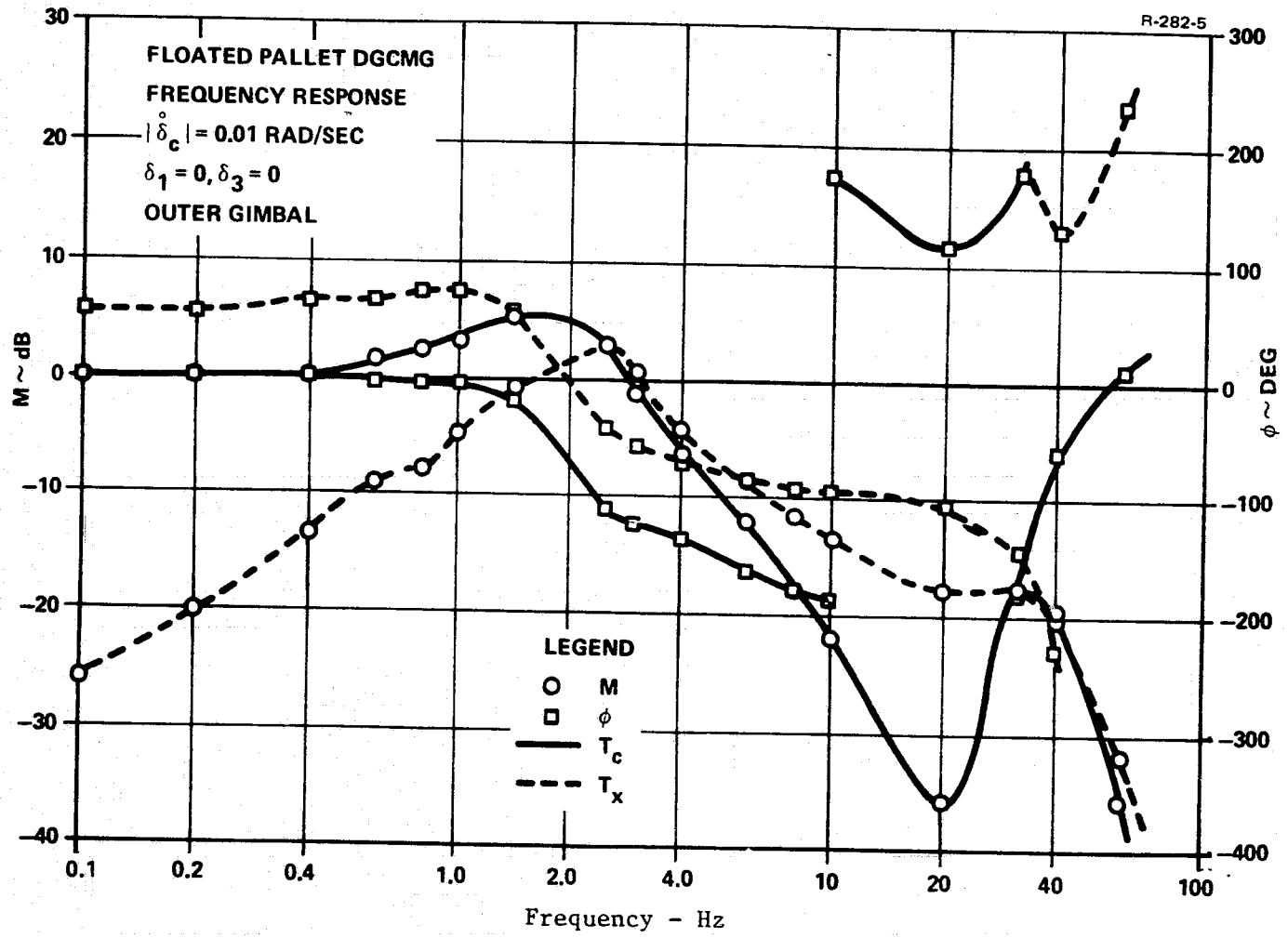

Figure 6-4. Floated Pallet CMG Frequency Response to Outer Gimbal Rate Command

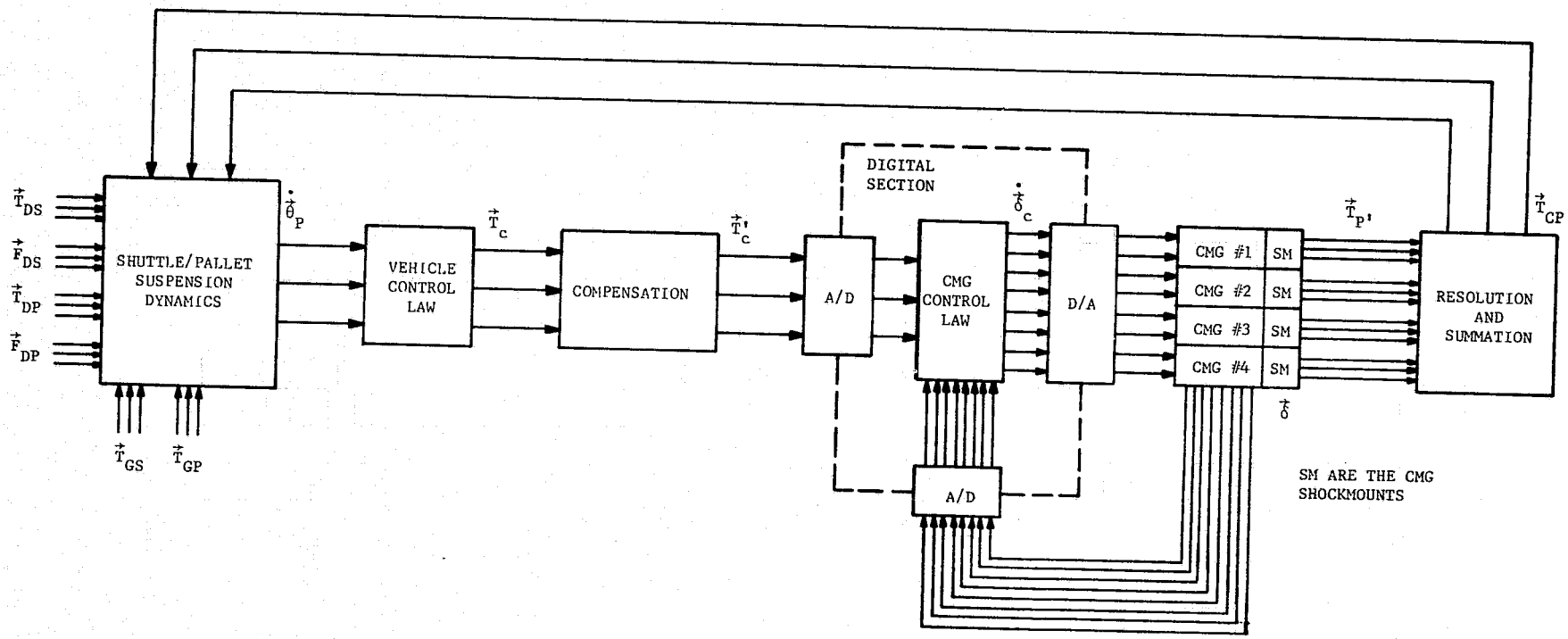

Figure 6-5. Floated Pallet Pointing Performance Study Hybrid Simulation Model

Table 6-1. Floated Pallet Pointing Performance Study Vehicle Parameters

Parameter	Symbol	Nominal Magnitude	Units
Reciprocal of Pallet Inertia	A_{Pxx}	4.696×10^{-5}	$1/kg\text{-}m^2$
Reciprocal of Pallet Inertia	A_{Pyy}	7.204×10^{-6}	$1/kg\text{-}m^2$
Reciprocal of Pallet Inertia	A_{Pzz}	7.384×10^{-6}	$1/kg\text{-}m^2$
Reciprocal of Orbiter Inertia	A_{Sxx}	1.015×10^{-6}	$1/kg\text{-}m^2$
Reciprocal of Orbiter Inertia	A_{Syy}	1.385×10^{-7}	$1/kg\text{-}m^2$
Reciprocal of Orbiter Inertia	A_{Szz}	1.354×10^{-7}	$1/kg\text{-}m^2$
Suspension Spring Const.	$K_{\phi x}$	8,420	N-m
Suspension Spring Const.	$K_{\phi y}$	21,555	N-m
Suspension Spring Const.	$K_{\phi z}$	53,432	N-m
Suspension Damping	$C_{\phi x}$	2,679	N-m-sec
Suspension Damping	$C_{\phi y}$	6,860	N-m-sec
Suspension Damping	$C_{\phi z}$	17,007	N-m-sec

Table 6-2. Floated Pallet Pointing Performance Study CMG Parameters

Parameter	Symbol	Nominal Magnitude	Units
Inner Axis Compensator Gain	K_1	10.54	vdc/vdc
Outer Axis Compensator Gain	K_3	12.80	vdc/vdc
Inner Gimbal Amplifier Gain	K_{a1}	10.0	amp/vdc
Outer Gimbal Amplifier Gain	K_{a3}	10.0	amp/vdc
Inner Gimbal Motor Gain	K_{m1}	1.559	N-m/amp
Outer Gimbal Motor Gain	K_{m3}	1.559	N-m/amp
Inner Gimbal Tachometer Gain	K_{R1}	0.995	vdc/rad/sec
Outer Gimbal Tachometer Gain	K_{R3}	0.995	vdc/rad/sec
Compensator Lead Corner Frequency	ω_N	20.0	rad/sec
Compensator Lag Corner Frequency	ω_D	0.2	rad/sec
Motor Deadzone	-	0.003	ampere
Gimbal Motor Static Friction	S_m	0.1	N-m
Gimbal Motor Running Friction	R_m	0.08	N-m
Zero Gimbal Rate Band	ϵ_g	0.00005	rad/sec
Zero Motor Rate Band	ϵ_m	0.002828	rad/sec
Gear Ratio	N_g	56.55	
Inner Gimbal Motor Inertia	J_{m1}	0.0068	$kg-m^2$
Outer Gimbal Motor Inertia	J_{m3}	0.0068	$kg-m^2$
Inner Gimbal Gear Train Stiffness	K_{g1}	203,370	N-m/rad
Outer Gimbal Gear Train Stiffness	K_{g3}	203,370	N-m/rad
Moment of Inertia of Wheel About Axis Perpendicular to Spin Axis	J_d	1.803	$kg-m^2$
Gimbal Static Friction	S_g	0.5	N-m
Gimbal Running Friction	R_g	0.4	N-m
Bearing Compliance	$K_{\gamma 1}$	542,320	N-m/rad
Bearing Compliance	$K_{\gamma 3}$	542,320	N-m/rad
Compliance Damping	$\beta_{\gamma 1}$	20	N-m-sec/rad
Compliance Damping	$\beta_{\gamma 3}$	20	N-m-sec/rad
Angular Momentum of Wheel	H_r	3115.0	N-m-sec
Inner Gimbal Inertia	J_{a11}	0.746	$kg-m^2$
Inner Gimbal Inertia	J_{a22}	0.868	$kg-m^2$
Inner Gimbal Inertia	J_{a33}	1.003	$kg-m^2$

Table 6-2. Floated Pallet Pointing Performance Study CMG Parameters (Concluded)

Parameter	Symbol	Nominal Magnitude	Units
Outer Gimbal Inertia	J_{c11}	0.76	$kg\text{-}m^2$
Outer Gimbal Inertia	J_{c22}	4.3	$kg\text{-}m^2$
Outer Gimbal Inertia	J_{c33}	3.9	$kg\text{-}m^2$
Equivalent Outer Gimbal Inertia	J'_{c33}	4.834	$kg\text{-}m^2$
CMG Base Inertia	J_{b11}	5.35	$kg\text{-}m^2$
CMG Base Inertia	J_{b22}	7.9	$kg\text{-}m^2$
CMG Base Inertia	J_{b33}	3.63	$kg\text{-}m^2$
Shockmount Spring Const.	K_{Sx}	170,000	N-m/rad
Shockmount Spring Const.	K_{Sy}	208,000	N-m/rad
Shockmount Spring Const.	K_{Sz}	58,000	N-m/rad
Shockmount Damping	D_{Sx}	402	N-m-sec/rad
Shockmount Damping	D_{Sy}	490	N-m-sec/rad
Shockmount Damping	D_{Sz}	137	N-m-sec/rad

Table 6-3. Floated Pallet Pointing Performance Study
Vehicle Control Law Gains

GAIN \ BANDWIDTH		(Hz) 0.5	1.0	2.0	4.0
N-m-sec/rad	K_{Rx}	4.60×10^4	9.18×10^4	1.84×10^5	3.67×10^5
	K_{Ry}	3.00×10^5	5.98×10^5	1.20×10^6	2.40×10^6
	K_{Rz}	3.00×10^5	5.84×10^5	1.17×10^6	2.34×10^6
N-m/rad	K_{Px}	5.00×10^5	1.98×10^5	7.94×10^5	3.17×10^6
	K_{Py}	3.20×10^5	1.29×10^6	5.18×10^6	2.00×10^7
	K_{Pz}	3.20×10^5	1.26×10^6	5.05×10^6	2.00×10^7
N-m/rad-sec	K_{PIx}	5.75×10^3	4.59×10^4	3.68×10^5	7.40×10^5
	K_{PIy}	3.75×10^4	2.99×10^5	2.40×10^6	4.80×10^6
	K_{PIz}	3.65×10^4	2.92×10^5	2.34×10^6	4.60×10^6

7. FLOATED PALLET POINTING PERFORMANCE

Pallet control loop bandwidths of 0.5, 1.0, 2.0 and 4.0 Hz were considered in this study. Three types of hybrid simulation runs were made for the various system bandwidths:

1. No torque disturbance acting on the pallet or orbiter.

2. Step torque disturbance acting on the pallet.

   a) Each axis individually at the minimum value necessary to eliminate the undisturbed limit cycle on that axis.

   b) All axes simultaneously at the values determined in part a.

3. Crew motion torque disturbance acting on the orbiter as given by $\vec{T}_{DS}=\vec{R}x\vec{F}_{DS}$ where $\vec{R}=(-15,0,0)^T$ meter, and

   Case I $\quad \vec{F}_{DS}=(0,F_D,0)^T$ N

   Case II $\quad \vec{F}_{DS}=(0,0,F_D)^T$ N

   Case III $\quad \vec{F}_{DS}=(0,\frac{F_D}{\sqrt{2}},\frac{F_D}{\sqrt{2}})^T$ N

   where the crew motion disturbance F_D is as shown in figure 7-1.

The above runs were made for all bandwidths with all CMG gimbal angles at 0 degrees for the 0.5 and 1.0 Hz systems with all CMG gimbal angles at 45 degrees, and for the 2.0 and 4.0 Hz systems with CMG inner gimbal angles at 0 degrees and outer gimbal angles at 45 degrees. In addition, type 1 runs were made for the 1.0, 2.0, and 4.0 Hz systems with all CMG gimbal angles at 0 degrees with CMG friction levels of one-half and twice the nominal friction levels.

Time histories of various system variables were plotted on strip chart recorders. The variables chosen for display were the following:

$\dot{\delta}_{1j}, j = 1,2,3,4$ CMG inner gimbal rates

$\dot{\delta}_{3j}, j = 1,2,3,4$ CMG outer gimbal rates

$\dot{\theta}_{Si}, i = x,y,z$	orbiter angular rates
$\theta_{Si}, i = x,y,z$	orbiter attitude
$T_{DPi}, i = x,y,z$	torque disturbance on pallet
$T_{Ci}, i = x,y,z$	torque command from vehicle control law
$T'_{Ci}, i = x,y,z$	torque command from compensator
$T_{CPi}, i = x,y,z$	net CMG torque applied to pallet
$\dot{\theta}_{Pi}, i = x,y,z$	pallet angular rates
$\theta_{Pi}, i = x,y,z$	pallet attitude

Reproductions of typical computer runs are shown in figures 7-2 through 7-4. Figure 7-2 shows vehicle response in the absence of disturbance torques with the limit cycles about the pallet axes (i.e., the traces for $\theta_{Pi}, i = x,y,z$) being the most evident feature. Application of a small steady torque rapidly damps out the limit cycle as shown in figure 7-3. A typical crew motion disturbance run is shown in figure 7-4. The results of the computer study are summarized in table 7-1.

7.1 Effect of CMG Friction on Pointing - The dominant nonlinearity in the CMG is friction. With no vehicle disturbances, the friction causes limit cycles as shown in the computer traces (e.g., figure 7-2). In general, the limit cycle amplitude decreases with increasing loop bandwidth as shown in figure 7-5.

Studies were also made to determine the effect of friction level on limit cycle amplitude. For a 2 Hz system with gimbal angles set equal to zero, the pallet attitude error due to nominal CMG friction was approximately 0.1 arc-second about the pallet Y and Z axes, and approximately 1.1 arc-second about the pallet X axis. As the CMG friction level increases or decreases, the limit cycle amplitude varies proportionately. The effect of friction level for various system bandwidths is summarized in figure 7-6.

When small vehicle disturbance torques (T_{DPi}) are applied, approximately 1 N-m, steady CMG gimbal rates occur and the system stops limit cycling (e.g., figure 7-3). Disturbance torques (T_{DPi}) required to stop limit cycling at various system bandwidths are summarized in figure 7-7.

7.2 Crew Motion Disturbances - Crew motion is the largest disturbance expected affecting pallet pointing performance. For the 2 Hz system with CMG gimbal angles at zero, the worst case crew motion disturbance error was 0.25 arc-second about the pallet Z axis. In general, pointing error introduced as a result of crew motion disturbance decreases as system bandwidth increases. These results are summarized in figure 7-8.

7.3 Summary - Results of the pointing performance study show that the system will have a limit cycle attitude error due to the CMG friction when no external torques act on the vehicle. It also shows that the limit cycle amplitude to be a function of friction level and system bandwidth. This limit cycling can be stopped by applying torques to the vehicle and reduced in amplitude by increasing system bandwidth. In addition, crew motion disturbance causes attitude error which is reduced by increasing system bandwidth.

With reference to the statements above, it would seem that the higher the system bandwidth the better the system performance; however, the higher the system bandwidth, the less stable the system becomes. In fact, the 2 Hz system was unstable at 45 degree inner and outer gimbal angles and the 4 Hz system was unstable at both 45 degree inner and outer gimbal angles and zero inner gimbal angles and 45 degree outer gimbal angles. This instability was not predicted by an idealized CMG system analysis and thus must be attributed to CMG dynamics. However, it is anticipated that a redesign of the CMG rate loops, taking into account the effects of the CMG shockmount, will eliminate these instabilities.

In summary, the 2 Hz system could easily meet the 1 arc-second pointing requirement considering the fact that an orbital vehicle almost always has disturbance torques acting upon it. Redesign of the CMG rate loop is recommended to take into account the effects of the CMG shockmounts and eliminate system instabilities presently observed for the ATM CMG rate loop design. In addition, a redesign of the rate loops, to better compensate for the effects of friction at zero gimbal rate commands, will allow lower vehicle loop bandwidths (i.e., approximately 1 Hz) while still meeting the 1 arc-second pointing stability performance desired for all system states.

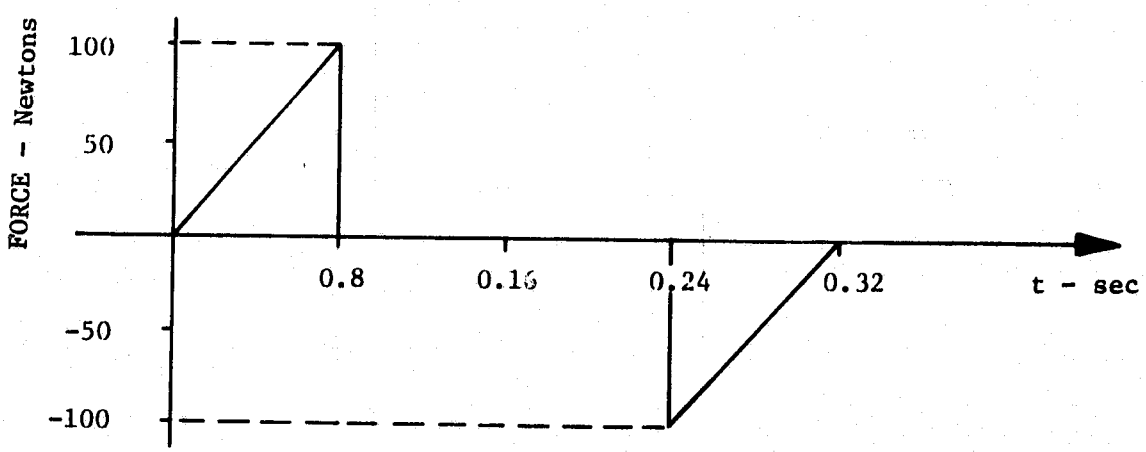

Figure 7-1. Crew Motion Disturbance Profile

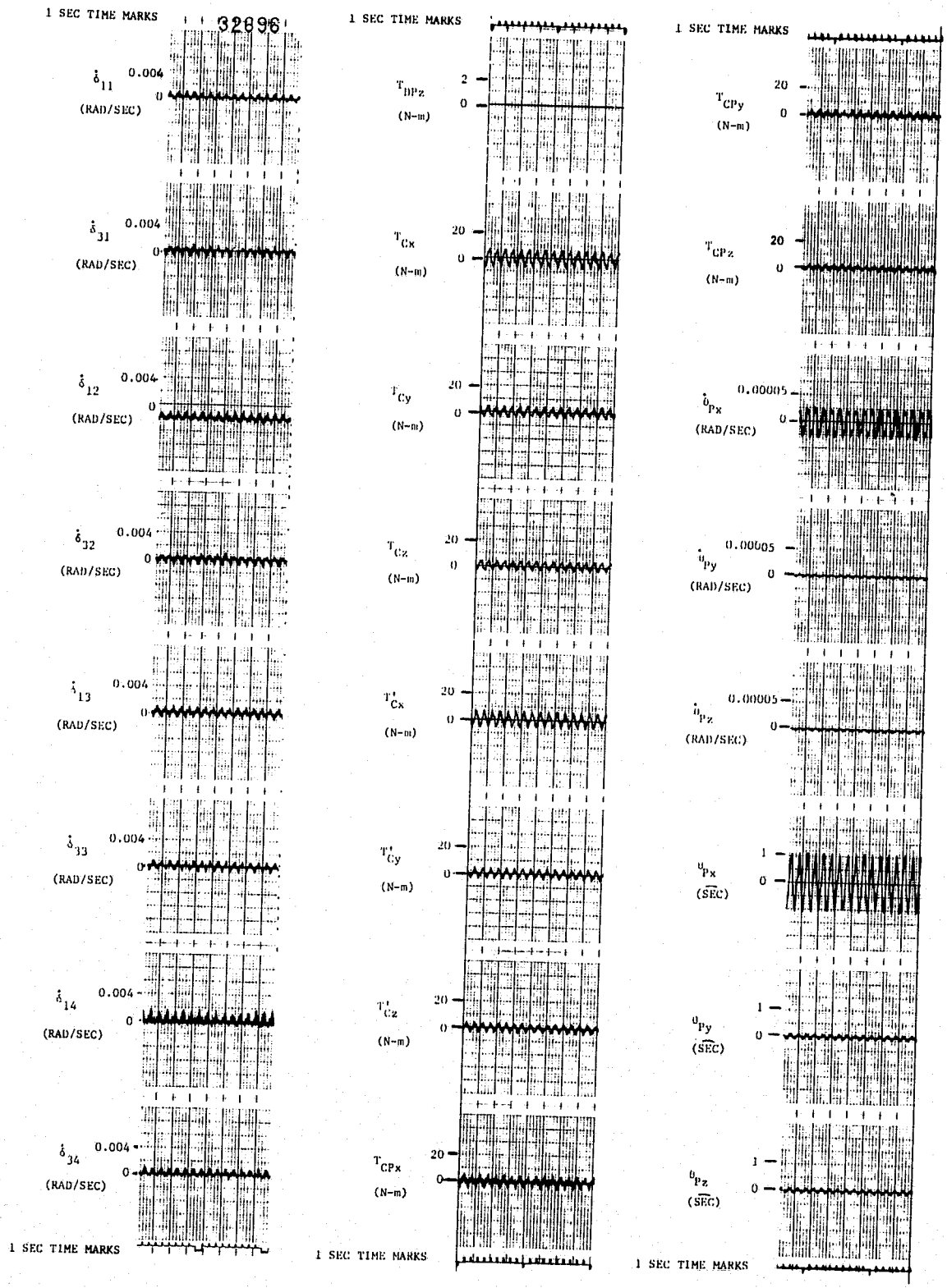

Figure 7-2. No Torque Disturbance, 2 Hz System, Zero Gimbal Angles

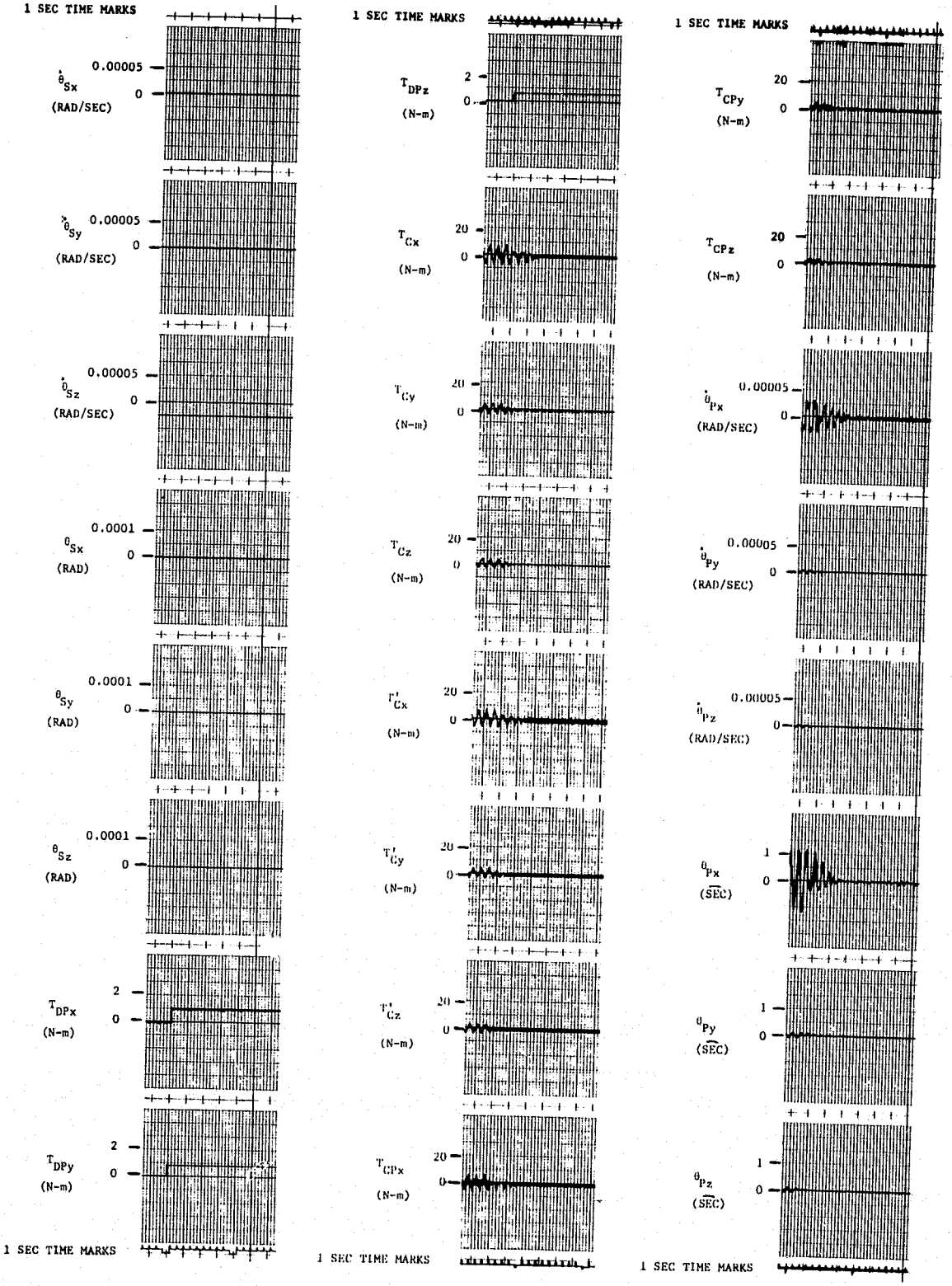

Figure 7-3. Step Torque Disturbance, 2 Hz System, Zero Gimbal Angles

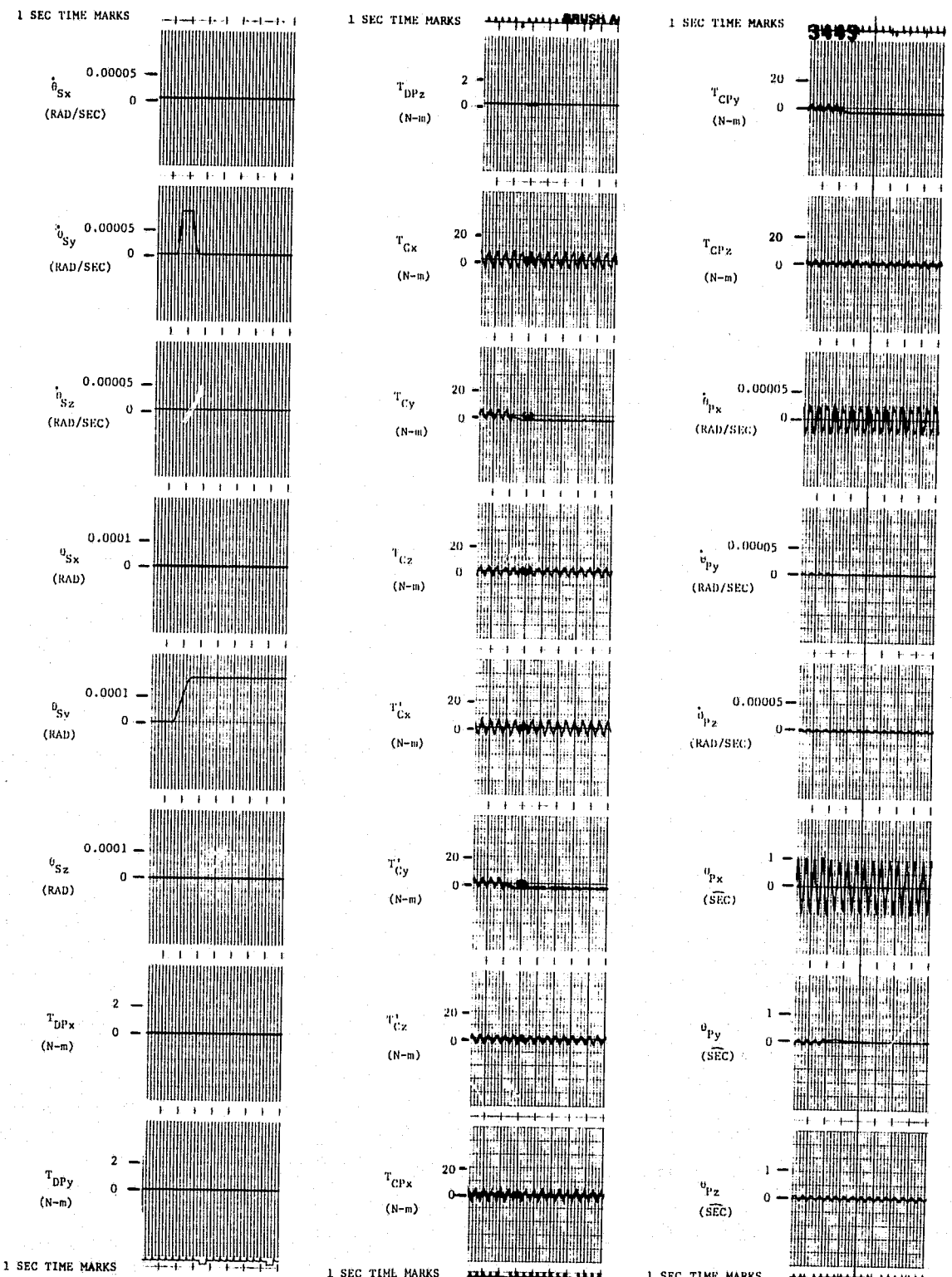

Figure 7-4. Crew Motion Torque Disturbance, 2 Hz System, Zero Gimbal Angles

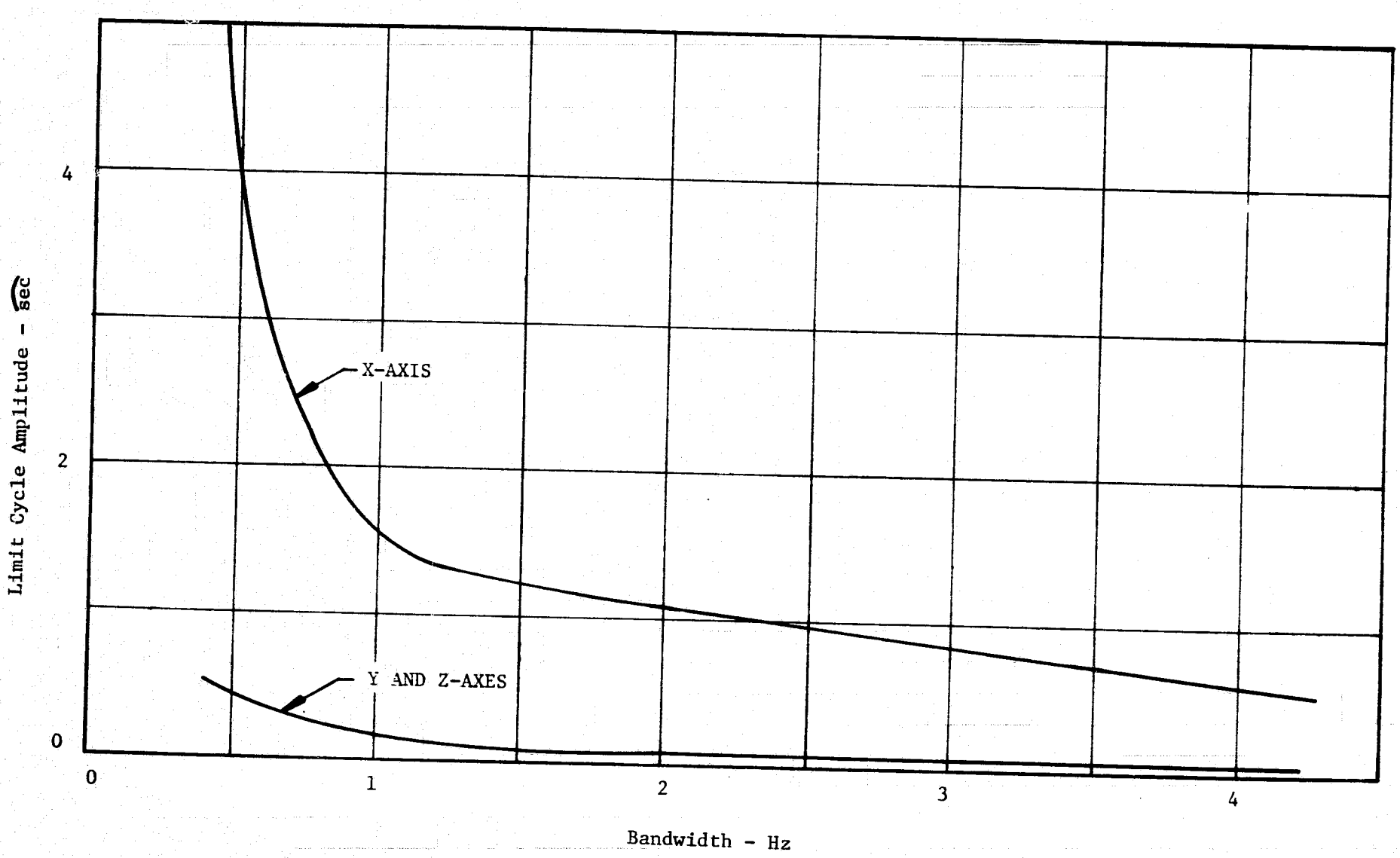

Figure 7-5. Unloaded Limit Cycle Peak Value Versus System Bandwidth (Zero Gimbal Angles)

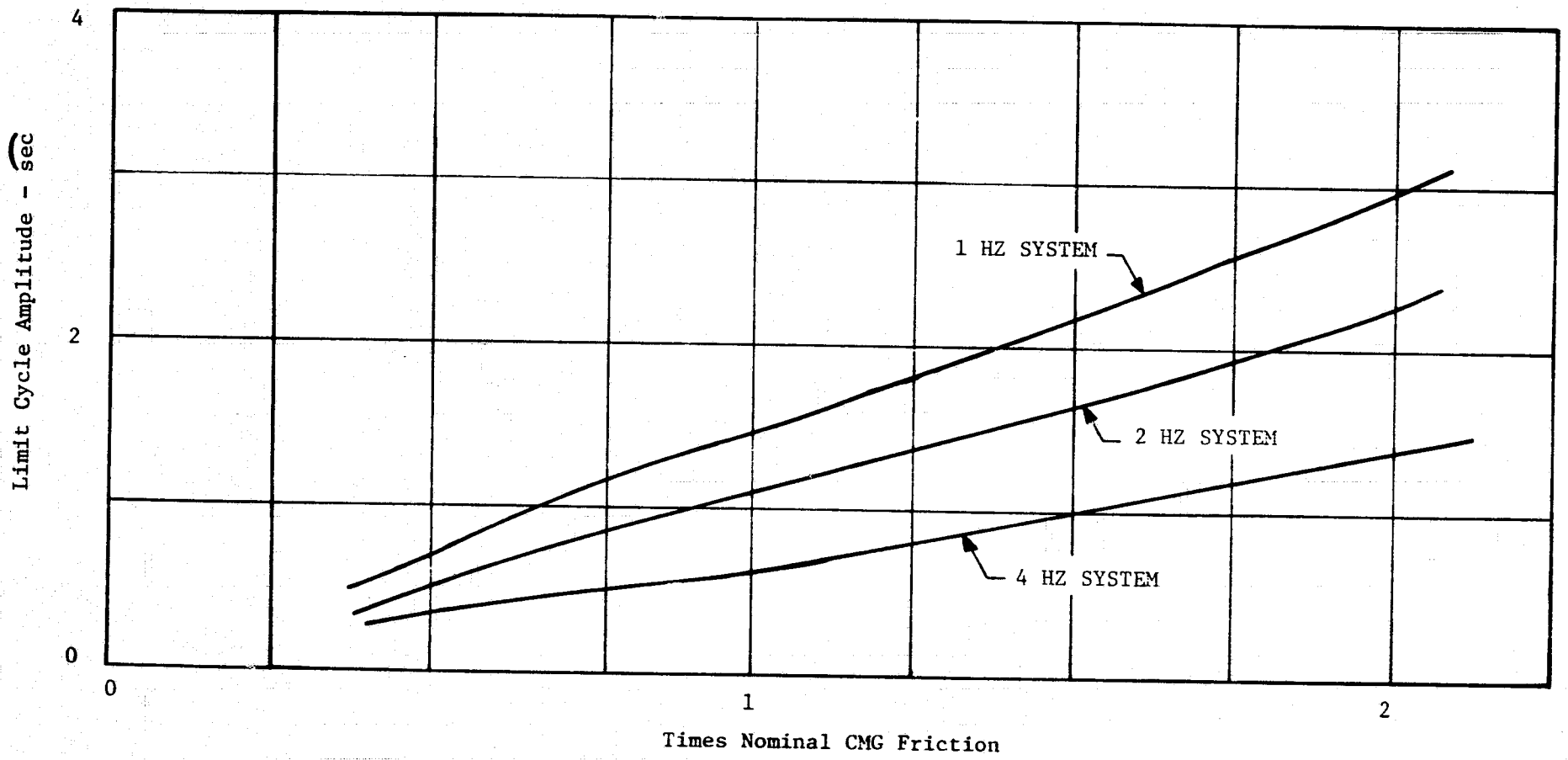

Figure 7-6. Unloaded Limit Cycle X-Axis Peak Value Versus CMG Friction Level (Zero Gimbal Angles)

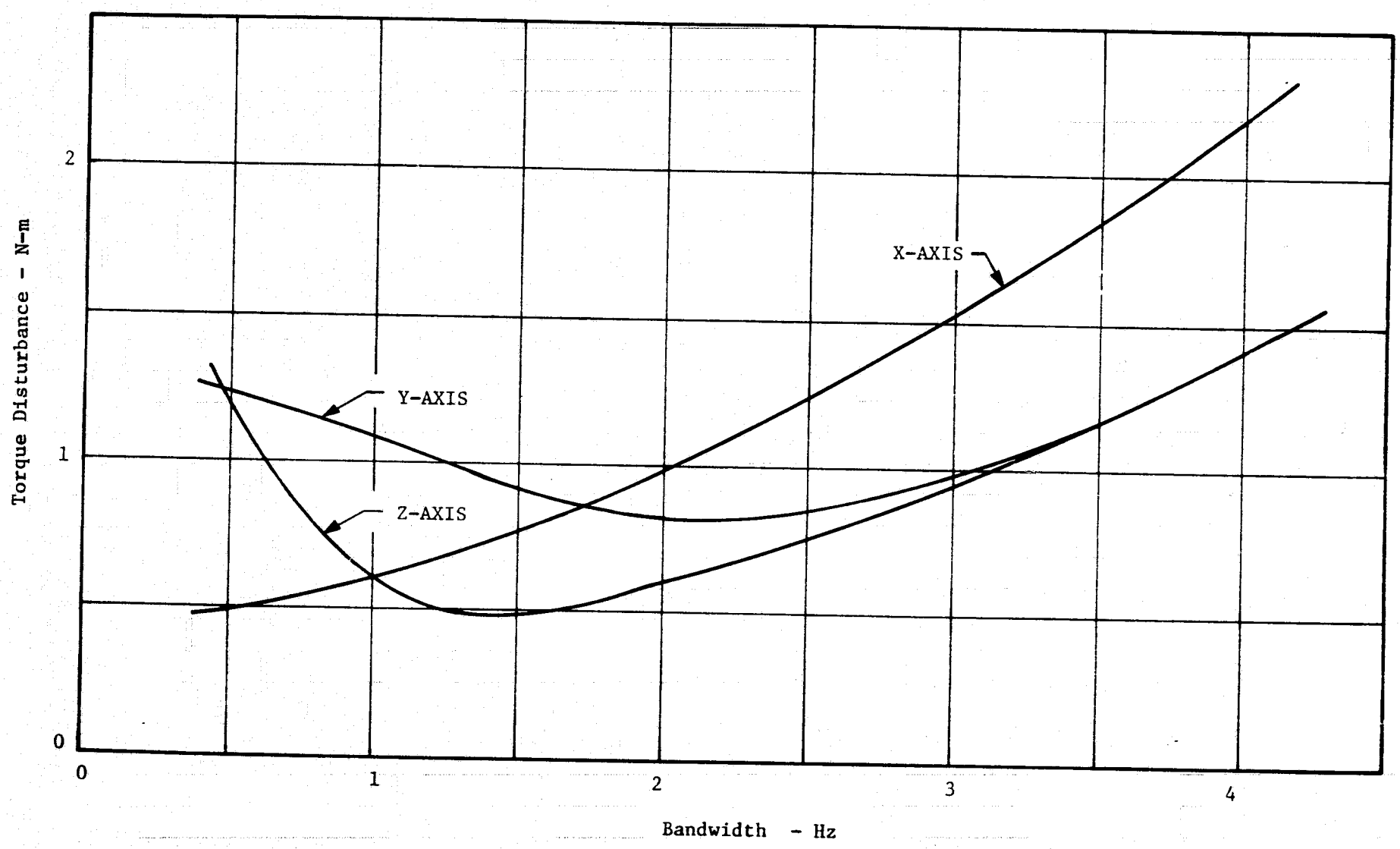

Figure 7-7. Torque Disturbance Required to Eliminate Limit Cycle Versus System Bandwidth (Zero Gimbal Angles)

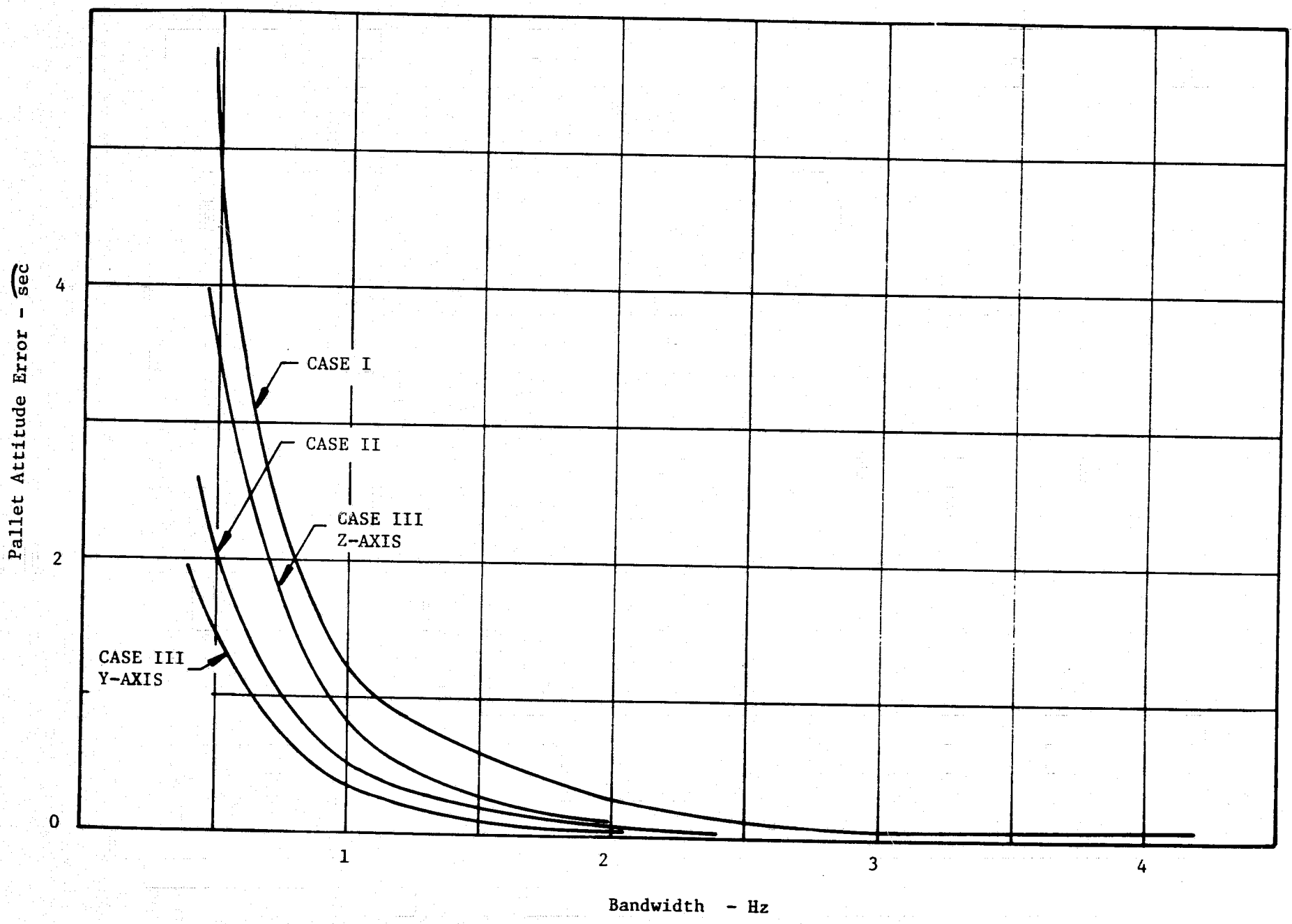

Figure 7-8. Crew Motion Disturbance Peak Error Versus System Bandwidth (Zero Gimbal Angles)

Table 7-1. Floated Pallet Hybrid Simulation Study Results

	SYSTEM BANDWIDTH			0.5 Hz	1.0 Hz	2.0 Hz	4.0 Hz
ZERO GIMBAL ANGLES	UNLOADED LIMIT CYCLE (PEAK VALUE) $\widehat{SEC}$	2 TIMES NOMINAL FRICTION	X axis	-	3.0	2.3	1.4
			Y axis	-	0.3	0.2	0.1
			Z axis	-	0.3	0.2	0.1
		NOMINAL FRICTION	X axis	4.0	1.5	1.1	0.6
			Y axis	0.4	0.15	0.1	0.05
			Z axis	0.4	0.15	0.1	0.05
		0.5 TIMES NOMINAL FRICTION	X axis	-	0.7	0.5	0.4
			Y axis	-	0.1	0.05	0.03
			Z axis	-	0.1	0.05	0.03
	TORQUE DISTURBANCE REQUIRED TO ELIMINATE LIMIT CYCLE (N-m)		X axis	0.5	0.6	1.0	2.2
			Y axis	1.2	1.1	0.8	1.4
			Z axis	1.2	0.6	0.6	1.4
	CREW MOTION DISTURBANCE (PEAK VALUE) $\widehat{SEC}$		Case I (Z axis)	5.0	1.2	0.25	0.05
			Case II (Y axis)	2.0	0.5	0.1	nil
			Case III (X axis)	1.5	0.35	0.05	nil
			(Z axis)	3.5	0.8	0.1	0.05
45 DEGREE GIMBAL ANGLES 0.5 and 1.0 Hz 45,45 2.0 and 4.0 Hz 0,45	UNLOADED LIMIT CYCLE (PEAK VALUE) $\widehat{SEC}$		X axis	1.5	0.1	0.5	*
			Y axis	0.5	0.25	0.2	*
			Z axis	0.5	0.2	0.2	*
	TORQUE DISTURBANCE REQUIRED TO ELIMINATE LIMIT CYCLE (N-m)		X axis	5.0	0.6	1.0	*
			Y axis	1.2	1.1	1.2	*
			Z axis	1.2	0.6	1.0	*
	CREW MOTION DISTURBANCE (PEAK VALUE) $\widehat{SEC}$		Case I (Z axis)	5.0	1.2	0.2	*
			Case II (Y axis)	2.0	0.5	nil	*
			Case III (Y axis)	1.5	0.4	nil	*
			(Z axis)	3.0	0.8	0.15	

*Unstable system, not run.

8. INSTRUMENT POINTING SYSTEM (IPS) DIGITAL SIMULATION MODELS

The stability and performance of IPS operation were investigated for pointing and slewing modes of operation. Mathematical models were defined and implemented digitally for these two modes of system operation. The derivation of these models is given in detail in volume I of this final report.

8.1 Pointing Performance Model - The mathematical model derived for the determination of pointing performance is a linear six body representation of the orbiter/pallet/IPS. The bodies are shown conceptually in figure 8-1 and are distributed as follows: body 1 represents the orbiter, bodies 2 and 3 represent the pallet, body 4 represents a gimbal base or pedestal, body 5 represents the inner gimbal or inertial gimbal of a proposed gimballing system and body 6 represents the instrument to be pointed. Features of the model include the following:

a. Six degree of freedom suspension dynamics between pallet and orbiter.

b. Pallet flexibility.

c. Six degree of freedom suspension dynamics between the pallet and the gimbal pedestal.

d. Gimbal and telescope interface flexibility.

e. Sensor and actuator dynamics.

By proper initialization this model can represent any of the three IPS (Inside-Out Gimbal, Standard Experiment Pointing Base or Floated Pallet) evaluated during the course of the pointing performance evaluation and comparison. A schematic representation of the model is shown in figure 8-2, with initial reaction parameters given in tables 8-1, 8-2, and 8-3 for the IOG, SEPB, and Floated Pallet, respectively.

Table 8-4 lists the set of general control gain functions from which the gains for any loop bandwidth and arbitrary inertia were computed for the control law structure of rate, position and integral of position.

8.2 Inside-Out Gimbal (IOG) Slewing Model - The model derived for the evaluation of IOG slewing is a nonlinear three body representation. The bodies are shown conceptually in figure 8-3 and are distributed as follows: body 1 represents the orbiter and

pallet, body 2 represents the gimbal pedestal and body 3 represents the inner gimbal and instrument. Features of the model include the following:

a. Full strapdown equations of motion for the telescope.

b. Nonlinear Euler terms due to telescope motion.

c. Six degree of freedom suspension dynamics between pallet and gimbal pedestal.

d. Quaternion type slew command logic.

e. Sensor and actuator dynamics.

A schematic representation of this model is shown in figure 8-4 with parameters given in table 8-5. The table contains double values for certain parameters since two telescopes were considered in the slewing study.

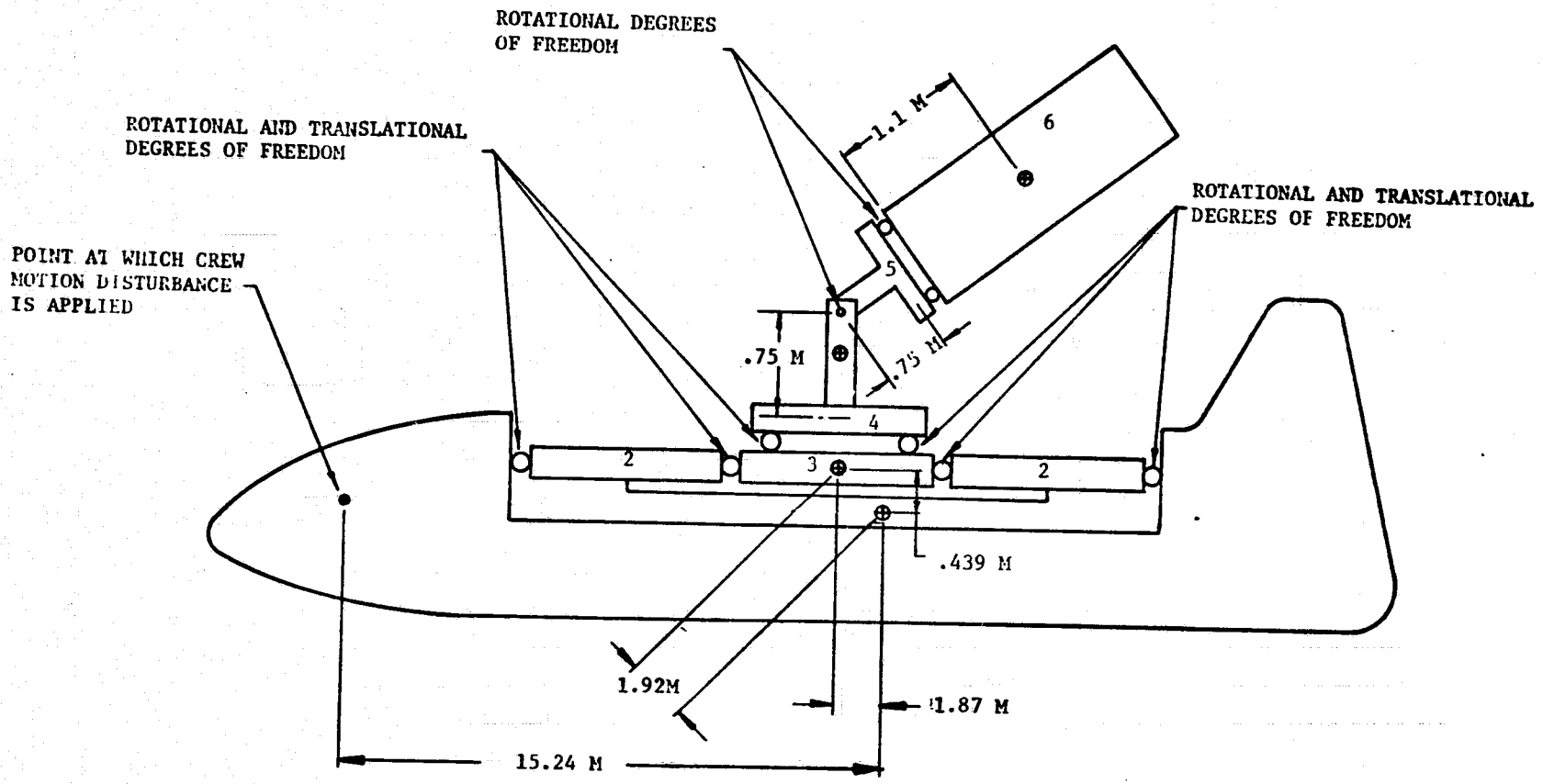

Figure 8-1. Conceptual Diagram of the Performance Evaluation Model

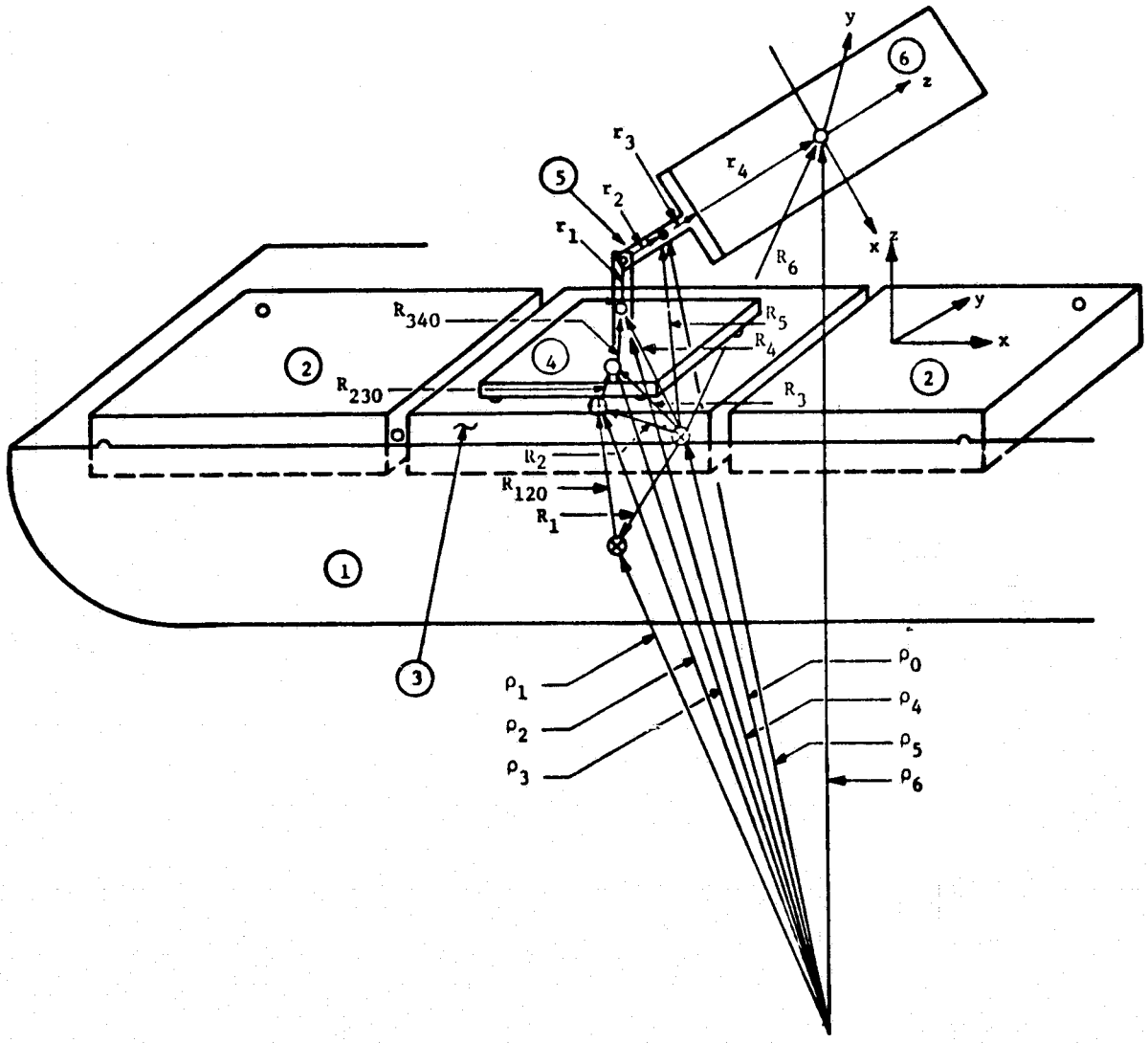

Figure 8-2. Schematic Diagram for the Linear Six Body Model

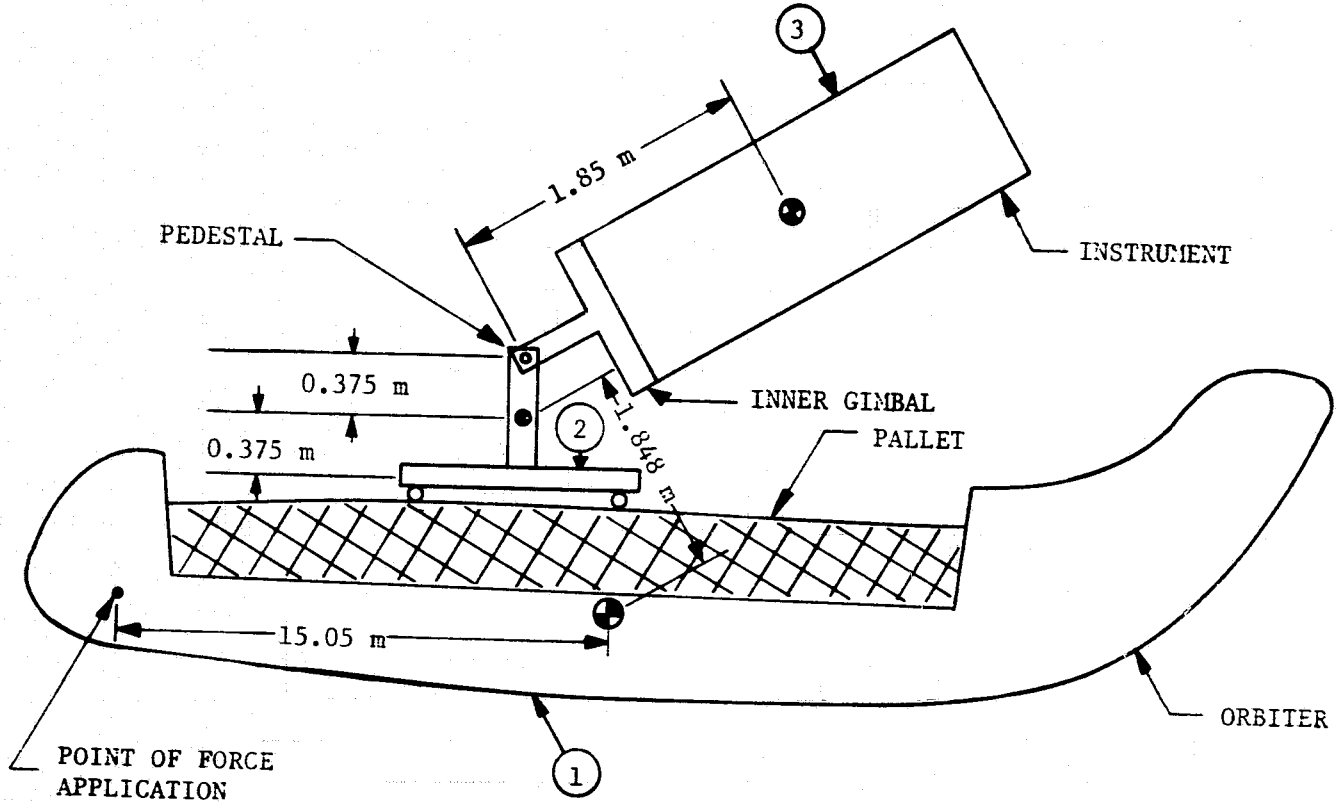

Figure 8-3. Conceptual Diagram of the Slewing Model

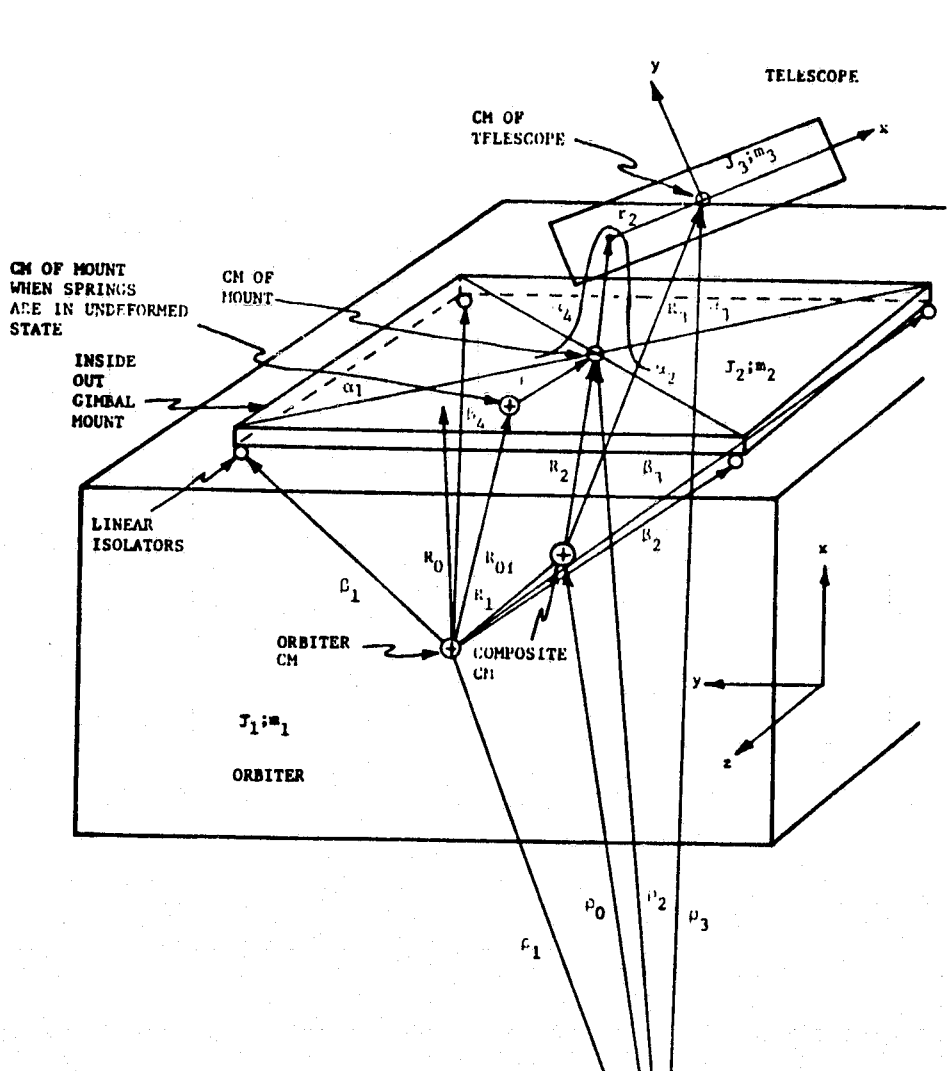

Figure 8-4. Schematic Diagram for the Nonlinear Slewing Model

Table 8-1. IOG System Parameters

Mass Properties

m_1=72,496 kg	J_1=diag{1.00x10^6,7.44x10^6,7.65x10^6} kg-m^2
m_2= 5,398 kg	J_2=diag{7.25x10^3,8.58x10^4,8.84x10^4} kg-m^2
m_3= 2,699 kg	J_3=diag{3.63x10^3,4.29x10^4,4.42x10^4} kg-m^2
m_4= 195 kg	J_4=diag{50.21,50.21,50.21} kg-m^2
m_5= 293 kg	J_5=diag{74.63,100.4,74.63} kg-m^2
m_6= 2,390 kg	J_6=diag{2.26x10^3,1.98x10^3,2.53x10^3} kg-m^2

Dimensional Parameters

$R_{11}=(-15.24,0,0)^T$ m	$R_{120}=(-1.87,0,0.439)^T$ m
$r_1=(0,0,0.375)^T$ m	$R_{230}=0$
$r_2=(0,0,0.375)^T$ m	$R_{340}=(0,0,0.375)^T$ m
$r_3=(0,0,0.375)^T$ m	$R_{E20}=0$
$r_4=(0,0,1.1)^T$ m	$R_{E30}=0$
$\alpha_{14}^{34}=(0.25,0.25,0.25)^T$ m	$R_{E40}=(0,0,-0.375)^T$ m

Table 8-1. IOG System Parameters (Concluded)

Nominal Spring and Damping Constants

D_{12}=diag{254.0,254.0,254.0} N-sec/m
K_{12}=diag{7.990×10^{4},7.990×10^{4},7.990×10^{4}} N/m
d_{12}=diag{1.367×10^{3},1.617×10^{4},1.606×10^{4}} N-m-sec/rad
k_{12}=diag{4.295×10^{5},5.081×10^{5},5.235×10^{5}} N-m/rad
D_{23}=diag{84.80,84.80,84.80} N-sec/m
K_{23}=diag{2.660×10^{4},2.660×10^{4},2.660×10^{4}} N/m
d_{23}=diag{4.562×10^{3},5.390×10^{3},5.554×10^{3}} N-m-sec/rad
k_{23}=diag{1.433×10^{5},1.694×10^{6},1.745×10^{6}} N-m/rad
D_{34}=diag{268.0,268.0,268.0} N-sec/m
K_{34}=diag{2.500×10^{3},2.500×10^{3},2.500×10^{3}} N/m
d_{34}=diag{66.90,66.90,133.8} N-m-sec/rad
k_{34}=diag{6.250×10^{2},6.250×10^{2},1.250×10^{3}} N-m/rad
$d_{56x}=2.840\times10^{2}$ f_{n56Rx} N-m-sec/rad
$d_{56y}=2.448\times10^{2}$ f_{n56Ry} N-m-sec/rad
$d_{56z}=3.179\times10^{2}$ f_{n56Rz} N-m-sec/rad
$k_{56x}=8.922\times10^{4}$ f^{2}_{n56Rx} N-m/rad
$k_{56y}=7.817\times10^{4}$ f^{2}_{n56Ry} N-m/rad
$k_{56z}=9.988\times10^{4}$ f^{2}_{n56Rz} N-m/rad
f_{n56Ri},i=x,y,z = Desired rotational natural frequency of the body 5 - body 6 interface

Table 8-2. SEPB System Parameters

Mass Properties

m_1=72,496 kg	J_1=diag{7.00x10^6,7.44x10^6,7.65x10^6} kg-m^2
m_2= 5,081 kg	J_2=diag{7.237x10^3,8.576x10^4,8.838x10^4} kg-m^2
m_3= 2,541 kg	J_3=diag{3.618x10^3,4.288x10^4,4.419x10^4} kg-m^2
m_4= 675 kg	J_4=diag{2.402x10^3,2.102x10^3,2.603x10^3} kg-m^2
m_5= 287 kg	J_5=diag{4.437x10^2,1.224x10^3,1.541x10^3} kg-m^2
m_6= 2,390 kg	J_6=diag{2.265x10^3,1.981x10^3,2.532x10^3} kg-m^2

Dimensional Parameters

$R_{11}=(-15.24,0,0)^T$ m	$R_{120}=(-1.87,0,0.429)^T$ m
$r_1=(0,0,2.0)^T$ m	$R_{230}=0$
$r_2=0$	$R_{340}=(0,0,0.9332)^T$ m
$r_3=0$	$R_{E20}=0$
$r_4=0$	$R_{E30}=0$
	$R_{E40}=(0,0,-2.0)^T$ m

Table 8-2. SEPB System Parameters (Concluded)

Nominal Spring and Damping Constants

$D_{12}=\text{diag}\{2.3950\text{x}10^{2},2.3950\text{x}10^{2},2.3950\text{x}10^{2}\}$ N-sec/m
$K_{12}=\text{diag}\{7.523\text{x}10^{4},7.523\text{x}10^{4},7.523\text{x}10^{4}\}$ N/m
$d_{12}=\text{diag}\{1.364\text{x}10^{3},1.617\text{x}10^{4},1.606\text{x}10^{4}\}$ N-m-sec/rad
$k_{12}=\text{diag}\{4.285\text{x}10^{5},5.079\text{x}10^{5},5.234\text{x}10^{5}\}$ N-m/rad
$D_{23}=\text{diag}\{79.83,79.83,79.83\}$ N-sec/m
$K_{23}=\text{diag}\{2.508\text{x}10^{4},2.508\text{x}10^{4},2.508\text{x}10^{4}\}$ N/m
$d_{23}=\text{diag}\{4.547\text{x}10^{3},5.388\text{x}10^{3},5.553\text{x}10^{3}\}$ N-m-sec/rad
$k_{23}=\text{diag}\{1.428\text{x}10^{5},1.693\text{x}10^{6},1.745\text{x}10^{6}\}$ N-m/rad
$D_{34}=\text{diag}\{1.053\text{x}10^{2},1.053\text{x}10^{2},1.053\text{x}10^{2}\}$ N-sec/m
$K_{34}=\text{diag}\{3.308\text{x}10^{4},3.308\text{x}10^{4},3.308\text{x}10^{4}\}$ N/m
$d_{34}=\text{diag}\{26.33,26.33,52.65\}$ N-m-sec/rad
$k_{34}=\text{diag}\{8.270\text{x}10^{3},8.270\text{x}10^{3},1.654\text{x}10^{4}\}$ N-m/rad
$d_{56x}=2.846\text{x}10^{2}\ f_{n56Rx}$ N-m-sec/rad
$d_{56y}=2.489\text{x}10^{2}\ f_{n56Ry}$ N-m-sec/rad
$d_{56z}=3.182\text{x}10^{2}\ f_{n56Rz}$ N-m-sec/rad
$k_{56x}=8.942\text{x}10^{4}\ f^{2}_{n56Rx}$ N-m/rad
$k_{56y}=7.821\text{x}10^{4}\ f^{2}_{n56Ry}$ N-m/rad
$k_{56z}=9.996\text{x}10^{4}\ f^{2}_{n56Rz}$ N-m/rad
$f_{n56Ri}, i=x,y,z$ = Desired rotational natural frequency of the body 5 - body 6 interface

Table 8-3. Floated Pallet System Parameters

Mass Properties

m_1=72,496 kg	J_1=diag{1.00×10^6, 7.47×10^6, 7.67×10^6} kg-m^2
m_2= 7,338 kg	J_2=diag{1.42×10^4, 9.29×10^4, 9.06×10^4} kg-m^2
m_3= 3,662 kg	J_3=diag{7.12×10^3, 4.64×10^4, 4.53×10^4} kg-m^2

Dimensional Parameters

$\alpha_{120}^{12}=(3.66,2.28,0)^T$ m	R_{230}=0
$R_{11}=(-15.24,0,0)^T$ m	R_{E20}=0
$R_{120}=(-1.87,0,0.528)^T$ m	R_{E30}=0

Nominal Spring and Damping Constants

D_{12}=diag{229.0,229.0,229.0} N-sec/m	
K_{12}=diag{719.0,719.0,404.0} N/m	
d_{12}=diag{2.682×10^3, 6.912×10^3, 1.703×10^4} N-m-sec/rad	
k_{12}=diag{8.401×10^3, 2.165×10^4, 5.340×10^4} N-m/rad	
$D_{23x}=D_{23y}=D_{23z}=84.79\ f_{n23T}$ N-sec/m	
$K_{23x}=K_{23y}=K_{23z}=2.664\times10^4\ f_{n23T}^2$ N/m	
$d_{23x}=8.951\times10^2\ f_{n23Rx}$ N-m-sec/rad	
$d_{23y}=5.836\times10^3\ f_{n23Ry}$ N-m-sec/rad	
$d_{23z}=5.693\times10^3\ f_{n23Rz}$ N-m-sec/rad	
$k_{23x}=2.812\times10^5\ f_{n23Rx}^2$ N-m/rad	
$k_{23y}=1.833\times10^6\ f_{n23Ry}^2$ N-m/rad	
$k_{23z}=1.789\times10^6\ f_{n23Rz}^2$ N-m/rad	
$D_{34x}=D_{34y}=D_{34z}=0$	$K_{34x}=K_{34y}=K_{34z}=0$
$d_{34x}=d_{34y}=d_{34z}=0$	$k_{34x}=k_{34y}=k_{34z}=0$

Table 8-4. Generalized Control Gains

$$K_{Rj}=4.736\ J_j f_n \quad \text{N-m-sec /rad}$$

$$K_{Pj}=8.41\ J_j f_n^2 \quad \text{N-m/rad}$$

$$K_{Ij}=6.64\ J_j f_n^3 \quad \text{N-m/sec}$$

where

J_j = inertia of the j^{th} vehicle axis ($kg\text{-}m^2$)

f_n = loop bandwidth defined as the -3 db point of the output torque to command torque transfer function (Hz)

Table 8-5. IOG Slewing Parameters

Mass Properties

m_1=80,593 kg	J_1=diag{1.011x10^6,7.569x10^6,7.783x10^6} kg-m^2
m_2= 195 kg	J_2=diag{50.21,50.21,50.21} kg-m^2
m_3= {2,683 kg; 1,225 kg}	J_3= {diag{2.335x10^3,2.080x10^3,2.605x10^3} kg-m^2; diag{5.918x10^2,6.176x10^2,1.794x10^3} kg-m^2}

Dimensional Parameters

R_{11}=(-15.05,0,-4.411x10^{-2})^T m	r_1=(0,0,-0.375)^T m
R_{120}=(-1.680,0,0.7699)^T m	r_2= {(0,0,1.850)^T m; (0,0,1.039)^T m}
R_{E20}=(0,0,-0.375)^T m	

Spring and Damping Constants

D_{12}=diag{59.93,59.93,59.93} N-sec/m

K_{12}=diag{125.0,125.0,125.0} N/m

d_{12}=diag{14.96,14.96,29.92} N-m-sec/rad

k_{12}=diag{31.25,31.25,62.50} N-m/rad

Control Loop Gains

K_{R3}= {diag{2.214x10^4,1.972x10^4,2.470x10^4} N-m-sec/rad; diag{3.674x10^3,3.674x10^3,1.628x10^4} N-m-sec/rad}

K_{P3}= {diag{7.856x10^4,7.000x10^4,8.764x10^4} N-m/rad; diag{1.306x10^4,1.306x10^4,5.784x10^4} N-m/rad}

K_{I3}= {diag{1.240x10^5,1.105x10^5,1.384x10^5} N-m/sec; diag{2.061x10^4,2.061x10^4,9.131x10^4} N-m/sec}

9. IPS OPERATING CHARACTERISTICS AND PERFORMANCE

The manner of operation and the operational characteristics of the IOG, SEPB, and Floated Pallet are discussed in this section, as is the effect of vehicle flexibility on the performance of each of the systems. In addition, the slewing performance of the IOG system is described.

9.1 IPS Characteristics - The following paragraphs describe the operation of each of the three IPS considered in this study. The control loop bandwidths and, where applicable, the suspension characteristics are defined in order to meet the ±1 sec pointing requirement in the presence of the crew motion disturbance shown in figure 7-1.

9.1.1 Inside-Out Gimbal System (IOG) - The IOG system is unique in that it is designed for exclusive operation in a zero gravity environment. A relatively large moment arm (1.85 m) exists between the telescope center of mass and the gimbal intersection points resulting in significant torque coupling into the telescope if the IOG gimbal pedestal is linearly accelerated. Rotational coupling is small in comparison to the translational.

In order to overcome the effects of this large CM offset the IOG base (pedestal) is isolated from pallet motion through a six degree of freedom suspension. This suspension must be soft enough such that the disturbances introduced into the telescope will not result in pointing error in excess of ±1 $\widehat{\text{sec}}$ peak for both realistic pointing loop bandwidths and control torque levels. The suspension must ultimately provide torques equal and opposite to the applied telescope control torques in order to keep the IOG pedestal from rotating and hence acts as a momentum desaturator for the IOG base. The suspension characteristics have minimal effect on the bandwidth and damping that can be realized with the pointing control loop.

Using the nominal IOG suspension parameters of table 8-1 with the telescope directed straight up out of the orbiter payload bay (zero look angle), a control loop bandwidth of 2 Hz is required to maintain pointing within ±1 $\widehat{\text{sec}}$ under the influence of crew motion disturbance. However, as the telescope look angle was varied from zero it was found the pointing error is a strong function of the angle as shown in figure 9-1. This result can be viewed as a juggling phenomenon where the hinge point tends to remain directly under the telescope center of mass when the telescope look angle is zero. However, when the telescope has a look angle of 90 degrees and the crew motion disturbance is applied along the orbiter z axis, no hinge translation can take

place that would reduce the translational coupling into the telescope. This is apparent since the translational coupling into the telescope occurs along the z axis and, for the given geometrical arrangement, initial hinge point translation due to telescope control torque along the z axis is not possible.

If the explanation given above were valid then it would directly follow that nearly equivalent operation as that exhibited when the telescope look angle is 90 degrees would be achieved with a zero telescope look angle when the distances between the IOG center of mass, the hinge point, and the suspension center of elasticity are zero. This was done and the results are shown in figure 9-2. Examination of this figure indicates that essentially equivalent pointing performance was obtained for zero look angle as that achieved for a 90 degree look angle once the hinge point, center of elasticity of the IOG suspension, and the pedestal center of mass coincide.

It is therefore apparent that in choosing an IOG loop bandwidth the telescope should be positioned at the worst possible look angle consistent with its operational range. For the orbiter/IOG/telescope system being considered the telescope maximum look angle is $\pm$65 degrees. Examination of figure 9-1 indicates that a pointing error of approximately 9 $\widehat{\text{sec}}$ results at a telescope look angle of 65 degrees for a 2 Hz control loop bandwidth in the presence of a crew motion disturbance. Increasing the loop bandwidth much beyond 2 Hz is not desirable from structural and noise (i.e., sensor and actuator) viewpoints. Hence the only way to achieve the desired pointing stability of $\pm$1 $\widehat{\text{sec}}$ peak is to soften the suspension.

Figure 9-2 shows pointing error as a function of suspension stiffness for various telescope look angles for a 2 Hz pointing control loop bandwidth. Examination of the curve for a 65 degree telescope look angle (the maximum look angle projected for IOG operation) shows that a reduction in suspension stiffness by approximately a factor of 20 would result in a peak pointing error of 0.5 $\widehat{\text{sec}}$ for a 2 Hz control loop bandwidth. This then is the recommended reduction in suspension stiffness in order to meet the pointing performance of 1 $\widehat{\text{sec}}$ peak without increasing the pointing control loop bandwidth beyond 2 Hz.

Figure 9-3 shows IOG pointing performance as a function of distance from the hinge point to the telescope center of mass (i.e., moment arm) for several pointing control loop bandwidths for 1/20 nominal suspension stiffness and a telescope look angle of 65 degrees. Examination of this figure shows that pointing error increases as the telescope moment arm increases. However,

it is apparent that the pointing error is approaching a maximum value as the telescope moment arm is increasing. In fact if the moment arm were to keep on increasing, the telescope incurred pointing error would begin to decrease. The reason for this phenomenon is that the telescope rotation about its center of mass required to track the translation of the hinge point due to crew motion disturbances, decreases as the moment arm is increased. This is apparent since the linear translation of the hinge point must be equal to "$r\theta$", where "r" is the telescope moment arm and θ is the telescope angular rotation. Figure 9-4 shows telescope pointing error as a function of pointing control loop bandwidth for various values of telescope moment arm, for 1/20 nominal suspension stiffness, and a telescope look angle of 65 degrees. As expected, telescope pointing error decreases as the pointing control loop bandwidth increases.

9.1.2 Standard Experiment Pointing Base (SEPB) - The SEPB is a conventional gimballing system in which the telescope center of mass is located in the vicinity of the gimbal intersection point. The base of the SEPB is hard mounted to the pallet. Isolation from crew motion is achieved by maintaining the telescope CM close to the gimbal intersection points in order to keep translational coupling into the telescope small without the use of a suspension. It is clearly seen that if the telescope CM were located exactly at the gimbal intersection point and in the absence of gimbal friction telescope isolation from crew motion would be achieved without the need for a pointing control loop. However, it is not possible to keep the telescope CM precisely at the gimbal intersection points, hence a pointing control loop is required to control the disturbances that couple into the telescope due to crew motions. The required pointing control loop bandwidth is a direct function of the telescope CM offset from the gimbal intersection or hinge point. This dependence is shown in figure 9-5 for a 1 and 2 Hz pointing control loop bandwidth.

Examination of figure 9-5 shows that a telescope CM offset of 3.2 and 8.9 centimeters (1.26 and 3.5 inches) for control loop bandwidths of 1 and 2 Hz, respectively, will result in peak pointing errors of ± 1 $\widehat{\text{sec}}$ in the presence of crew motion disturbances. Both of these allowable mass offsets require telescope mass balancing. Since it is not anticipated that balancing the telescope to 3 centimeters is no more difficult than balancing it to 9 centimeters, the smaller telescope mass offset is recommended, thus allowing the use of a 1 Hz pointing control loop for the SEPB. This would result in advantages when considering the effects of structural flexibility and system noise over a 2 Hz pointing control loop bandwidth.

9.1.3 Floated Pallet - In the floated pallet concept for the Spacelab, the total pallet is isolated with respect to the orbiter through a passive spring damper suspension. Four Skylab double gimbal CMGs are mounted on the pallet in order to control the total pallet to ± 1 sec peak pointing error in the presence of crew motion disturbances. The isolation system not only acts to isolate the pallet from crew motion disturbances but also allows the gross attitude control of the orbiter through the pallet suspension system via the control moment gyros mounted on the pallet. Hence the orbiter Reaction Control System (RCS) is not required to maintain orbiter attitude. Therefore the floated pallet concept eliminates the contaminants from the orbiter hypergolic RCS that are present in both the IOG and SEPB concepts.

It was anticipated and subsequently verified that a suspension natural frequency in the area of 0.1 Hz both in rotation and translation not only yields satisfactory isolation from crew motion disturbances, but will also allow the maintenance of orbiter attitude through the suspension system without large elongations of the pallet suspension system. Figure 9-6 shows a plot of peak pointing error as a function of floated pallet control loop bandwidth for the recommended suspension configuration in the presence of crew motion disturbances. From this figure it is seen that a pallet control loop bandwidth of approximately 1 Hz will limit the peak pointing error due to crew motion disturbance within ± 1 sec.

Figure 9-7 shows a plot of pallet pointing error vs suspension damping for nominal suspension stiffness and a 1 Hz pallet pointing control loop bandwidth. As the plot shows, pallet pointing error is only affected slightly as the damping ratio is varied by an order of magnitude. In fact, pointing error increases slightly as the damping ratio is increased from its nominal value of 0.1. Therefore suspension damping, the most uncertain quantity of the suspension parameters, does not require precise control in order to meet satisfactory pallet pointing stability performance.

Figure 9-8 shows a plot of pointing error vs pallet suspension natural frequency for a constant damping ratio of 0.1 for a 1 Hz pointing control loop bandwidth. As expected, the pointing error incurred is a fairly sensitive function of suspension natural frequency increasing appreciably as the suspension natural frequency is increased.

9.2 Effects of Flexibility on the Pointing Control Loop - The problem of flexibility can be divided into two broad classes:

a. Flexibility between sensors and actuators as exemplified by the classical booster problem.

b. Sensors and actuators mounted on a relatively rigid structural portion which is in turn connected through a flexible interface to the remaining structure. Skylab was an example of this type of problem.

Both of these effects cause stability problem, however, they are different in nature. When flexibility exists between sensors and actuators the flexibility acts as a lag in the control system which can be grossly viewed as the equivalent of having low bandwidth actuators thus causing instability. When sensors and actuators are mounted on a relatively rigid portion of structure which is connected through a flexible interface to the remaining structure, the effect of the flexibility is to cause an apparent decrease in the controllable vehicle inertia when the natural frequency of the flexible interface is exceeded. This decrease in inertia can be viewed as an increase in loop gain which can cause instability if the inertia reduction is appreciable, and the stiffness of the interface does not yield a sufficiently high structural natural frequency.

The instabilities caused by flexure in both classes of the problem can be compensated for by two general techniques:

a. Design the bandwidth of the control loop below the natural frequencies of the vehicle flexibilities (i.e., gain stabilization). This type of design results in a low control loop bandwidth and hence pointing performance will not be met under the influence of disturbances, particularly those due to crew motion.

b. Use phase stabilization techniques which would yield adequate control loop bandwidth thus enabling high accuracy system pointing performance. However, this technique requires the accurate knowledge of the vehicle bending characteristics which are not readily available and can necessitate on-board measurement of vehicle flexibility characteristics.

Therefore, the approach taken in this study was to evaluate the loop bandwidth required to meet 1 $\widehat{\text{sec}}$ system pointing performance assuming a rigid structure as described previously. Flexibility was then inserted and the structural stiffness (i.e., structural natural frequencies) required to yield satisfactory system stability and performance determined without the use of bending mode filters. This determination was conducted for both classes of the flexibility problem outlined above.

9.2.1 Effects of Flexibility on the IOG Pointing Control Loop - Using an IOG loop bandwidth of 2 Hz with sensors and actuators mounted on the inertial gimbal of the IOG, the flexible interface between the gimbal and the telescope was varied in order to determine the interface frequency required for system stability. The result of this investigation showed that an interface frequency of approximately 8 Hz corresponding to an interface stiffness of 1.291×10^7 N-m/rad was required to achieve natural stability.

When the sensors are mounted on the telescope the interface frequency required for system neutral stability was approximately 2.8 Hz corresponding to an interface stiffness of 1.647×10^6 N-m/rad. This is approximately a factor of 2.8 less than the interface frequency required when sensors and actuators are mounted on the IOG inertial gimbal. Figure 9-9 shows the interface frequency required for neutral stability as a function of loop bandwidth for sensors mounted on the telescope.

Variations in the flexibility characteristics of the pallet and the interface between pallet and orbiter over wide ranges had little effect on overall IOG system stability and performance.

In summary the conclusions that are drawn from the investigation of the effects of flexibility on the IOG system performance and configuration are the following:

a. In order to minimize the interface and telescope frequency and stiffness required for stability sensors should be mounted on the telescope rather than the inertial gimbal of the IOG. This would necessitate both a mechanical and electrical interface with the various telescopes that are to be mounted on the IOG.

b. The interface frequency and corresponding stiffness required for neutral stability is approximately 2.8 Hz and 1.647×10^6 N-m/rad, respectively. It should be noted that these values are required for neutral stability. In order to achieve adequate stability margins the interface frequency should be increased between a factor of 1.5 to 2 corresponding to an increase in stiffness of 2.25 to 4. It should be noted that the interface stiffness represents the gimbal stiffness, telescope mounting interface stiffness, and the stiffness of the telescope support module as a lumped parameter. The reason for this is that the sensors will be mounted on the optical bench in order to control

the telescope line of sight while the attach point to the IOG will be on the back end of the telescope. Therefore, the IOG gimbal compliance, interface compliance, and telescope support module compliance can be roughly viewed as springs in series. Hence it is seen that severe stiffness requirements will be placed on the telescope support module in order to achieve system stability thus complicating the structural design. If bending mode filters are to be employed to alleviate the telescope stiffness requirements accurate knowledge of system bending modes would be required and each telescope would require its own bending mode filter design making the IOG very payload sensitive.

9.2.2 Effects of Flexibility on the SEPB - Using the 1 Hz pointing control loop, the interface frequency and stiffness requirements were determined when sensors were mounted on the inertial gimbal of the SEPB and when they were mounted on the telescope.

Examination of the inertias of the SEPB inner gimbal and the telescope (table 8-2) indicate that they are of the same order for the y and z axes and differ by a factor of 5 for the x axis. This is much smaller than the factors of 34 or 70 encountered for the IOG. Hence when sensors are mounted on the inertial gimbal of the SEPB an apparent loop gain increase of a factor of 5 occurs for the x axis and only requires a structural interface frequency of 0.5 Hz to achieve neutral stability. In fact the x axis is the only axis for which a minimum interface stiffness is required for stability. For the y and z axes there is no interface stiffness required for absolute stability about these axes. However, if pointing stability is to be maintained to within ± 1 sec peak the interface frequency and stiffness required is 3 Hz and 9.0×10^5 N-m/rad, respectively. It should be noted that this interface frequency and stiffness requirement is only needed to meet pointing performance but not for stability. Hence it is not necessary that margins of 1.5 or 2 be applied to these numbers in order to assure satisfactory system performance which would be the case as pointed out above when structural interface frequency and stiffness requirements are necessary from a stability viewpoint.

When the sensors are mounted on the telescope the interface frequency and stiffness requirement for neutral stability are 6 Hz and 3.6×10^6 N-m/rad, respectively. Since the inertias about the y and z axes for the SEPB inertial gimbal and the telescope differ by only a factor of 1.6 a large system lag results, therefore, the interface frequency and stiffness has to be relatively high in order to set the second order break frequency high enough with respect

to the control loop bandwidth in order to achieve stability. In fact the axes which govern the interface frequency and stiffness requirements are the y and z axes. The value of interface frequency and stiffness required for the x axis is appreciably below that which is required for the y and z axes.

In summary the following are the conclusions that are drawn from the investigations performed on the effects of flexibility on SEPB pointing control loop performance:

a. Sensors should be mounted on the SEPB inertial gimbal in order to minimize the structural frequency and interface requirements for stability. The interface frequency and stiffness required for stability is 0.5 Hz and 2.5×10^4 N-m/rad and is governed by the x axis.

b. The interface frequency and stiffness required to maintain ± 1 sec peak pointing stability in the presence of crew motion disturbances is 3 Hz and 9.0×10^5 N-m/rad, respectively. This value of interface stiffness is approximately half that required for the IOG thus alleviating the structural requirements for the telescope. In addition it should be noted that the SEPB would attach to the telescope metering truss which is traditionally quite stiff due to thermal and dimensional stability requirements. Hence a 3 Hz interface frequency with its corresponding interface stiffness should be easier to achieve than a similar interface stiffness for the IOG.

c. The interface frequency and stiffness required for neutral stability if sensors are mounted on the telescope is 6 Hz and 3.6×10^6 N-m/rad, respectively. This is an increase of a factor of 2 in interface frequency and a factor of 4 in interface stiffness over that which is required when sensors are mounted on the inertial gimbal of the SEPB.

9.2.3 Effects of Flexibility on the Floated Pallet - Using the 1 Hz control loop bandwidth, the interface frequency and stiffness requirements for stability and pointing performance were determined for the following cases; where body 2 represents the outer pallet segments and body 3 the central segment:

1. Sensors and actuators mounted on body 3 which corresponds to one-third of the pallet inertia.

2. Actuators mounted on body 2 and sensors mounted on body 3.

3. Sensors and actuators mounted on body 2.

For case 1 where sensors and actuators were mounted on body 3 there was no interface frequency or stiffness requirement between bodies 2 and 3 from an absolute stability viewpoint. However, if ± 1 sec peak pointing stability is to be met in the presence of crew motion disturbances over the total pallet structure the rotational and translational interface frequency, rotational stiffness, and translational stiffness had to be 4 Hz, 2.93×10^7 N-m/rad, and 5.78×10^5 N/m, respectively.

For case 2 where sensors were mounted on body 3 and actuators on body 2 the rotational and translational interface frequency, rotational stiffness, and translational stiffness had to be 8 Hz, 1.44×10^8 N-m/rad, and 2.313×10^6 N/m, to achieve neutral stability. It should be noted that the same results would be obtained if the actuators were mounted on body 3 and the sensors were mounted on body 2 since the system is reciprocal and the system characteristic equation does not change.

For case 3 where both sensors and actuators were mounted on body 2 there was no interface frequency or stiffness requirement between bodies 2 and 3 required from the standpoint of absolute stability. However, approximately a 0.5 Hz interface frequency corresponding to linear interface stiffness of 3.6×10^4 N/m and a rotational stiffness of 4.58×10^5 N/m was required in order to meet ± 1 sec pointing stability over the total pallet. The significance of this result is that it gives an estimate as to the interface frequency and stiffness required by instruments that are mounted to the pallet. Since body 3 gets perturbed only through the flexible interface between bodies 2 and 3, body 3 can be considered as an experiment bolted to the pallet which can be considered as body 2. It is therefore seen that the interface frequency between experiments and pallet which is being stabilized to ± 1 sec peak is only required to be in the vicinity of 0.5 Hz. Therefore, the floated pallet places the least restriction on telescope and positioning gimballing structural design. It should also be noted that the pallet pointing control system is least sensitive to payload characteristics and hence truly acts as an experiment base which can accommodate a wide variety of payloads requiring precise pointing accuracies.

In summary the following are the conclusions derived from the investigations on the effect of flexibility on the floated pallet:

a. In order to minimize the floated pallet stiffness requirements sensors and actuators should be mounted on a relatively stiff section of pallet corresponding to approximately 30 percent of the total pallet inertia having a first significant bending mode in excess of 8 Hz. The interface frequency between this section and the rest of the pallet should be 4 Hz if 1 sec pointing stability is to be maintained over the total pallet.

b. The interface structural frequency between instruments mounted on a pallet stabilized to ±1 sec in order to meet ±1 sec pointing stability on the instrument is approximately 0.5 Hz. This poses the least restriction on telescope structural design of any of the systems investigated and can easily be met. This makes the pallet quite insensitive to payload characteristics and hence truly acts as an experiment base capable of accommodating a large variety of instruments requiring precise pointing.

Table 9-1 summarizes the results obtained for the IOG, SEPB, and Floated Pallet with respect to the effects of structural flexibility.

9.3 IOG Slewing Performance - Two slew profiles provided by NASA were used in this evaluation, profile 1 representing the rate required to track an earth fixed point, profile 2 chosen to give rates 50 percent higher than earth tracking. Two telescopes were also used in the IOG slewing evaluation. One of the telescopes is the same as that used in the IOG pointing performance evaluations described in the preceding sections, the parameters of which are listed in table 8-5. The second telescope evaluated was considerably lighter than that used in the pointing performance studies. The configuration and mass properties for this telescope are shown in figure 9-10. In all of the slewing studies the suspension stiffness was set at 1/20 nominal. For convenience, the telescope used above in the IOG pointing performance evaluations will be referred to as the "baseline telescope" while the second telescope will be called the "slewing telescope."

Both of the slew profiles were applied to the baseline and slewing telescopes. The telescopes were slewed about the -y axis for both profiles. In addition, both telescopes were slewed using profile 1 about an axis in the xy plane making an angle of 45 degrees with both the -x and -y telescope axes and IOG pedestal axes. A satisfactory slew about this axis would imply satisfactory slewing about any axis located in the x-y plane.

Examination of table 9-2 indicates that the IOG is capable of satisfactorily slewing the "slewing telescope" through both slew profiles about any axis in the xy plane. The maximum resulting pedestal rotation and isolator elongation is approximately 9.12×10^{-2} rad (5 degrees) and 2.65×10^{-2} m (1.04 inches), respectively. These values especially for the isolator elongation are within state-of-the-art isolator design. In addition, the maximum control torque required was 1.69 N-m when using profile 2 which is well within the capability of direct drive DC torquers of feasible size and volume. Direct drive DC torquers are desirable from a pointing control viewpoint since they eliminate the nonlinearities that usually accompany geared torquers. The largest tracking error incurred was 1.474 $\widehat{\text{sec}}$ when using slew profile 2. However, it is anticipated that this error could be reduced to less than an arc second by a slight increase in telescope control loop gains.

Further examination of table 9-2 shows that slewing the baseline telescope evely through slew profile 1 results in relatively large rotations and translations of the IOG pedestal accompanied by substantial elongations of the IOG isolators. The IOG pedestal rotated .176 rad (10 degrees) and 0.179 rad (10.3 degrees) about the x and y axes, respectively, and was accompanied by an isolator elongation of 9.161×10^{-2} m (3.61 inches) when the telescope was slewed about an axis in the xy plane making an angle of $\pi/4$ rad (45 degrees) with respect to the telescope -x and -y axes. It is difficult to design a suspension that will give satisfactory performance and have uniform characteristics for elongations in the order of 10.16 cm (4 inches). When attempting to slew the baseline telescope through slew profile 2, pedestal rotations and isolator elongations are appreciably more severe than those incurred using slew profile 1, as table 9-2 indicates. It should be noted that when using slew profile 2, the rotations of the IOG pedestal are so severe that the assumptions of small angular rotation of the IOG pedestal, made in the derivation of the equations of motion for the slewing model, are no longer valid.

The results of the IOG slewing studies further indicate the sensitivity of IOG performance to payload characteristics. It is doubtful that the IOG will be able to satisfactorily track a point on earth with a telescope whose inertia is in excess of 10^3 kg-m^2 within acceptable pedestal rotations and translations, and isolator elongations. This sensitivity of IOG performance to payload characteristics, also shown in section 9.2, is the most significant shortcoming of the IOG system.

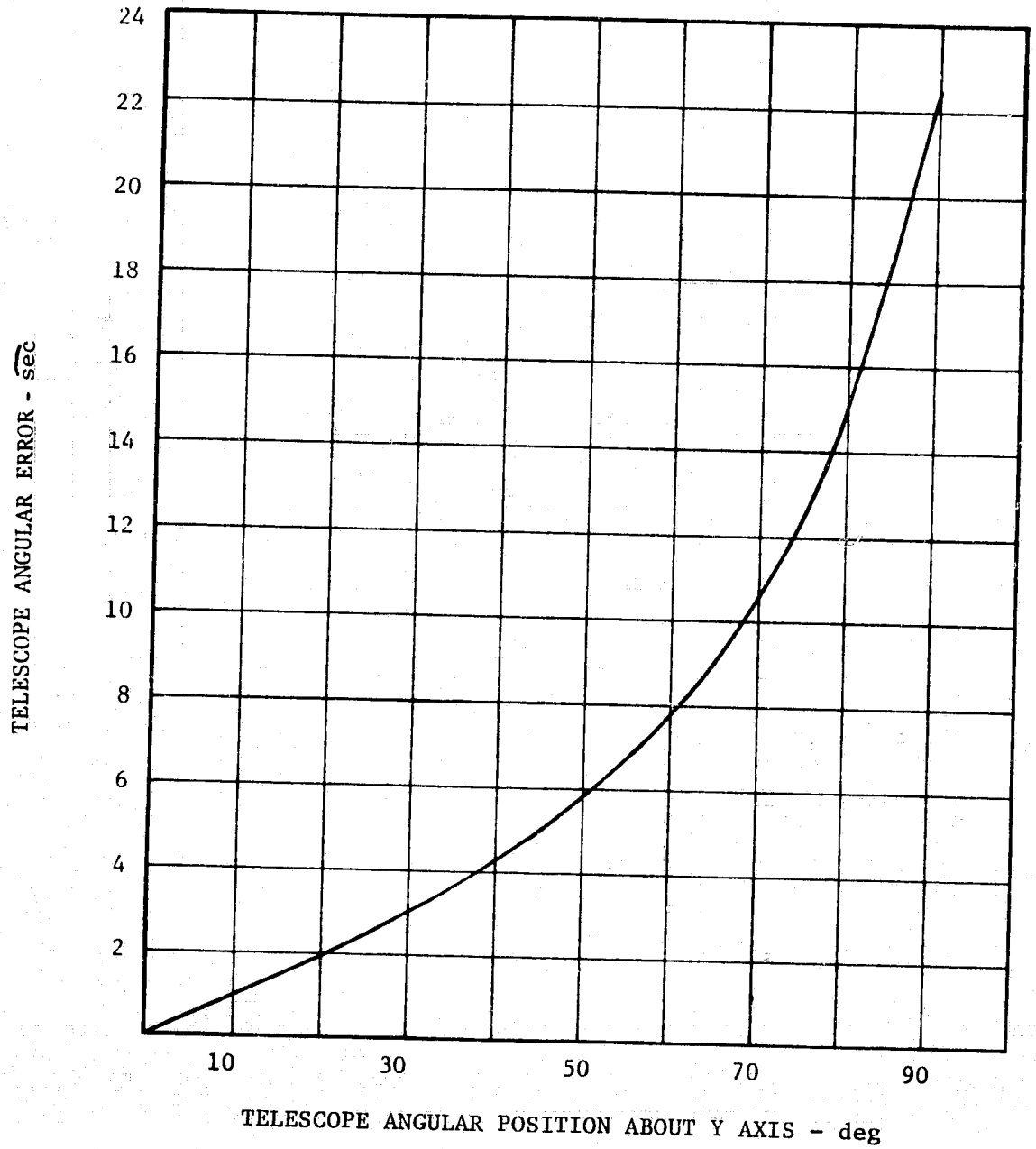

Figure 9-1. IOG Pointing Error vs Telescope Pointing for Nominal Suspension System and 2 Hz Pointing Control Loop Bandwidth

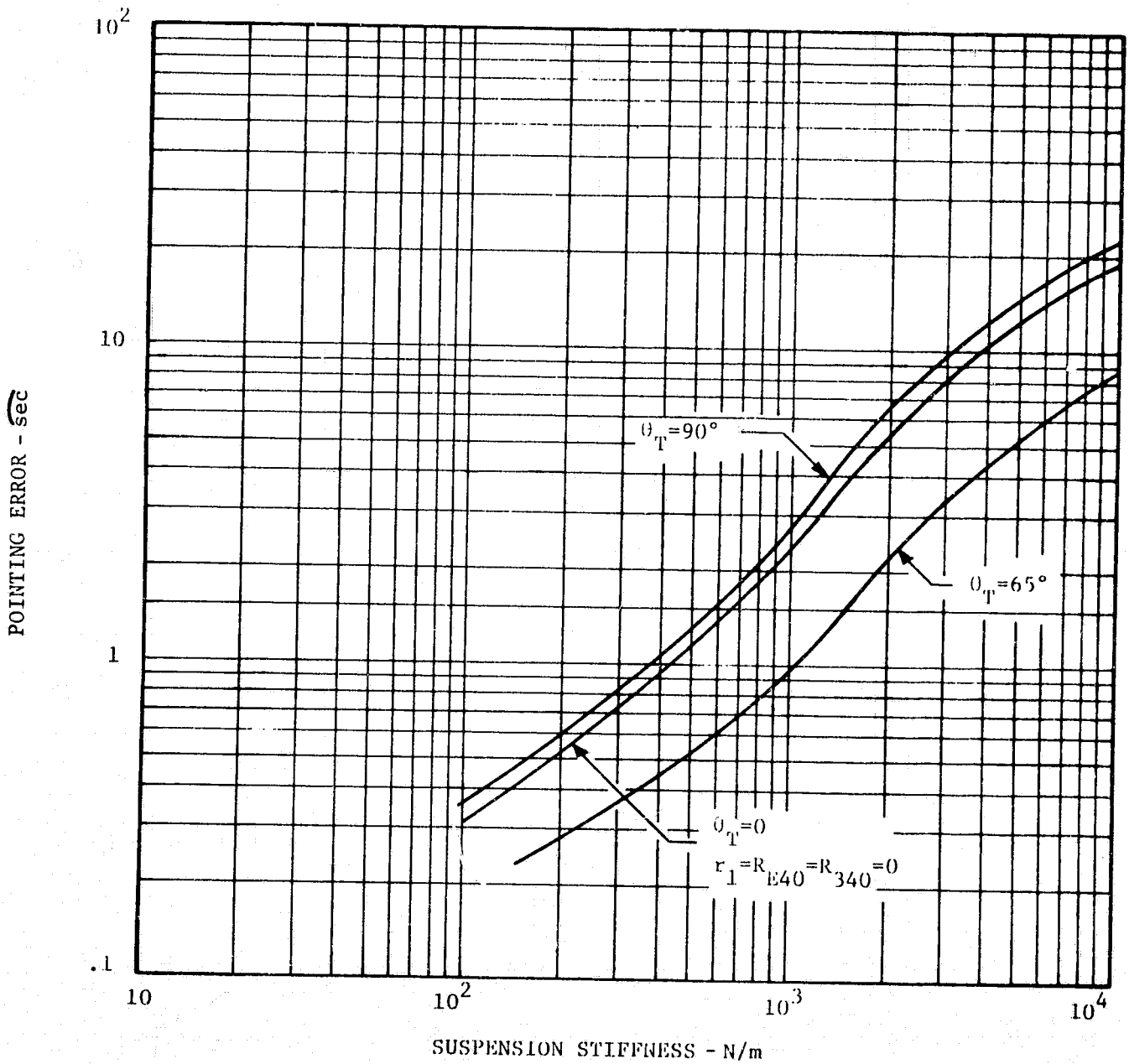

Figure 9-2. IOG Pointing Error vs Suspension Stiffness for 2 Hz Pointing Control Loop Bandwidth

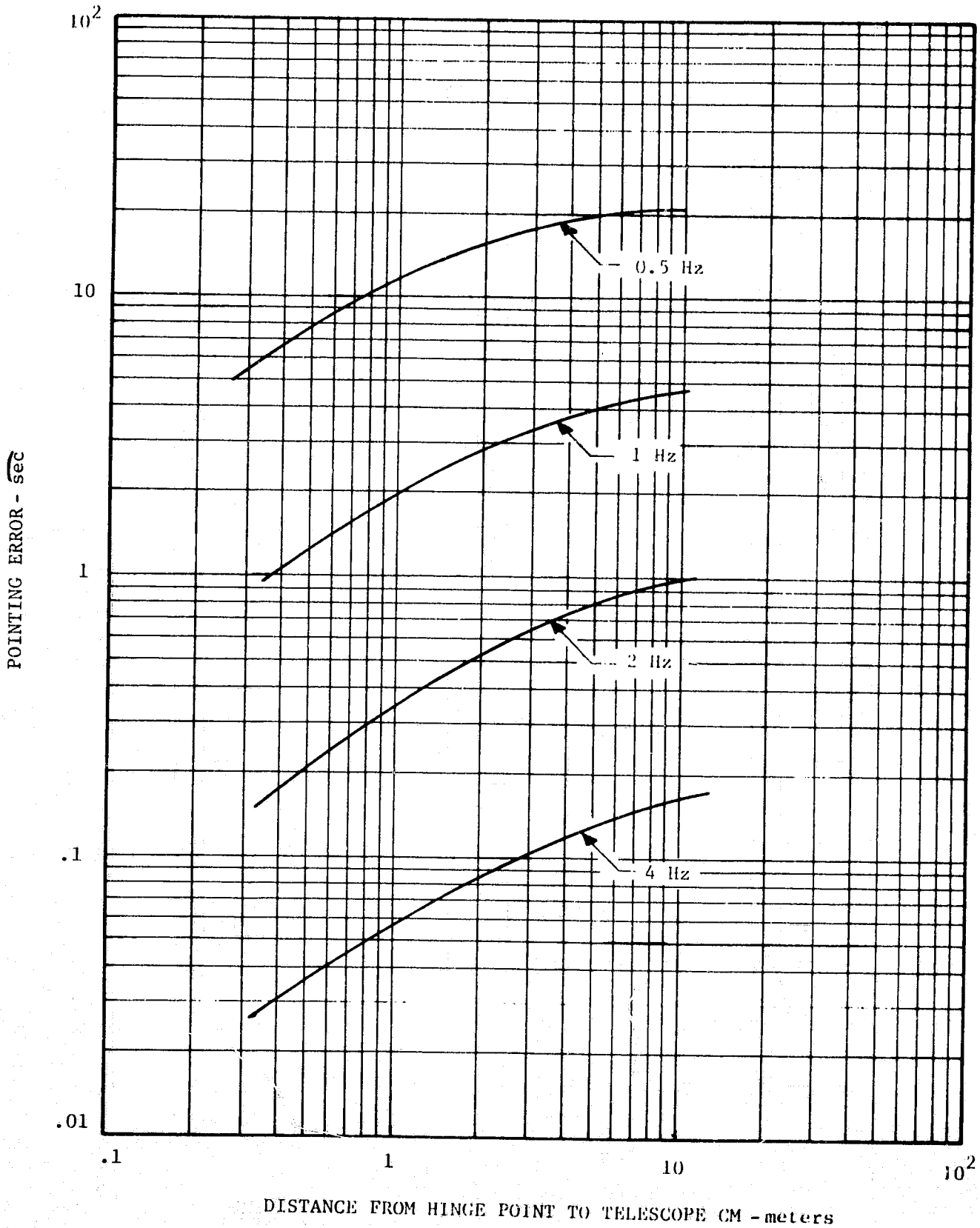

Figure 9-3. IOG Pointing Error vs Telescope Moment Arm for 1/20 Nominal Suspension Stiffness and 65 Degree Telescope Look Angle

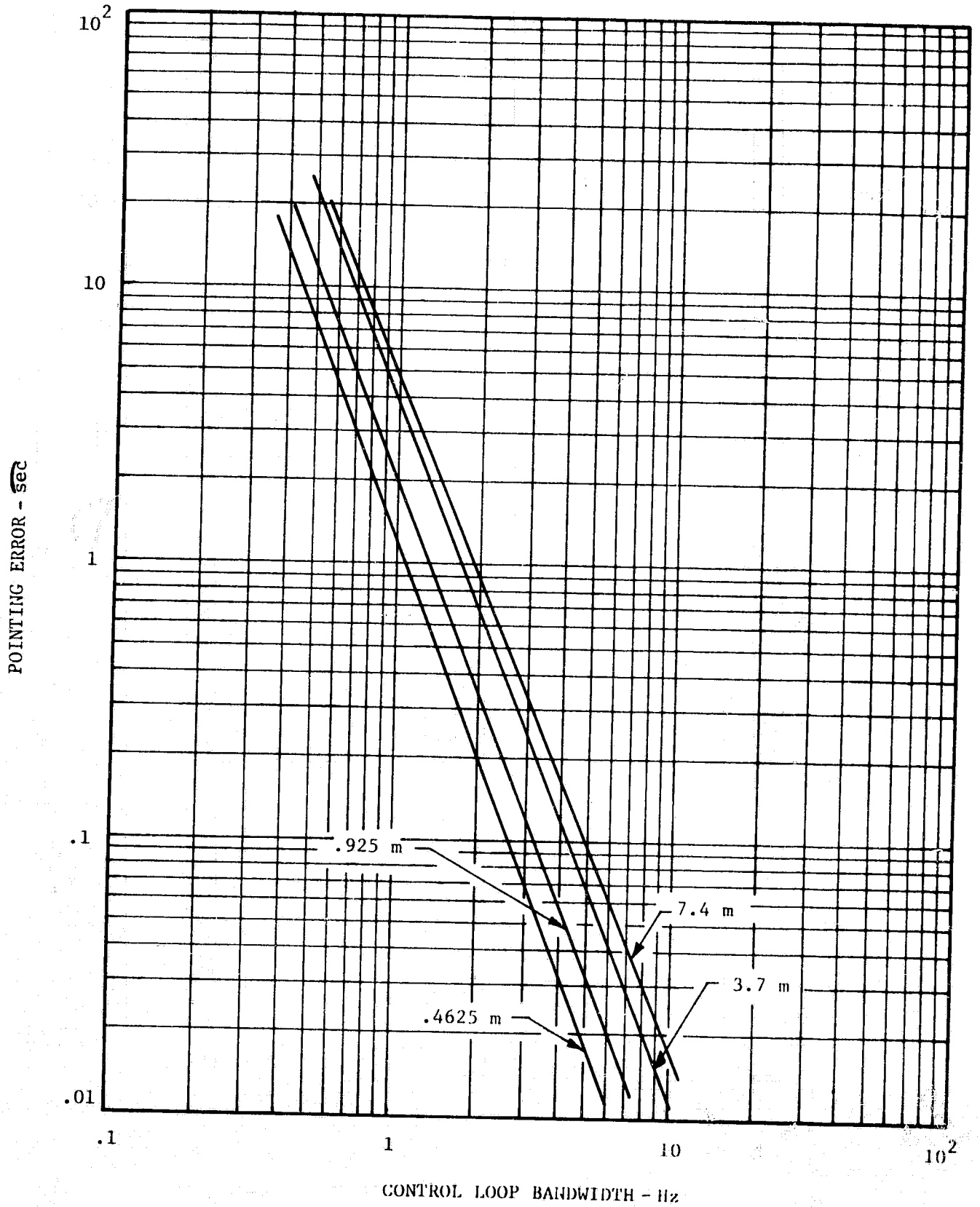

Figure 9-4. IOG Pointing Error vs Pointing Control Loop Bandwidth for 1/20 Nominal Suspension Stiffness and 65 Degree Telescope Look Angle

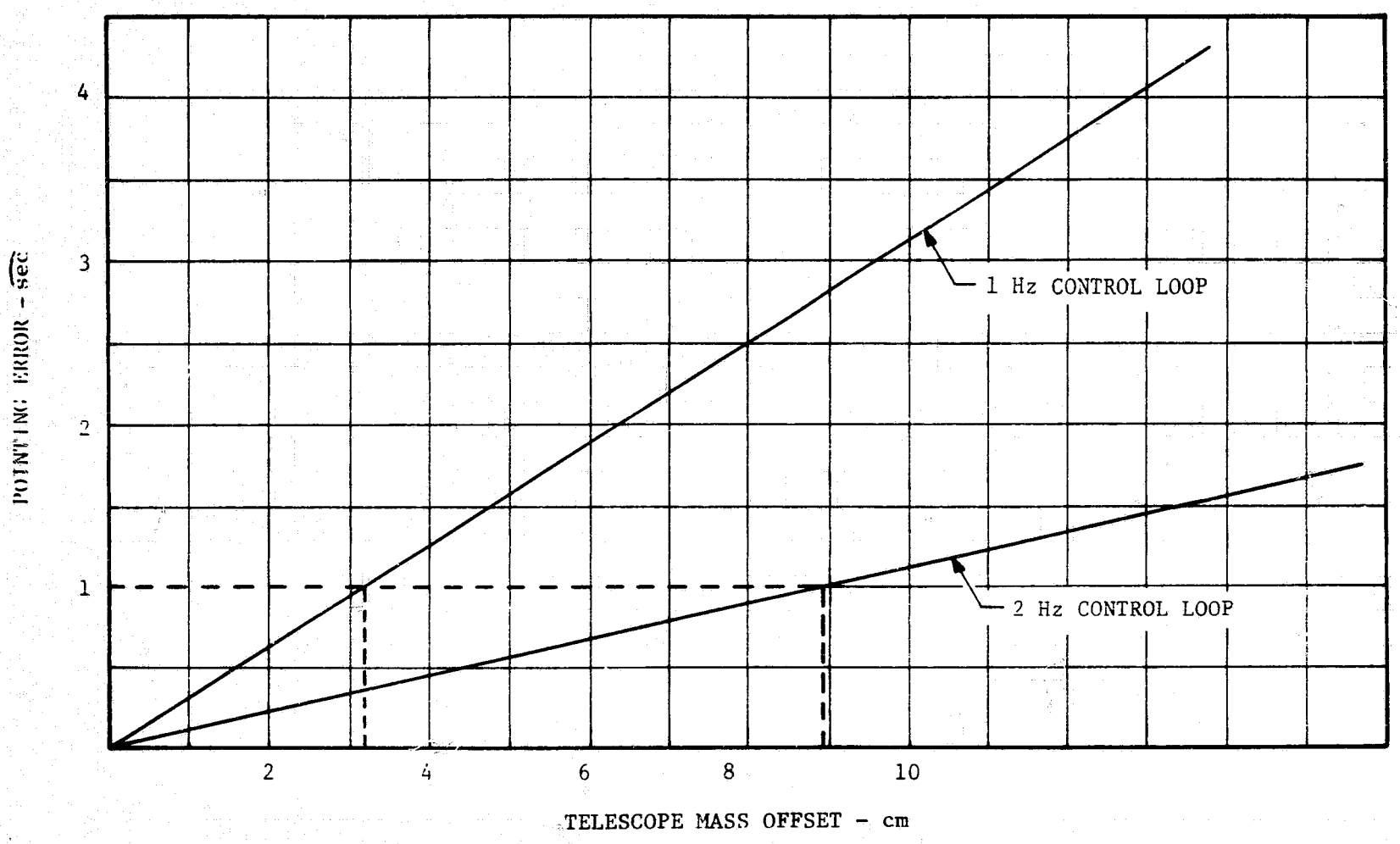

Figure 9-5. SEPB Pointing Error vs Telescope Mass Offset

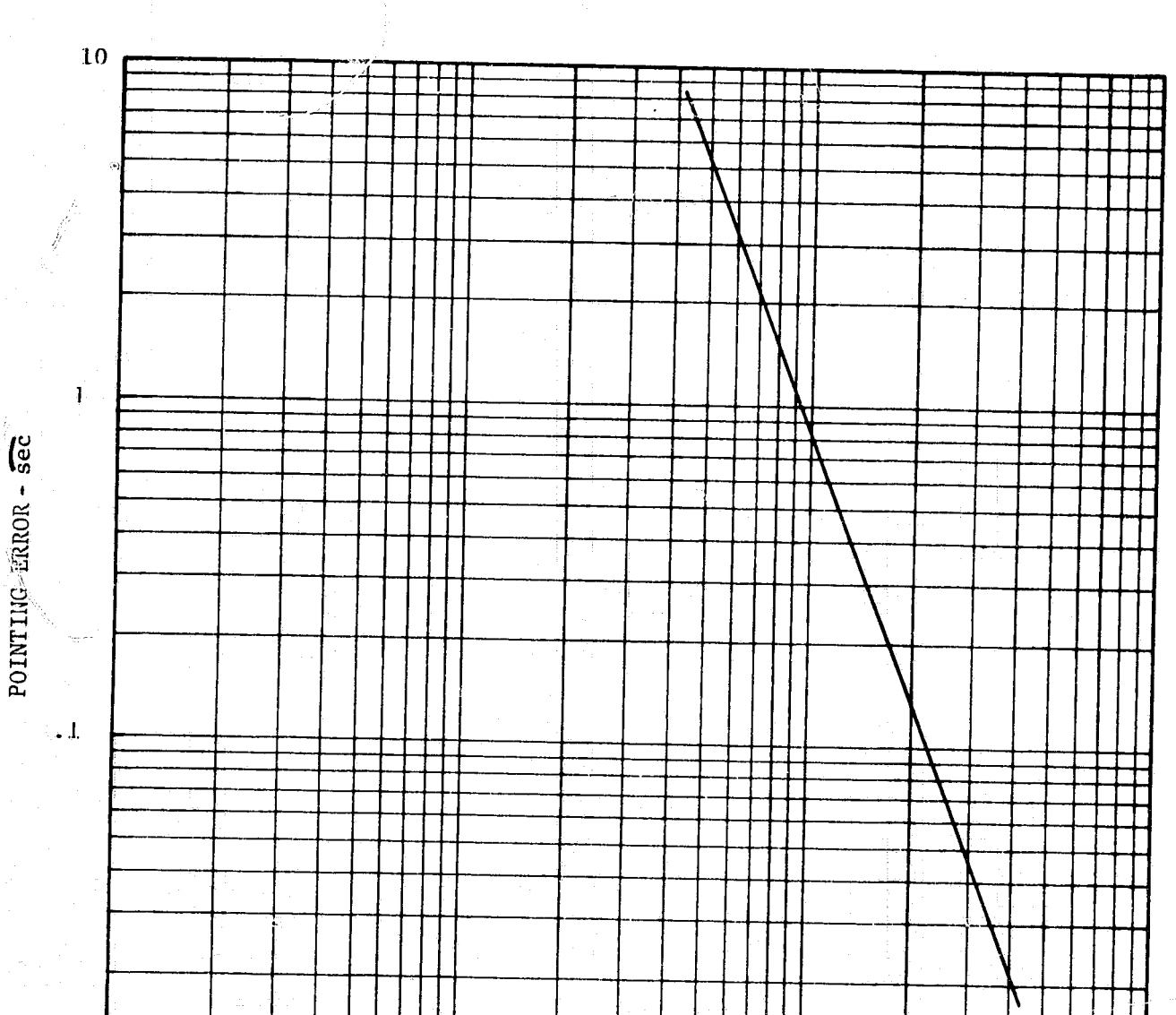

Figure 9-6. Floated Pallet Pointing Error vs Control Loop Bandwidth for 0.1 Hz Suspension Natural Frequency

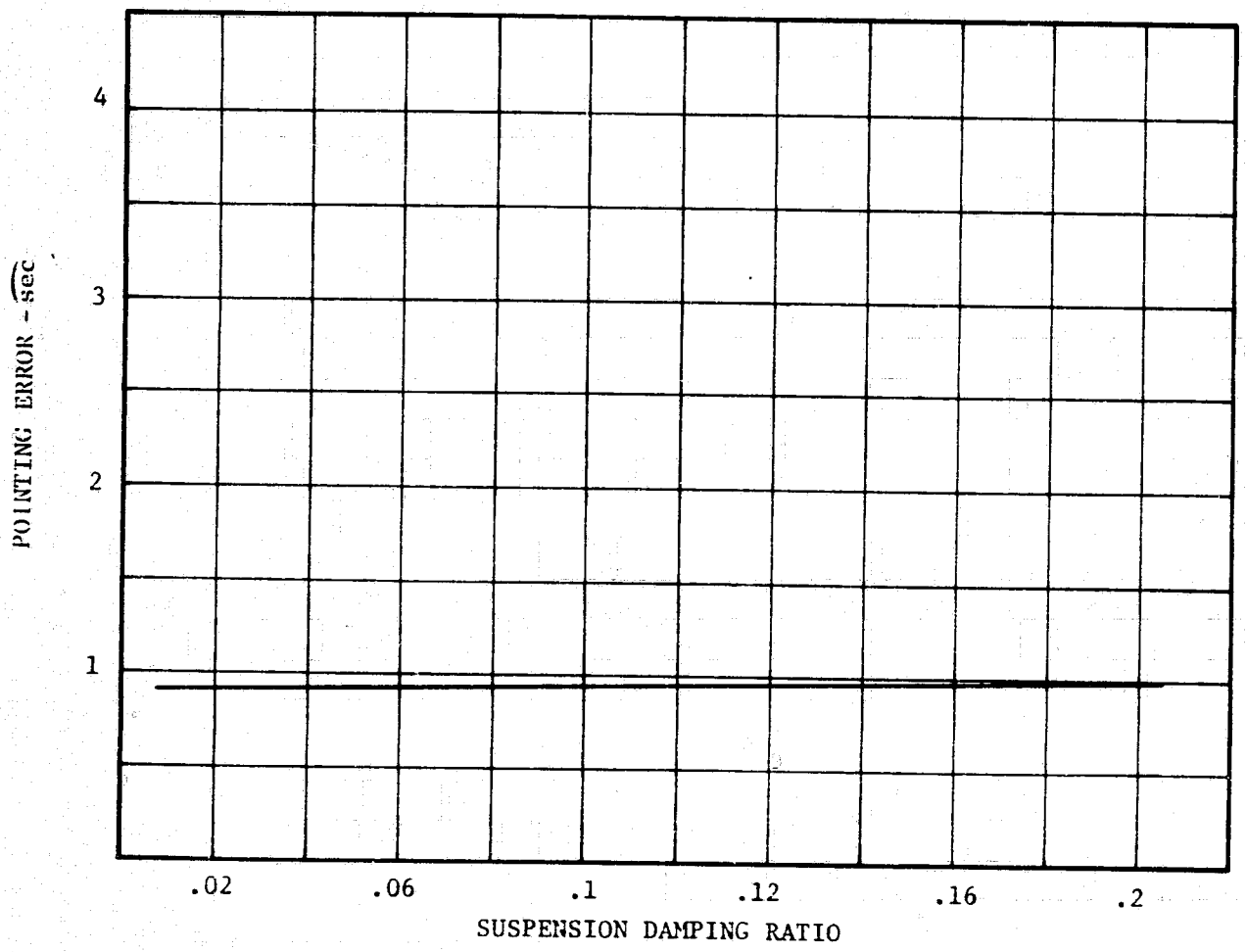

Figure 9-7. Floated Pallet Pointing Error vs Suspension Damping Ratio for 1 Hz Loop Bandwidth and 0.1 Hz Suspension Natural Frequency

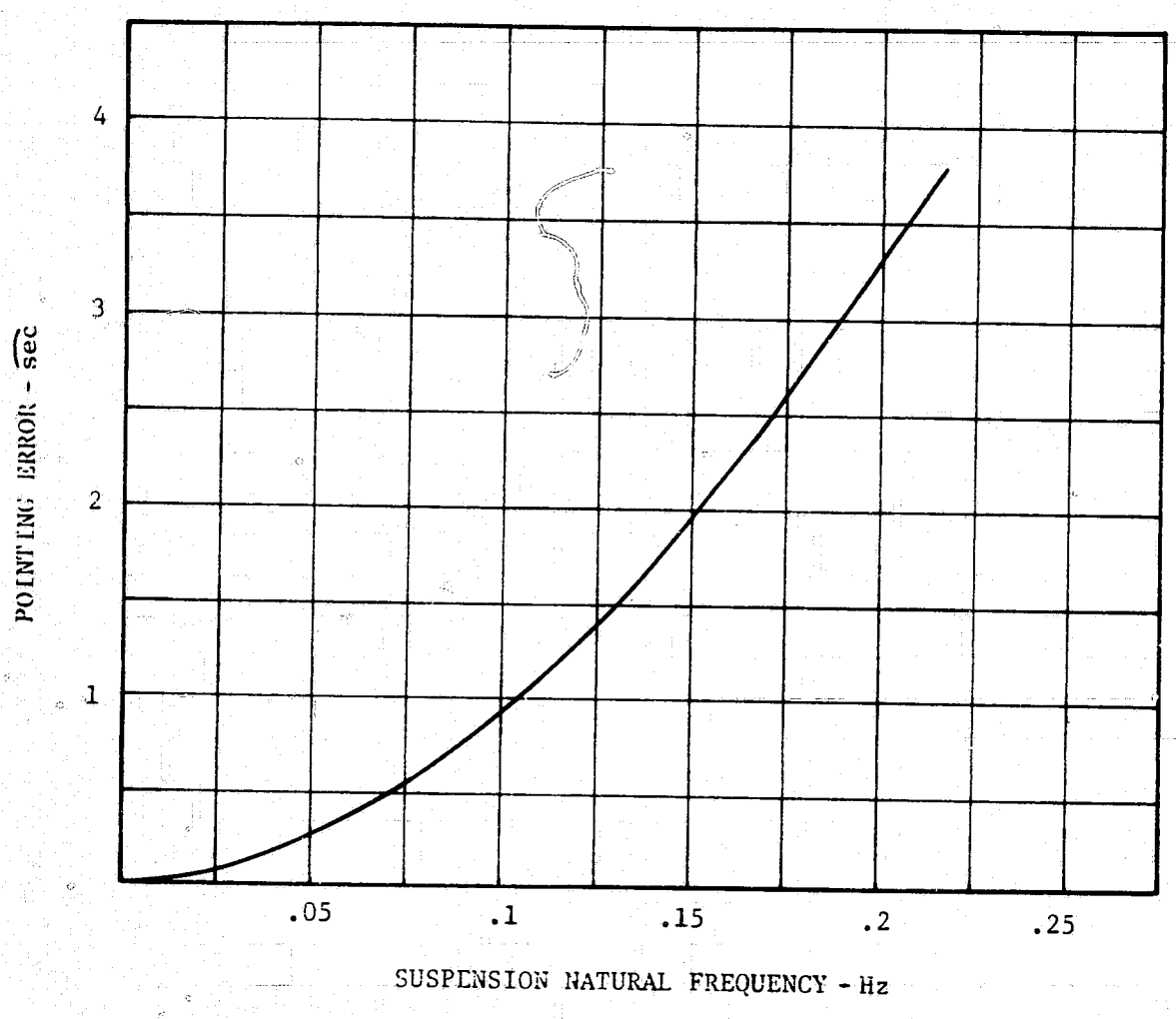

Figure 9-8. Floated Pallet Pointing Error vs Suspension Natural Frequency for 1 Hz Control Loop and 0.1 Suspension Damping Ratio

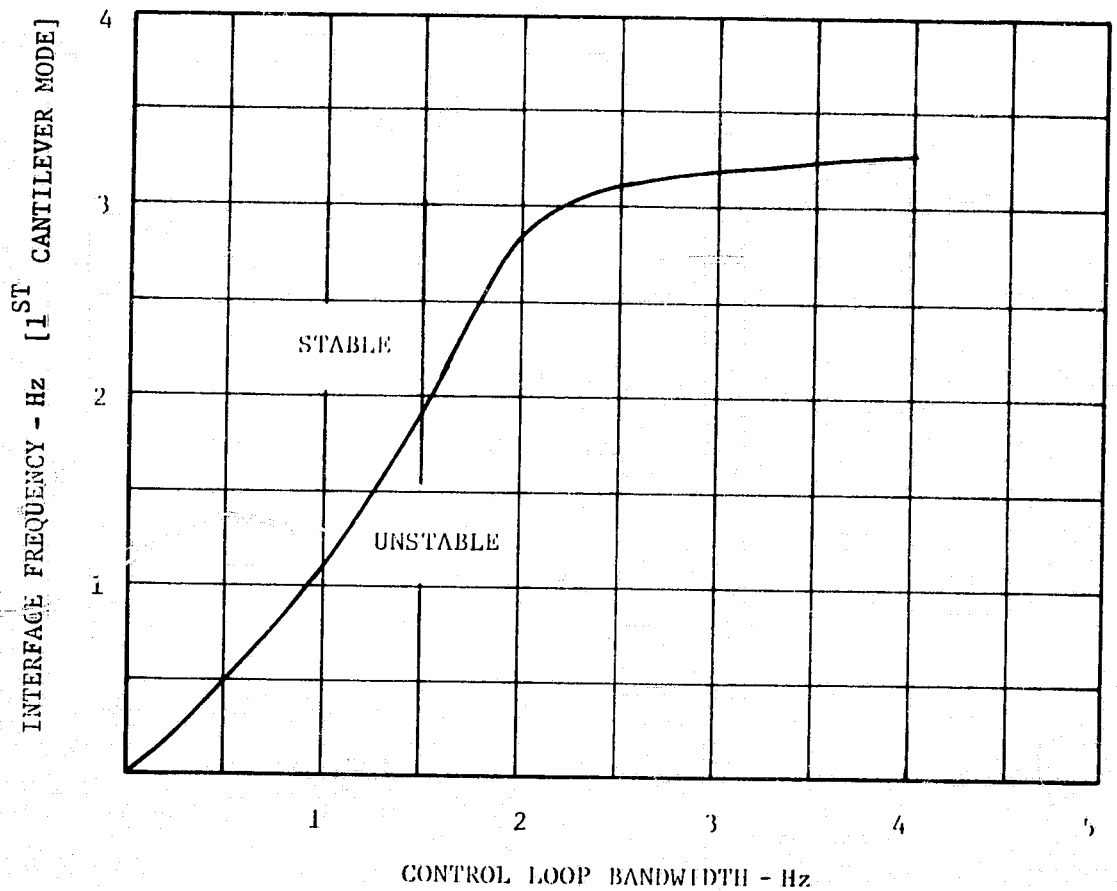

Figure 9-9. Gimbal Interface Frequency vs IOG Control Loop Bandwidth (Sensors Mounted on the Telescope)

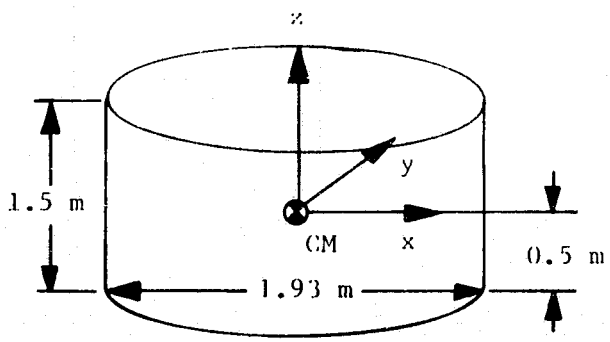

M=932 kg

J_x=388 kg-m^2

J_y=388 kg-m^2

J_z=1,719 kg-m^2

Figure 9-10. IOG Slewing Telescope Configuration and Mass Properties

Table 9-1. Effects of Structural Flexibility for the IPS

SYSTEM	INTERFACE STIFFNESS FOR STABILITY WITH FLEXIBLE INTERFACE BETWEEN SENSORS AND ACTUATORS	INTERFACE STIFFNESS FOR STABILITY WITH SENSORS AND ACTUATORS MOUNTED ON RIGID STRUCTURE	INTERFACE STIFFNESS TO MEET POINTING STABILITY REQUIREMENT OF $\pm\widehat{1}$ SEC PEAK
Inside-Out Gimbal System (IOG) 2 Hz Control Loop 2.5×10^3 kg-m^2 Instrument	1st Cantilever Mode f_n=2.846 Hz k=1.647×10^6 N-m/rad Should at least be increased by a factor of 2 (5.692 Hz) to achieve adequate system response	1st Cantilever Mode f_n=7.967 Hz k=1.291×10^7 N-m/rad	Not applicable
Standard Experiment Pointing Base (SEPB) 1 Hz Control Loop 2.5×10^3 kg-m^2 Instrument	f_n=6 Hz k=3.599×10^6 N-m/rad	f_n=0.5 Hz k=2.499×10^4 N-m/rad	f_n=3 Hz k=8.996×10^5 N-m/rad
Floated Pallet 1 Hz Control Loop	f_n=8 Hz k=1.73×10^8 N-m/rad K=2.313×10^6 N/m	None required as long as rigid (i.e., 8 Hz) section corresponds to approximately 30 percent of the total pallet inertia	f_n=4 Hz k=2.93×10^7 N-m/rad K=5.784×10^5 N/m

Table 9-2. IOG Slewing Performance

	SLEW PROFILE	TELESCOPE SLEW AXIS	TRACKING ERROR (rad)	IOG PEDESTAL ROTATION (rad)	IOG PEDESTAL CM TRANSLATION (meters)	ISOLATOR ELONGATION (meters)	CONTROL TORQUE (N-m)
Slewing Telescope (932 kg)	1	-y axis	$\theta_{xE}=0$	$\theta_x=0$	$\varepsilon_x=1.88\times10^{-2}$ (.7402 in)	$x=1.588\times10^{-3}$ (.0625 in)	$T_{cx}=0$
			$\theta_{yE}=4.89\times10^{-6}$ (1.008 sec)	$\theta_y=4.59\times10^{-2}$ (2.63 deg)	$\varepsilon_y=0$	$y=0$	$T_{cy}=0.836$
			$\theta_{zE}=0$	$\theta_z=0$	$\varepsilon_z=1.26\times10^{-3}$ (.05 in)	$z=1.182\times10^{-2}$ (.4652 in)	$T_{cz}=0$
	2	-y axis	$\theta_{xE}=0$	$\theta_x=0$	$\varepsilon_x=3.72\times10^{-2}$ (1.465 in)	$x=3\times10^{-3}$ (.118 in)	$T_{cx}=0$
			$\theta_{yE}=7.15\times10^{-6}$ (1.474 sec)	$\theta_y=9.12\times10^{-2}$ (5.225 deg)	$\varepsilon_y=0$	$y=0$	$T_{cy}=1.69$
			$\theta_{zE}=0$	$\theta_z=0$	$\varepsilon_z=2.61\times10^{-3}$ (.103 in)	$z=2.29\times10^{-2}$ (.902 in)	$T_{cz}=0$
	1	In xy plane $\pi/4$ rad with respect to telescope -x and -y axes	$\theta_{xE}=4.53\times10^{-6}$ (.934 sec)	$\theta_x=5.27\times10^{-2}$ (3.02 deg)	$\varepsilon_x=2.18\times10^{-2}$ (.858 in)	$x=1.85\times10^{-3}$ (.073 in)	$T_{cx}=0.949$
			$\theta_{yE}=4.59\times10^{-6}$ (.9464 sec)	$\theta_y=5.32\times10^{-2}$ (3.048 deg)	$\varepsilon_y=2.17\times10^{-2}$ (.854 in)	$y=1.938\times10^{-3}$ (.076 in)	$T_{cy}=0.963$
			$\theta_{zE}\approx0$	$\theta_z\approx0$	$\varepsilon_z=2.04\times10^{-3}$ (.08 in)	$z=2.653\times10^{-2}$ (1.044 in)	$T_{cz}\approx0$
Baseline Telescope (2.39×10^3 kg)	1	-y axis	$\theta_{xE}=0$	$\theta_x=0$	$\varepsilon_x=9.92\times10^{-2}$ (3.906 in)	$x=5.725\times10^{-3}$ (.2254 in)	$T_{cx}=0$
			$\theta_{yE}=4.17\times10^{-6}$ (0.86 sec)	$\theta_y=0.249$ (14.27 deg)	$\varepsilon_y=0$	$y=0$	$T_{cy}=5.33$
			$\theta_{zE}=0$	$\theta_z=0$	$\varepsilon_z=4.39\times10^{-3}$ (.1728 in)	$z=6.592\times10^{-2}$ (2.595 in)	$T_{cz}=0$
	2	-y axis	$\theta_{xE}=0$	$\theta_x=0$	$\varepsilon_x=0.270$ (10.6 in)	$x=1.725\times10^{-2}$ (.679 in)	$T_{cx}=0$
			$\theta_{yE}=8.05\times10^{-6}$ (1.66 sec)	$\theta_y=0.674$ (38.6 deg)	$\varepsilon_y=0$	$y=0$	$T_{cy}=14.1$
			$\theta_{zE}=0$	$\theta_z=0$	$\varepsilon_z=8.62\times10^{-3}$ (.339 in)	$z=0.1726$ (6.795 in)	$T_{cz}=0$
	1	In xy plane $\pi/4$ rad with respect to telescope -x and -y axes	$\theta_{xE}=2.09\times10^{-6}$ (.431 sec)	$\theta_x=0.176$ (10.08 deg)	$\varepsilon_x=7.15\times10^{-2}$ (2.815 in)	$x=4.375\times10^{-3}$ (.172 in)	$T_{cx}=3.89$
			$\theta_{yE}=2.26\times10^{-6}$ (.466 sec)	$\theta_y=0.179$ (10.26 deg)	$\varepsilon_y=6.71\times10^{-2}$ (2.642 in)	$y=3.975\times10^{-3}$ (.157 in)	$T_{cy}=3.85$
			$\theta_{zE}\approx0$	$\theta_z\approx0$	$\varepsilon_z=3.93\times10^{-3}$ (.155 in)	$z=4.161\times10^{-2}$ (3.61 in)	$T_{cz}\approx0$

10. COMPARISON OF THE IOG, SEPB, AND FLOATED PALLET SYSTEMS

In this section the IOG, SEPB, and Floated Pallet are compared relative to each other. The format for this comparison is a tabular listing giving the advantages and disadvantages of each of the systems investigated. Comparison between system weight and the pallet/telescope interface stiffness requirements is also presented. However, before presenting the comparison tables some general comments on the systems investigated are in order.

The one main disadvantage of the IOG system is its extreme sensitivity to payload characteristics. This payload sensitivity manifests itself in three ways:

a. Severe stiffness requirements are placed upon the telescope structural design. These stiffness requirements apply to the total telescope structure including the instrument and subsystem compartment behind the actual telescope (i.e., optical bench), which traditionally does not require a stiff structural design. Hence telescope structural design will be driven to a great degree by IOG stability and performance needs rather than the requirements primarily placed upon its design from the scientific mission it is to perform. Compensation for telescope flexibility can be designed in order to alleviate the requirements for structural rigidity. However, if this approach is adopted, a phase stabilization technique would be required in order to maintain the 2 Hz control loop bandwidth required to meet pointing performance. This would necessitate accurate knowledge of telescope and interface flexibility characteristics, which can possibly require on-board measurement, and the capability of varying compensator characteristics as a function of these measurements.

b. Sensors required for IOG control should be mounted on the telescope in order to minimize the interface and telescope structural stiffness required for system stability. This detracts from the IOG as a general purpose experiment accommodator and requires a mechanical and an additional electrical interface.

c. Pedestal rotations, translations, and isolator elongation as a function of telescope mass, inertia characteristics, and slew profiles. This sensitivity probably will not allow the slewing of telescopes larger than 1,000 kg-m^2, even for earth point tracking, in order to maintain pedestal motion and isolator elongations within tolerable limits.

The advantage of the IOG system is that it does not require payload mass balancing, thus making it ameanable to changing telescope instrument packages as desired without telescope rebalancing. In addition, the IOG is the lowest weight system of options investigated. The IOG will also be the minimum cost option of the Instrument Pointing Systems considered, however, in light of the payload sensitivity described above it is not apparent that minimum overall program cost would result.

The SEPB does not exhibit the degree of payload sensitivity as the IOG, however, it does place relatively severe gimbal to telescope interface stiffness requirements in order to meet telescope pointing stability performance. However, there is one significant difference between the SEPB and IOG. Since the SEPB is a center of mass mount (i.e., telescope CM must be constrained to a "small" radius sphere with respect to the gimbal intersection point), it can conveniently be attached to the telescope optical bench. The optical bench is normally made quite stiff due to thermal and dimensional stability considerations. Thus the stiffness required to meet pointing stability will probably not drive telescope structural design. In addition, the stiffness requirements for the SEPB is to meet pointing performance and is not required for absolute system stability. This means that the interface stiffness does not have to be designed with any safety margins. Also from structural considerations the stiffness requirements across the interface are minimized if the sensors are mounted on the SEPB inner or inertial gimbal. This eliminates a mechanical and electrical interface and makes the SEPB a piece of general experiment accommodation equipment.

The SEPB exhibits the best slewing capability of the three systems investigated. There is no restriction on the size of telescope used or the slew profile that could be performed from a dynamic viewpoint. The only restriction is that the gimbal torquer has sufficient torque to execute a desired slew profile for a particular telescope being considered.

There are two primary disadvantages to the SEPB systems. These are:

a. The need for telescope mass balancing in order to achieve satisfactory pointing performance. This would complicate the logistics of changing telescope experiment packages thus detracting from its role as an overall experiment accommodator.

b. It is projected to be the heaviest of the systems considered particularly when considering multiple telescope operations.

There are two principal disadvantages to the Floated Pallet system:

a. The Floated Pallet requires a control moment gyro system.

b. It would not be feasible to maneuver the total orbiter in order to perform telescope slewing due to control moment gyro system size and torque considerations. Hence a separate gimballing system would be required in order to perform accurate telescope slewing. If there are slew requirements for many of the projected Spacelab experiments, this would require the use of essentially redundant Instrument Pointing Systems.

The three prime advantages of the Floated Pallet concept are:

a. The total pallet is stabilized to ± 1 sec thus making it an ideal experiment carrier or base for all types of experiments requiring precise pointing accuracy.

b. The Floated Pallet is not sensitive to payload characteristics making it an ideal piece of experiment accommodation equipment. There are virtually no requirements on telescope structural integrity that would probably not be met by standard structural design. In addition, all control gear would be mounted on the pallet thus eliminating mechanical and electrical interfaces with the various pallet mounted experiments.

c. Use of the Floated Pallet system will eliminate the contaminants due to maintaining the orbiter attitude with the presently defined hypergolic reaction control system. It should be noted that if contamination considerations require the use of CMGs in order to eliminate the contamination effects of the orbiter RCS, one of the prime objections to the Floated Pallet concept, both from a cost and complexity viewpoint, is removed. The additional effort required to float the pallet does not appear to be appreciable, hence it would be a real contender for the Spacelab Instrument Pointing System. Even if separate gimballing systems would be required to perform accurate telescope slewing, the Floated Pallet should still be considered for development once CMGs become a necessity from a contamination viewpoint. This would eliminate the interface and telescope structural stiffness requirements that would otherwise be present in gimballing concepts, thus yielding payload insensitive performance characteristics.

Table 10-1 shows the weight comparison between the IOG, SEPB, and Floated Pallet concepts. Table 10-2 shows the comparison between the structural interface stiffness requirements for the systems considered. Tables 10-3, 10-4, and 10-5 summarize the overall advantages and disadvantages of the Spacelab Instrument Pointing Systems.

Table 10-1. Instrument Pointing System Weight Summary

Inside-Out Gimbal System (IOG)		
Weight of Gimbal and Pedestal = 488 kg (1,076 lb)		
Standard Experiment Pointing Base (SEPB)		
Weight of SEPB = 962 kg (2,121 lb)		
Floated Pallet		
Suspension Weight	[11 kg/corner (24.25 lb)]	44 kg (97 lb)
Retention System Weight	[4 kg/mechanism (8.818 lb)]	20 kg (44.09 lb)
CMG Mounting Rack	(Four CMGs)	90 kg (198.4 lb)
CMG Weight	[190 kg/CMG (418.9 lb)]	760 kg (1,676 lb)
CMG Electronics	[9.07 kg/box (20 lb)]	18.14 kg (40 lb)
Total Floated Pallet Weight		932.1 kg (2,055 lb)

Table 10-2. Effects of Flexibility on Instrument Pointing System

SYSTEM	INTERFACE STIFFNESS FOR STABILITY WITH FLEXIBLE INTERFACE BETWEEN SENSORS AND ACTUATORS	INTERFACE STIFFNESS FOR STABILITY WITH SENSORS AND ACTUATORS MOUNTED ON RIGID STRUCTURE	INTERFACE STIFFNESS TO MEET POINTING STABILITY REQUIREMENT OF ±1 SEC PEAK
Inside-Out Gimbal System (IOG) 2 Hz Control Loop 2.5×10^3 kg-m^2 Instrument	1st Cantilever Mode f_n=2.846 Hz k=1.647×10^6 N-m/rad Should at least be increased by a factor of 2 (5.692 Hz) to achieve adequate system response	1st Cantilever Mode f_n=7.967 Hz k=1.291×10^7 N-m/rad	Not Applicable
Standard Experiment Pointing Base (SEPB) 1 Hz Control Loop 2.5×10^3 kg-m^2 Instrument	f_n=6 Hz k=3.599×10^6 N-m/rad	f_n=0.5 Hz k=2.499×10^4 N-m/rad	f_n=3 Hz k=8.996×10^5 N-m/rad
Floated Pallet 1 Hz Control Loop	f_n=8 Hz k=1.73×10^8 N-m/rad K=2.313×10^6 N/m	None required as long as rigid (i.e., 8 Hz) section corresponds to approximately 30 percent of the total pallet inertia	f_n=4 Hz k=2.93×10^7 N-m/rad K=5.784×10^5 N/m

Table 10-3. Inside-Out Gimbal System (IOG)

ADVANTAGES	DISADVANTAGES
• Projected to be the minimum weight option. • Does not require payload mass balance. • Projected to be minimum cost option. However, it is not at all apparent that the IOG would result in overall minimum program cost. • Does not require a stiff pallet. • Does not require pallet suspension. • Shuttle attitude can be maintained by RCS. • Does not require accurate roll (i.e., about telescope line-of-sight) stabilization if consistant with experiment requirements.	• Sensors should be mounted on telescope in order to minimize the telescope and gimbal/interface stiffness requirements for stability. This would force an IPS/experiment mechanical and electrical interface detracting from the IOG utility as a piece of experiment accommodation equipment. • Severe stiffness requirements on the total telescope structure and telescope gimbal interface result, even if sensors are mounted on the telescope. • High gimbal/pallet and telescope stiffness required for stability. Hence, must be designed with proper margins. • If flexible body compensation is to be employed in order to achieve stability while alleviating telescope and gimbal stiffness requirements, the resulting design would have to be performed for each payload individually, thus making the IOG extremely payload sensitive. • Since loop bandwidths of 2 Hz or better are required for meeting system performance, phase stabilization techniques would be needed for flexible body compensation. This requires an accurate knowledge of flexible body characteristics which can possibly necessitate an on-board measuring system. • Slewing payloads in excess of 10^3 kg-m^2 to perform earth point tracking is not feasible if pedestal motions and isolator elongations are to be kept within tolerable limits. • Since the IOG mounts to the back end of the telescope, large volumes are swept out as the telescope is positioned, making the mounting of multiple telescopes difficult.

Table 10-3. Inside-Out Gimbal System (IOG) (Concluded)

ADVANTAGES	DISADVANTAGES
	• Acquisition star trackers would be required for each telescope since accurate location of one telescope with respect to the other would be difficult in light of the IOG shockmount. This is aggravated as the shockmount is made softer, as is presently indicated (i.e., the shockmount stiffness should be reduced by a factor of 20 to 30 from the present nominal stiffness value of 10^4 n/m). • Separate servos and retention/releasing mechanism would be required for each IOG. • Shuttle attitude would be maintained by a hypergolic RCS, thus maximizing the possibility of experiment contamination. • As mission time increases, an increasing RCS weight penalty results.

Table 10-4. Standard Experiment Pointing Base (SEPB)

ADVANTAGES	DISADVANTAGES
• Does not require stiff pallet. • Does not require pallet suspension. • Shuttle attitude can be maintained by RCS. • Sensors and actuators can be and should be mounted on the SEPB inner gimbal, thus eliminating an electrical/mechanical interface present for the IOG. • Although a 3 Hz interface stiffness is required for the gimbal and the gimbal-to-telescope interface, the attach point to the telescope is at the cm. It is therefore relatively simple to attach to the telescope truss structure which is usually very stiff from optical, thermal, and dimensional stability consideration. • Would not require separate acquisition star trackers. • Telescope slewing easily achieved for a large variety of payloads and slew profiles. • Sweeps out minimum volume when positioning telescope. • System not as payload sensitive as IOG. • Does not require accurate roll (i.e., about the telescope line-of-sight) if consistant with experiment requirements.	• Requires experiment mass balance. • Projected to be heaviest of the systems considered, particularly when considering multiple telescopes. • Each telescope requires a separate SEPB. This will only allow the mounting of two telescopes without exceeding the pallet weight capability. • Shuttle attitude would be maintained by hypergolic RCS, maximizing the possibility of experiment contamination. • As mission time is extended, an increasing RCS fuel weight penalty is paid.

Table 10-5. Floated Pallet

ADVANTAGES	DISADVANTAGES
• Stabilizes total pallet to 1 sec accuracy, thus making total pallet a stable experiment carrier. • Requires only positioning gimbals for the various telescopes mounted on the pallet. Gimbals do not have to be actively servoed. This only applies to experiments that require pointing and not those that require slewing. • Does not require separate acquisition star trackers for each telescope. • Will result in minimum gimbal/telescope interface stiffness requirements (i.e., between 0.5 and 1 Hz). • Minimizes experiment contamination probability since shuttle attitude is maintained via CMGs. • As mission duration is increased, the weight penalty due to the addition of CMGs decreases. • Experiment mass balancing is not required. • System is essentially payload insensitive and is adaptable to a wide variety of payloads.	• Requires CMGs for pallet/shuttle stabilization. • Requires stiff pallet (4 Hz first significant bending mode). • Requires pallet suspension/retention system. • Requires separate servoed gimballing system to perform experiment slewing and tracking. • Requires accurate (i.e., $< \pm 1$ $\widehat{\text{sec}}$) three axis stabilization.

11. RECOMMENDED FUTURE EFFORT

The following tasks are recommended to continue and extend the investigations performed in this study to better evaluate, specify, and compare the IOG, SEPB, and Floated Pallet systems.

a. Determine the stability of the IOG system as a function of the following system parameters:

1) Suspension characteristics (i.e., stiffness and damping).

2) Telescope look angle.

3) Telescope mass and inertia characteristics.

4) Variation in telescope cm location.

5) Sensor and actuator characteristics.

6) Interface stiffness.

7) Control law structure.

The interrelationship between these parameters and their effect on IOG stability should be determined.

b. Determine the adaptability of the IOG in accommodating various projected payload performance requirements. Establish whether one suspension design would be adequate to meet the requirements for the projected payloads or multiple suspension designs would be required.

c. Establish the effects of gimbal friction, wire torques, and other pertinent gimbal nonlinearities on IOG and SEPB pointing and slewing performance.

d. Determine the effect of wire torques on the pointing performance of the Floated Pallet.

e. Determine the effects of sensor and actuator noise on the pointing performance of the IOG, SEPB, and Floated Pallet. Establish the allowable levels of these noise sources consistent with meeting ± 1 $\widehat{\text{sec}}$ pointing stability.

f. Determine the effects of sampling and quantization on the pointing performance of the IOG, SEPB, and Floated Pallet. Establish the required sampling rate and quantization levels that would yield satisfactory system performance.

g. Define in detail the hardware complement required for the IOG, SEPB, and Floated Pallet concepts. Particular emphasis should be given to determining the hardware needed for multiple telescope operation. In addition, the modifications to the pallet structure required to yield the needed stiffness for satisfactory Floated Pallet stability and pointing performance be defined in enough detail to make an accurate evaluation of the level of effort involved.

h. Perform a detailed cost analysis of the IOG, SEPB, and Floated Pallet systems in order to enable the optimum choice or possible choices of Instrument Pointing Systems.

i. Review the instruments and payload experiment combinations which are candidates for the Floated Pallet to revise and update mission requirements as they affect the total control loop.

j. Review the instruments and payload experiment combinations which are candidates for the Floated Pallet to determine center of mass envelopes as they affect the suspension system.

k. Investigate the relative motions of the pallet/orbiter mounting points as they affect the suspension system and the retention system.

l. Define candidate CMG control system configurations including sensors that could meet pallet mission requirements. Perform indepth trade studies between the various CMG control system configurations in order to determine the optimum CMG configuration that will meet overall mission requirements in a cost effective manner. These studies should include detailed hardware trade-offs with respect to size, weight, power consumption, reliability and cost as well as the impact various CMG configurations have on software complexity and overall software cost. In addition candidate types of control logic (e.g., CMG gimbal rate control laws, singularity avoidance laws, etc.) required to satisfactorily manage the CMG control system should be evaluated from the standpoint of software complexity and required computer capacity for implementation as well as overall performance.

12. CROSS-REFERENCE TO TECHNICAL VOLUMES

For more detailed information (i.e., derivations, discussion, etc.) the technical volumes I, II, and III of this final report should be consulted. The following cross-reference is provided to facilitate finding the appropriate material.

SUMMARY VOLUME SECTION	TECHNICAL VOLUME AND SECTION	
2	Volume II	Sections 5 and 6
	Volume III	Section 6
3	Volume III	Sections 4 and 5
4	Volume III	Section 7
5	Volume III	Section 8
6	Volume II	Sections 7, 8, 9, and 10
7	Volume II	Section 10
8	Volume I	Section 2
9	Volume I	Sections 3, 4, and 5
10	Volume I	Section 6